CHARACTERIZING AND MODELING PROTEIN-SURFACE INTERACTIONS IN LAB-ON-CHIP DEVICES

By

PARAG KATIRA

A DISSERTATION PRESENTED TO THE GRADUATE SCHOOL
OF THE UNIVERSITY OF FLORIDA IN PARTIAL FULFILLMENT
OF THE REQUIREMENTS FOR THE DEGREE OF
DOCTOR OF PHILOSOPHY

UNIVERSITY OF FLORIDA

2009

To my grandmother Dr. Jaya M. Katira

ACKNOWLEDGMENTS

There are a lot of people who have influenced, guided, helped and supported me throughout my educational career and I would like to thank them. Firstly, I would like to thank Dr. Henry Hess, who has been my mentor and guide for the past four years. I also thank my committee members, Dr. Tanmay Lele, Dr. Simon Phillpot, Dr. Rajiv Singh and Dr. Jiangeng Xue for their teachings, guidance and support. I have always been blessed with excellent teachers and mentors throughout my educational career. I would like to specifically thank my high school physics teacher Prof. M. B. Vichare and my undergraduate mentor Prof. A. N. Agarwal for the knowledge they imparted to me, the guidance they gave me and the faith they placed in me.

Next, I thank the two people who have made me the person I am today, my mom and dad. I can never thank them enough for everything that they have done for me, for their love and for all the sacrifices that they have made for me. I thank my sister, Dhara for being the greatest influence in my life, for keeping my feet grounded and for always showing me the right path to follow. I thank my fiancée Athmika, who is also my best friend and my greatest strength. Her love and warmth make every moment of my life wonderful. I thank my Aunt Babita and Uncle Chetan, who have always made me feel at home, even though I am far away from it.

Finally, I thank all my friends and colleagues in the Hess group - Ashutosh, Rob, Yoli, Isaac, In-kook, Shruti and Thorsten - for bearing with me and for making graduate school thoroughly enjoyable. I also thank my friends Ashwin, Raja, Mihir, Apurv, Krishna, Saurabh, Karthik, Mahesh and Pankaj for all the fun we have had together and for all their help and support.

TABLE OF CONTENTS

page

LIST OF TABLES

LIST OF FIGURES

Abstract of Dissertation Presented to the Graduate School
of the University of Florida in Partial Fulfillment of the
Requirements for the Degree of Doctor of Philosophy

CHARACTERIZING AND MODELING PROTEIN-SURFACE INTERACTIONS IN LAB-ON-CHIP DEVICES

By

Parag Katira

August 2009

Chair: Henry Hess
Major: Materials Science & Engineering

Protein adsorption on surfaces determines the response of other biological species present in the surrounding solution. This phenomenon plays a major role in the design of biomedical and biotechnological devices. While specific protein adsorption is essential for device function, non-specific protein adsorption leads to the loss of device function. For example, non-specific protein adsorption on bioimplants triggers foreign body response, in biosensors it leads to reduced signal to noise ratios, and in hybrid bionanodevices it results in the loss of confinement and directionality of molecular shuttles. Novel surface coatings are being developed to reduce or completely prevent the non-specific adsorption of proteins to surfaces.

A novel quantification technique for extremely low protein coverage on surfaces has been developed. This technique utilizes measurement of the landing rate of microtubule filaments on kinesin proteins adsorbed on a surface to determine the kinesin density. Ultra-low limits of detection, dynamic range, ease of detection and availability of a ready-made kinesin-microtubule kit makes this technique highly suitable for detecting protein adsorption below the detection limits of standard techniques.

Secondly, a random sequential adsorption model is presented for protein adsorption to PEO-coated surfaces. The derived analytical expressions accurately predict the observed

experimental results from various research groups, suggesting that PEO chains act as almost perfect steric barriers to protein adsorption. These expressions can be used to predict the performance of a variety of systems towards resisting protein adsorption and can help in the design of better non-fouling surface coatings.

Finally, in biosensing systems, target analytes are captured and concentrated on specifically adsorbed proteins for detection. Non-specific adsorption of proteins results in the loss of signal, and an increase in the background. The use of nanoscale transducers as receptors is beneficial from the point of view of signal enhancement, but has a strong mass transport limitation. To overcome this, the use of molecular shuttles has been proposed that can selectively capture analytes and actively transport them to the nanoreceptors. The effect of employing such a two-stage capture process on biosensor sensitivity is theoretically investigated and an optimum design for a kinesin-microtubule-driven hybrid biosensor is proposed.

CHAPTER 1
INTRODUCTION

Adsorption of proteins to surfaces plays a major role in the functioning of biosensors and other lab-on-chip based devices. Prevention of non-specific adsorption of proteins to the biosensor surface is extremely important to achieve high signal-to-noise ratio in biosensors.*[1-6]* This is because non-specific adsorption of target analytes to the sensor surface results in the loss of signal at the receptor, while non-specific adsorption of other proteins in the solution at the receptor results in increased background signal. Preventing non-specific protein adsorption is also crucial to the design and development of hybrid bionanodevices.*[7-10]* Hybrid bionanodevices utilize motor proteins*[11, 12]* adsorbed on surfaces to generate micro- and macro-scale movement of associated filaments which can act as molecular shuttles for various cargos.*[10, 13-17]* Hybrid bionanodevices that can manipulate macromolecules and nanoscale particles have many promising applications,*[18-22]* but require stringent protein adsorption conditions such as patterns of protein fouling and non-fouling regions for controlling cargo movement within these devices.*[23, 24]* Non-specific adsorption of proteins (in amounts as low as 0.01% of a monolayer) within the non-fouling regions can result in loss of device function. *[25]* To this effect novel surface coatings are being developed to reduce or completely prevent the adsorption of proteins to surfaces.

In this thesis, the role of protein adsorption in various medical and biotechnology applications, various techniques to control protein adsorption and standard methods to quantify protein adsorption are discussed in brief in chapters one and two. In chapter three, a novel quantification technique for extremely low protein coverage on surface is described. This technique utilizes the measurement of landing rates of labeled microtubule filaments on kinesin proteins adsorbed on a surface to determine the protein density. Ultra-low limits of detection,

dynamic range, ease of detection and availability of a ready-made kinesin microtubule kit makes this technique highly suitable for detecting protein adsorption below the detection limits of standard techniques. This method is used to determine the performance of standard surfaces, surface polymer coatings by poly(ethylene oxide) (PEO) and a new type of polymer coating for preventing protein adsorption.

Understanding the ability of polymer coatings to resist protein adsorption requires the development of theoretical models that explain the observed experimental results. Some of the important theoretical modeling techniques for adsorption of proteins to various surfaces that increase the understanding of this phenomenon are discussed in chapter four. In chapter five, a random sequential adsorption model is presented for adsorption of proteins to PEO-coated surfaces. This is a simple probabilistic model for protein adsorption that differs from a previous, generally accepted model called single chain mean field theory in that this model assumes the polymer chains to be perfect steric barriers to proteins and are randomly grafted on the surface. The simple analytical expressions derived from this model accurately predict the observed experimental results from various research groups, which suggests that PEO chains act as almost perfect steric barriers to protein adsorption. The analytical expressions can be directly applied to a large number of systems to predict their performance towards resisting protein adsorption and can help in the design of better non-fouling surface coatings.

Finally, in chapter six, the role of protein adsorption in biosensing applications and the limitations of current biosensor designs are discussed. Use of nanoscale receptors for the capture and detection of analytes can be useful in lowering the detection limits of biosensors due to a high signal-to-noise ratio. But, the application of nanoscale receptors in actual biosensors is limited due to the time it takes to capture sufficient analytes onto the receptors. It has been

suggested that molecular shuttles can be employed to capture and concentrate specific analytes from solution for rapid detection in these biosensors. Such a two-stage capture mechanism for analytes in synthetic biosensors is theoretically modeled to determine the optimum conditions where such a molecular motor driven transport system can be advantageous. The obtained analytical expressions are used to design and optimize a molecular shuttle-based biosensor where the analyte molecules are captured onto kinesin driven microtubules and concentrated at a receptor by active transport. The derived analytical expressions can also be used to improve the design of existing hybrid bionanodevices so that the integration of these with biosensors results in higher sensitivity.

Proteins and Protein-Surface Interactions

Proteins are essential biological macromolecules that participate in every process within cells. Proteins are made of amino acids arranged in a linear chain and polymerized by formation of peptide bonds between the carboxyl and amino groups of adjacent amino acids. The linear polymer chain forms the primary structure of the proteins (Figure 1-1 A). The amino acid composition is generally unique and specific to each particular protein. The hydrogen bonding characteristics of the polyamide bonds in the linear chain results in various secondary structures in proteins such as α – helix, β – sheet or random coil (Figure 1-1 B). Further intramolecular interactions between the various groups of constituent amino acids give rise to a unique tertiary structure to each polypeptide chain (Figure 1-1 C). These intramolecular interactions can be ionic interactions, salt bridges, hydrogen bonding, hydrophobic interactions or covalent disulphide bonds which give specific structural and mechanical properties to the proteins. Two or more polypeptide chains, each with its own primary, secondary and tertiary structure associate to form the quaternary structure of the protein (Figure 1-1 D). Further details on amino acid sequences and resulting protein structures can be found in related references.*[26-29]*

A large variety of proteins are found within cells. Each protein has unique structural and functional properties. Many proteins are enzymes that specifically bind to other molecules and catalyze biochemical reactions that are vital to metabolism. Other proteins such as collagen, elastin, actin and myosin are present for structural functions such as formation of the scaffolding that supports the cell shape. Some proteins act as energy producing components of the cell such as dynein and kinesin which are involved in intracellular cargo transport. Proteins present in the cell membrane are important in cell-cell and cell-surface interactions such as signaling, immune response, cell adhesion and cell migration. Due to their diversity and functionality proteins perform most of the tasks within cells, and the human body has tens of thousands of protein types.*[30, 31]*

The importance of proteins in the biological environment, as major drivers of intracellular process makes protein structure and function studies extremely important. Proteins interact with surfaces by one or more of the following general force classes: 1) Electrostatic forces due to the presence of two or more charged groups near the interface, 2) hydrophobic interactions in the presence of water molecules at the protein-surface interface and 3) hydrogen bonding due to dipole-dipole interactions.*[28]* These interactions can result in proteins adsorbing to surfaces in different configurations, and change in adsorbed protein configuration over time *[32, 33]* which further dictate the response of other biomaterials such as other proteins,*[34]* protein agglomerates*[35]* and cells *[36, 37]* in the solution to the surface. Furthermore, adsorption of proteins on surfaces can result in changes to the material interface properties such as its hydrophobicity or surface charge.*[32, 38]* Controlled protein adsorption to surface is important in the functioning of any device exposed to a biological environment. Examples of such devices and the role of protein adsorption in their application are discussed in the following section.

Applications for Controlled Protein Surface Interactions

Proteins are known to adsorb on almost all surfaces *[39, 40]*, hydrophilic or hydrophobic. Adsorption of proteins on surfaces determines the response of other biological species within the surrounding solution towards the surface. Extensive developments in the fields of biotechnology, medicine and food processing have given rise to a large variety of applications which require different protein-surface interactions such as adsorption of specific proteins in functional conformations, localized adsorption of specific proteins and in many cases complete prevention of protein adsorption to the surface. This requires designing surfaces that fulfill the requirements of these applications. The diversity in protein structure and functions makes it challenging to design biomaterial interfaces that trigger only specific protein interactions. Extensive research towards developing such material interfaces has resulted in some success over the years. A significant degree of control over specific and non-specific protein adsorption has been attained by the development of surface coatings and surface modifiers.*[41-47]* Also, basic theoretical concepts that govern various protein-surface interactions have been developed and detailed modeling of these systems has been attempted with some degree of success.*[48-50]* Yet the required degree of control over protein adsorption desired for practical biomedical*[51]* and biotechnological applications,*[23]* as well as a clear understanding of the protein adsorption phenomenon and its prevention*[52]* have not been achieved. Some of the major applications and the required protein-surface interactions are discussed in the following sections.

Biomedical Applications

Artificial joints, pacemakers, stents, artery grafts, and dental implants are just a few examples of biomedical devices that require controlled protein-surface interactions. Biomaterials implanted into the body trigger what is known as foreign body reaction. Nonspecific adsorption of proteins immediately occurs on implanted materials. This non-specific adsorption which does

not normally occur in a biological environment causes a number of cells such as leukocytes, monocytes and platelets to adhere to the implant material triggering a process similar to normal wound healing. A cascade of events (Figure 1-2) results in chronic inflammation at the material interface which leads to the fusing of the adhered macrophages into multinucleated foreign body giant cells that often persist for the lifetime of the implant. This prevents the implant material from performing its expected functions. Detailed explanations of foreign body response and response to implant materials have been discussed in related reviews.*[51, 53-55]* To improve the host response to implant materials various strategies are being developed such as: 1) Developing materials that promote adsorption of specific proteins which in turn trigger specific cell responses that render the surface biocompatible,*[56]* 2) Maintaining protein conformations on surfaces to trigger only specific responses from cells adhering to the implanted material *[57]* and 3) Preventing protein adsorption to implanted materials altogether as cell adhesion is initiated on the adsorbed protein layer.*[58, 59]* Detailed reviews on design and compatibility of implant materials to cell adhesion and controlled response can be found in related reviews.*[38, 55]*

Biosensors and Lab-On-Chip Devices

Bioimplants involve protein surface interactions *in vivo*. While these are extremely important for the design of biocompatible materials in medicine, a large number of in vitro process also require a high degree of control over protein surface interactions. *In vitro* devices such as biosensors *[60, 61]* and lab-on-chip devices *[62, 63]* are important for the detection of various biomolecules and observation of various biological interactions which have applications in medicine, food processing, and biotechnology and bio warfare. In biosensors, the presence of specific target species within a particular solution is probed by the interaction of that species with a receptor biomolecule or biomolecules. In a large number of cases the receptor biomolecules are proteins specifically adsorbed on a surface. The species being detected could be

antibodies, viruses, bacteria or other proteins. This requires the surfaces to be modified such that the receptor molecules are adsorbed at only specific spots on the surface. Furthermore, the adsorption of target species has to be prevented on non-specific locations on the sensor surface. This requires a strong control over the biomolecule (proteins) surface interactions (Figure 1-3).*[64-66]* In other lab-on-chip devices, various reactions chambers are developed to probe the design of enzymatic networks, protein-ligand and protein-protein interactions. Here it is once again essential to prevent non-specific protein surface interactions that would result in loss of protein concentration or even result in change of protein conformations due to adsorption that result in changed reactivity of proteins.*[67-70]* Lab-on-chip devices that probe cellular functions such as cell growth, migration and cell multiplication to study signaling pathways or the formation of cellular networks require protein adsorption in patterned areas on surfaces and with maintained functionality.*[70-72]*

Hybrid Bionanodevices

An emerging field of bioengineering is the design of bionanodevices that utilize mechanical properties of specific proteins to develop nanoscale actuators.*[73-75]* These devices have applications in nanorobotics,*[17, 21, 76-79]* self assembly of dynamic structures,*[80-82]* detection of molecular level forces,*[83]* and self-pumping systems for microfluidic applications.*[84-86]* One example of this is the design of molecular shuttles driven by motor proteins (Figure 1-4) for transport and manipulation of biomolecules,*[18, 87, 88]* nano-particles*[89-91]* and even micron-sized structures.*[19, 92, 93]* Motor proteins convert chemical energy to mechanical output within cells and are responsible for various force generation tasks as well as intracellular transport.*[10, 11, 94-96]* The application of these motor proteins *in vitro* requires design of specific interfaces that allow the motor proteins to adsorb in the right conformation. *[23]* Also, the ability to control and manipulate motor action for desired output in

some cases requires adsorption of these proteins in patterns on surfaces as shown in Figure 1-4.*[97-99]*

Techniques to Control Protein-Surface Interactions

The understanding and control of protein-surface interactions is a major challenge in the design of a large variety of medical and bioengineered devices. The diversity and complexity of protein structures as well as the sheer abundance of different types of proteins makes this problem even more complex and challenging for researchers. Various strategies are being developed to control protein-surface interactions such as: 1) Prevent non-specific adsorption, 2) Promote specific adsorption and 3) Conserve protein conformations. Some of these techniques for controlled protein-surface interactions are briefly discussed in the following section and detailed descriptions and discussions can be found in related literature.*[45, 51, 55, 100-103]*

Surface Modifications to Prevent Protein Adsorption

The earliest attempts towards making surfaces resistant to protein adsorption were by increasing their hydrophilicity. This method is only moderately successful for certain proteins while for others it has no effect. *[40, 104, 105]* This is because hydrophilic solid surfaces have either charged or polar groups at their surface. These can interact easily with the polar groups or oppositely charged regions on the protein surface resulting in protein adsorption. At best, hydrophilic surfaces can prevent the denaturation of proteins and conserve their conformation.*[106]* The reason for this is that proteins generally denature on surfaces by exposing the previously hidden hydrophobic regions of the folded protein to the hydrophobic regions on the surface. The lack of hydrophobic regions forces the protein to adsorb to the surface only by electrostatic interactions and maintain its folded structure.

The most widely used system to render a surface protein resistant (non-fouling) is by surface immobilization of poly(ethylene oxide) (PEO) chains of varying lengths (number of EO

units varying from 3 to 50). There have been many approaches to attaching PEO to material surfaces to render them non-fouling either through covalent immobilization, adsorption or interpenetration. One common approach is the adsorption of PEO-PPO-PEO triblock co-polymers onto hydrophobic surfaces through strong hydrophobic-hydrophobic interactions (Figure 1-5 A).*[107, 108]* This polymer class is also known as Poloxamers or Pluronics and has been extensively studied. Another important approach for PEO attachment to surfaces is by the formation of self assembled mono-layers of Oligo(ethylene oxide) (OEO) or PEO modified alkane-thiols on gold surfaces (Figure 1-5 B).*[109-111]* The OEO or PEO SAMs (self-assembled monolayers) best hinder the protein adsorption when the polymeric chains are densely packed*[111, 112]* except in the case of PEO chains attached with non-polar groups at the terminating end.*[113]* An alternative for modification of gold surfaces is based on PPS-PEO diblock or PEO-PPS-PEO triblock co-polymers with poly(propylene sulfide) PPS as the central block that binds to gold surfaces and PEO grafted chains.*[114]* Another approach of packing PEO or OEO chains on surfaces to render them protein non-fouling is by SIATRP (surface initiated atom transfer radical polymerization).*[47, 115, 116]* In one technique, the polymerization initiator molecule is functionalized by a thiol and a mixed SAM of this initiator and a diluent is formed on the gold surface. Poly (OEGMA) i.e. poly oligo(ethylene glycol) methyl methacrylate is then grown in a bottle brush morphology along the SIATRP initiator molecule (Figure 1-5 C). Other than PEO polymer chains, other polymeric structures such as tetraethlyeneglycol dimethylether (tetraglyme) have also been used.*[43, 117]* Tetraglyme forms a highly non-fouling cross-linked structure and even though in plasma-deposited tetraglyme there are no chains longer than 3 units, the surface is highly protein non-fouling. Surfaces grafted with oligosaccharide surfactant polymers have also been shown to resist protein adsorption by

the formation of a glycocalix like structure.*[118]* Apart from using PEO or PEO-like polymers to coat the surface, formation of stable phospholipid bilayers on surfaces also prevents adsorption of most proteins (Figure 1-5 D).*[119]*

Techniques to Promote Specificity of Protein-Surface Interactions

Some biomedical and biotechnological applications employ specifically adsorbed proteins on surfaces to trigger specific responses from other biological species in their surroundings. Examples of these are drug delivery systems, biosensors and lab-on-a-chip devices. For these applications, apart from reducing non-specific protein adsorption, spatial and conformational control over surface adsorption of specific proteins is desired. Various methods employing a combination of surface chemistry, surface coating with functionalized polymers and surface patterning techniques are used for controlled protein adsorption to specific regions of the surface. Examples of such surface modifications required for controlling specific aspects of protein adsorption are mentioned in this section.

Spatial control on protein adsorption can be obtained by surface patterning using lithography techniques. One can modify the surface chemistry and functionalization within specific regions of interest on the surface. For example, specific regions on a gold surface can be coated with hydrophobic alkanethiolates using microcontact printing.*[120, 121]* The remaining areas of the gold surface can then be treated with a solution containing PEO-linked alkanethiols which form a self-assembled monolayer on gold. The self assembled monolayers of PEO resist protein adsorption while the hydrophobic alkanethiols promote protein adsorption, thus localizing the adsorption of proteins to the microcontact printed pattern (Figure 1-6 A). Other lithography techniques can also be similarly used to locally render regions of a surface hydrophilic or hydrophobic/protein adsorbing or non-adsorbing. Details for these can be found in related literature.*[122-127]*

Control over specificity of protein adsorption requires the presence of a molecule or ligand on the surface that specifically binds to the target protein. This can be achieved by grafting the surface with polymer chains terminating with the specific ligand or molecule. This has been successfully shown for example by the specific adsorption of avidin to SAMs of biotin-terminated PEO chains (Figure 1-6 B),*[128]* adsorption of carbonic anhydrase to SAMs presenting benzenesulfonamide group,*[129]* and the attachment of integrins to arginine-glycine-aspartic acid (RGD) immobilized on the surface. *[46, 130]*

Conformational control on protein adsorption can be controlled by changing the surface chemistry of the surface. For example, adsorption of fibrinogen on gold surfaces exhibiting OH headgroups and COOH head groups conserves its conformation and functionality as compared to gold surfaces exhibiting NH_2 and CH_3 head groups.*[106]* In general, proteins spread more and denature easily on hydrophobic surfaces as compared to polar or charged surfaces. Another method of conserving protein conformation on adsorption is by embedding them within a dense layer of polymeric chains grafted on the surface or within lipid bilayers (Figure 1-6 C).*[131, 132]* Sometimes, adsorption of a layer of blocking protein such as albumin or casein helps preserve the conformation and functionality of secondary adsorbed proteins such as kinesin (Figure 1-6 D).*[133]* Similarly, immobilization of collagen type I protein on a poly (2-hydroxyethyl methacrylate) (pHEMA) surface binds osteopontin in a configuration that promotes endothelial cell adsorption. *[134]*

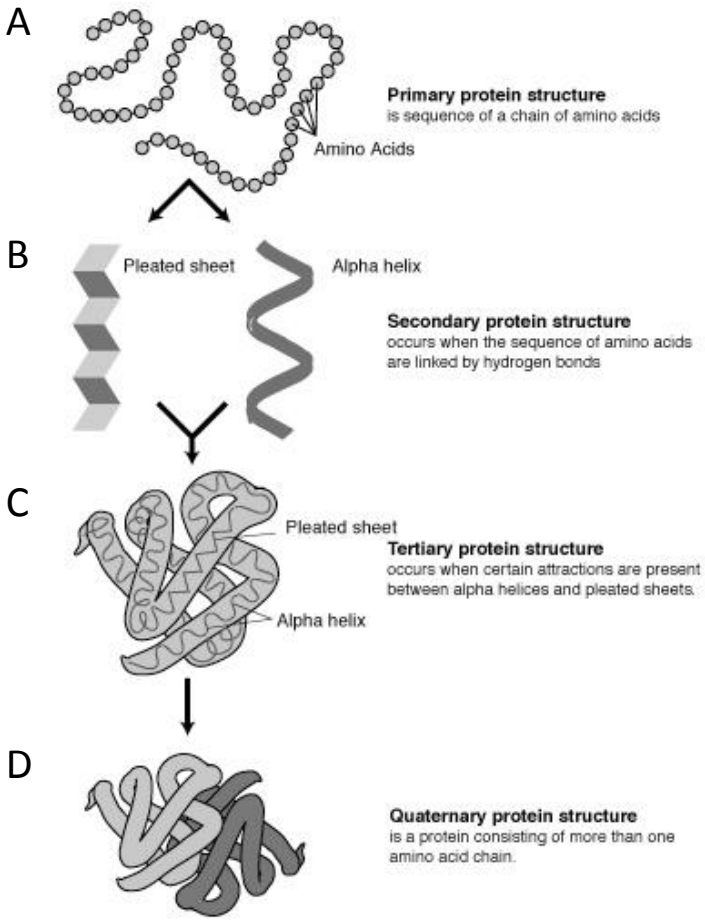

Figure 1-1. Structural Hierarchy of Proteins. A) Primary structure of proteins formed by linear amino acid chain. B) Secondary structure in the form of α – helices and β – sheets. C) Tertiary structure of proteins formed due to interactions between various side groups attached the polypeptide backbone. D) Quaternary structure of proteins formed by association of two or more tertiary structures. Figure adapted from reference *[135]*.

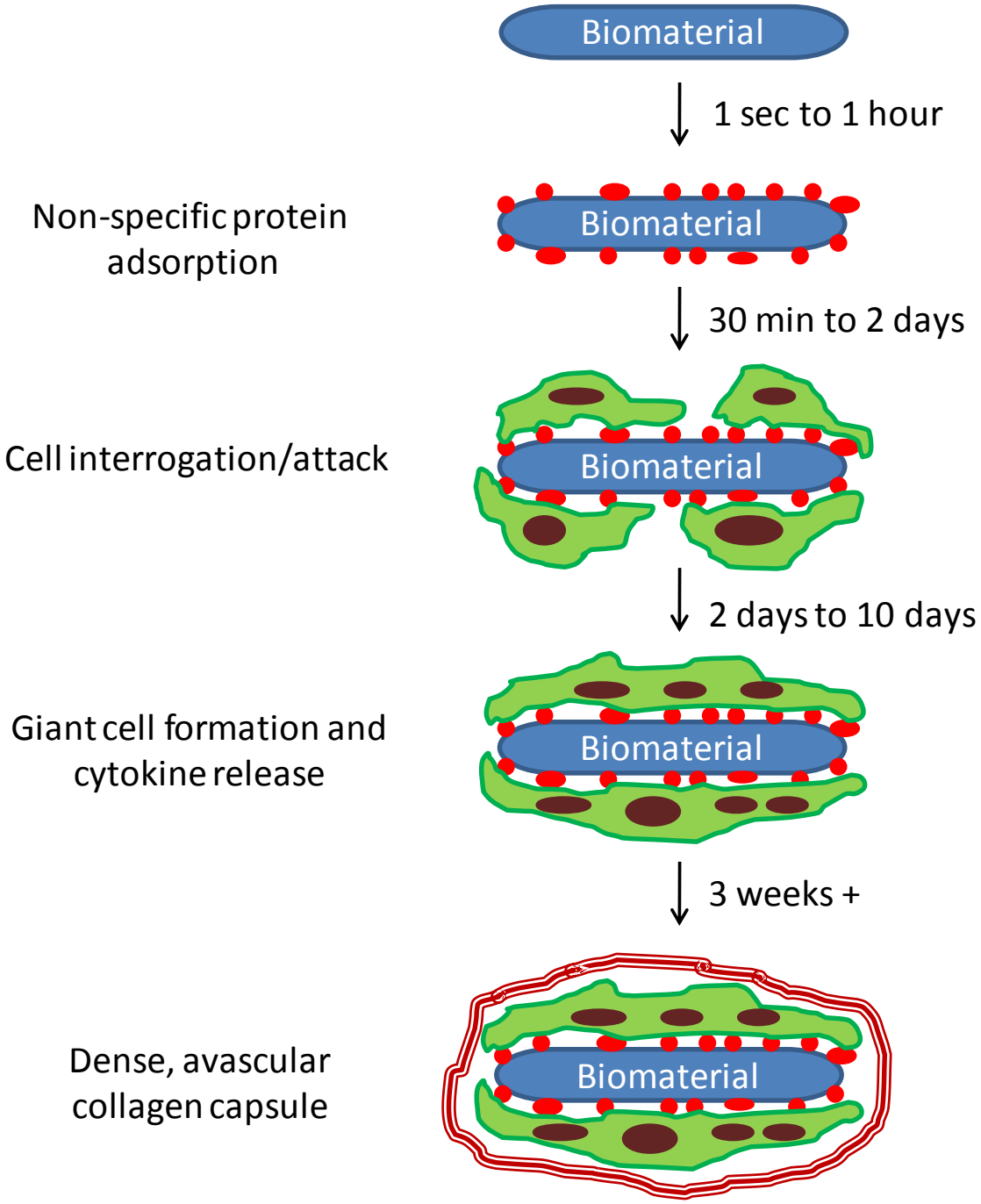

Figure 1-2. Foreign Body Response to Implant Material. The first step is adsorption of proteins to the implant material. Non-specific adsorption of proteins is detected by cells that begin to bind to the adsorbed proteins triggering the foreign body response. Over time a dense network or interconnected cells with multiple nuclei is formed. This triggers the formation of a dense collagen capsule that completely cuts off the implant material from the rest of the body. Figure adapted from reference *[51]*.

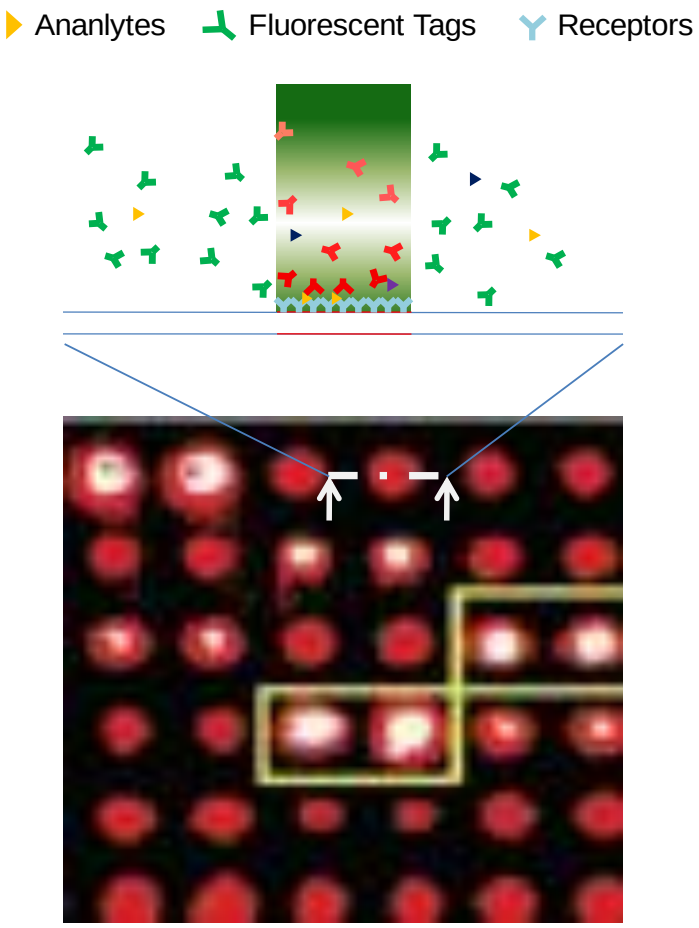

Figure 1-3. Protein-Surface Interactions in Biosensor Devices. The sample being analyzed may contain numerous biological species of which only a specific one needs to be detected. Prevention of non-specific adsorption and capture of target molecules by spatially localized receptor proteins is the basic principle of biosensor design. Sensor-chip adapted from *[136]*

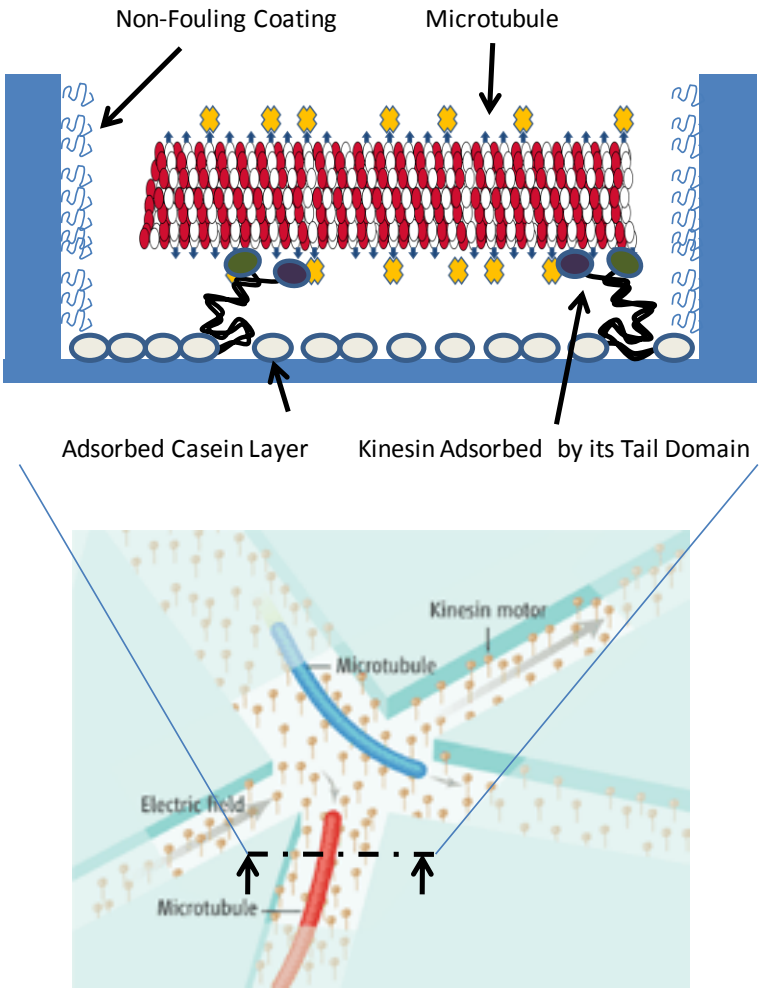

Figure 1-4. Protein-Surface Interactions in Hybrid Bionanodevices. Adsorption of motor proteins (kinesin) in functional conformations so that they can latch on to and drive the molecular shuttles (microtubules) along defined tracks. Partially adapted from *[13]*

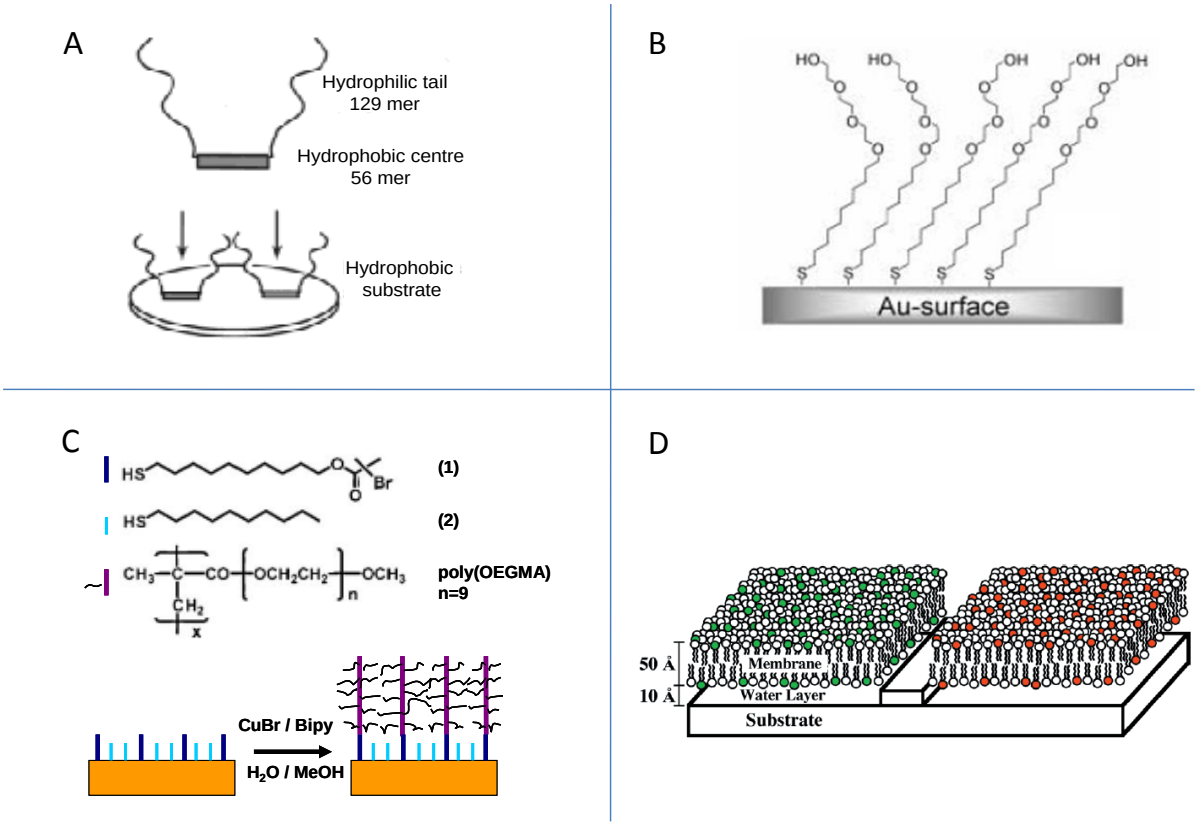

Figure 1-5. Surface Modifications to Prevent Protein Adsorption. A) Physically adsorbed PEO-PLL-PEO polymers to hydrophobic surfaces. Adapted from *[107]* B) Self-Assembled monolayers of alkanethiols attached to PEO chains. Adapted from *[137]* C) SIATRP based polymerization of poly (OEGMA) chains in a bottle brush morphology to obtain a dense packing of polymer chains. Adapted from *[115]* D) Surface patterned with lipid bilayers that prevent adsorption of non-membrane proteins. Adapted from *[132]*.

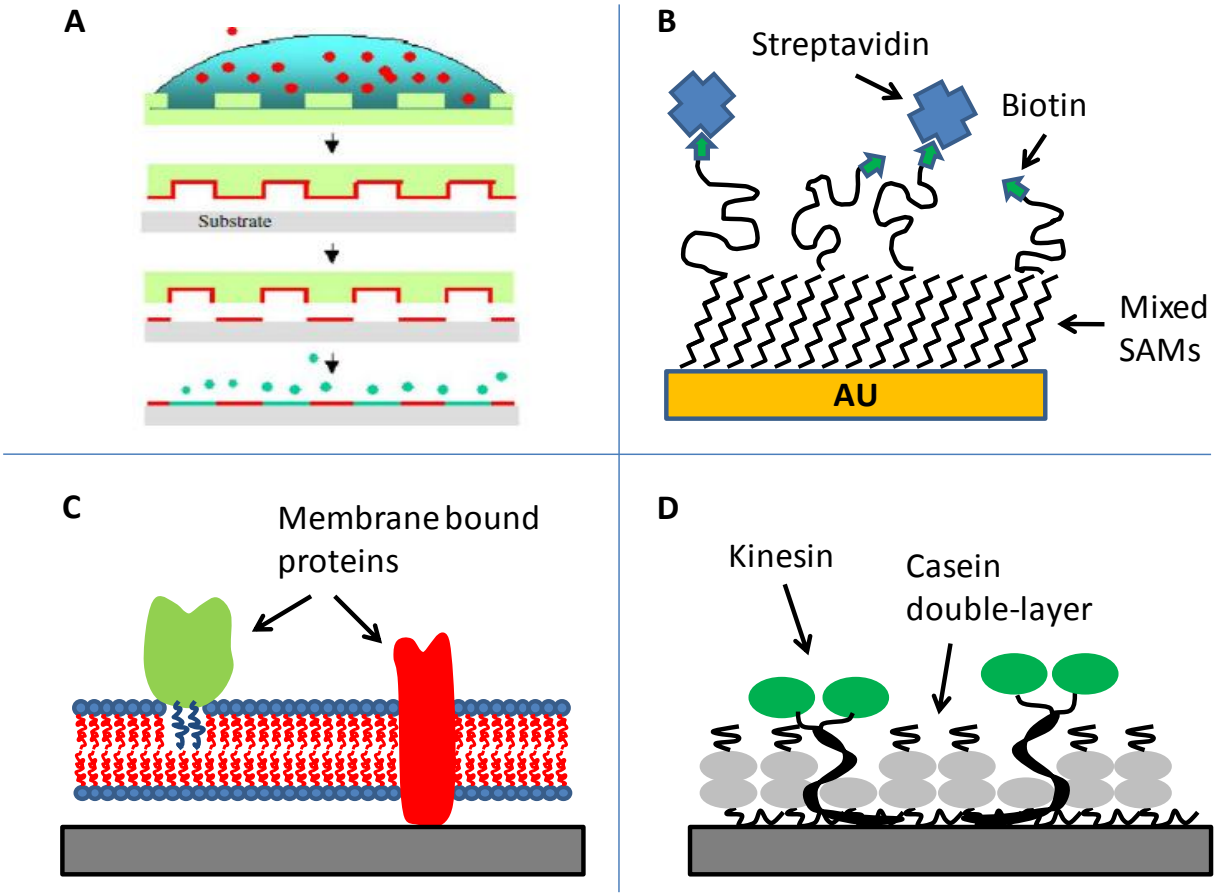

Figure 1-6. Surface Modifications for Controlled Protein Adsorption. A) Microconatct printing to spatially control protein adsorption. Adapted from *[125]* B) Self-Assembled monolayers of alkanethiols attached to PEO chains functionalized with biotin that specifically binds avidin from the solution. Partially adapted from *[138]* and *[139]* C) Immobilization of membrane proteins and conformational conservation by lipid bilayers. Adapted from *[131]* D) Adsorption of kinesin in controlled conformation to preserve functionality by adsorption of casein onto the surface. Partially adapted from *[133]*.

CHAPTER 2
QUANTIFYING PROTEIN ADSORPTION

Introduction

The importance of protein surface interactions for various medical and biotechnology applications as well as the various techniques that can be employed to control these interactions has been discussed in the previous chapter. A major portion of this control lies in the prevention of protein adsorption on surfaces i.e. in making the surfaces non-fouling. The most common technique is to coat the surface with hydrophilic polymer chains such as PEO. Various techniques to graft these hydrophilic chains are being developed as well as more complex polymeric structures are being developed to prevent protein adsorption and render surfaces non-fouling. With advances in non-fouling surface technology it becomes important to be able to characterize these surfaces both quantitatively and qualitatively for protein adsorption. A large number of different techniques to qualitatively and quantitatively measure protein adsorption have been developed over the years. Examples of these are Radiolabeling, Surface Plasmon Resonance (SPR) Spectrometry, Ellipsometry, Quartz Crystal Microbalance, Infrared Spectroscopy (IRS), X-ray Photoelectron Spectroscopy (XPS), Time of Flight-Secondary Ion Mass Spectroscopy (TOF-SIMS), Enzyme Linked Immuno Sorbent Assay (ELISA) and Single Molecule Detection techniques such as Confocal Microscopy, Atomic Force Microscopy and Scanning Tunneling Microscopy. Of these examples, XPS, TOF-SIMS, IRS and ELISA are mainly used to qualitatively characterize the adsorbed protein layer and are at best only semi-quantitative. The common techniques that are used to quantitatively determine the amount of protein adsorbed such as Ellipsometry and SPR are discussed in detail next.

Ellipsometry

Ellipsometry is one of the most commonly used techniques to quantify protein surface interactions. It is primarily provides information about the thickness of the adsorbed protein layer on surfaces. This thickness can be translated to the protein density on the surface.*[140]* The basic principle of ellipsometry is that when polarized light is reflected from a surface, there is a change in the polarization of reflected light from the incident light.*[141]* The difference in the polarization is a function of the refractive index of the materials at the interface and their extinction coefficients. In case of thin films on a surface, the difference in the polarization of reflected light is a combination of changes due to reflection from the thin film and the reflection of transmitted light from the surface below. In this case, the change in polarization is a function of the refractive index of the materials at both interfaces, the extinction coefficients of the materials and the film thickness. The difference in polarization is measured by – 1) Change in the phase difference between the parallel and perpendicular components of the wave upon reflection. This phase difference is given as shown in Equation 2-1.

$$\Delta = \delta_1 - \delta_2 \tag{2-1}$$

In the Equation 1-1, δ_1 is the phase difference between the parallel and the perpendicular components of the incident wave, and δ_2 is the phase difference between the parallel and perpendicular components of the reflected wave. 2) Change in the amplitude of both parallel and perpendicular components of the wave upon reflection. If the ratios of the amplitudes of the parallel and perpendicular components of the reflected wave to the amplitudes of parallel and perpendicular components of incident wave are represented by R^p and R^s, then the change in the amplitudes is given by the quantity ψ and expressed as in Equation 2-2.

$$\tan\psi = \frac{|R^p|}{|R^s|} \tag{2-2}$$

Based on the above principle, the fundamental equation*[141]* of ellipsometry is given as in Equation 2-3.

$$e^{j\Delta}\tan\psi = \frac{R^p}{R^s} \tag{2-3}$$

Here, Δ and ψ are the quantities measured by the ellipsometer. The information regarding the sample being analyzed is contained in R^p and R^s. By applying appropriate models for reflection at the interface, one can then determine the refractive index η_f and thickness d_f of the adsorbed film. Since and adsorbed protein layer is not an isotropic film, the film thickness obtained by ellipsometry can then be further expressed in terms of protein density Γ by Equation 2-4. *[142]*

$$\Gamma = d_f \frac{(\eta_f - \eta_m)}{(d_n / d_c)} \tag{2-4}$$

In Equation 2-4, η_f is the refractive index of the material on which protein is adsorbed and d_n/d_c is the refractive index increment. There are other methods as well by which the film thickness can be used to express the protein concentration.*[140]*

The most commonly used setup for ellipsometry is as follows (shown in Figure 2-1) –

1. A monochromatic light source
2. A polarizer that converts unpolarized light to linearly polarized light
3. A quarter wave plate that converts linearly polarized light to elliptically polarized light
4. The reflective interface that is being analyzed
5. An analyzer that determines the state of polarization of the reflected light beam
6. A detector to measure the light intensity
7. A calculation setup that can interpret the measured parameters using existing models to provide information regarding the interface

The commonly used ellipsometry technique employing the above mentioned setup is known as null-ellipsometry. When the analyzer is oriented at an angle such that no light passes

through, a null is said to be found. This is only possible if the reflected light beam is plane polarized. Usually upon reflection a plane polarized light gets reflected as an elliptically polarized light. If a quarter wave plate is used between the polarizer and the reflecting interface, under certain conditions, the elliptically polarized light from the quarter wave plate is reflected as a plane polarized light. This condition can be obtained by adjusting the angle of the polarizer and the quarter wave plate. The polarizer is rotated while the quarter wave plate is held fixed at 45^{o} until the reflected light from the interface is plane polarized and the analyzer is rotated until a null is found. The angles between the polarizer and the analyzer are a measure of the change in the phase of polarized light after reflection while the change in the intensity of reflected light is measured by the detector.

Ellipsometry is used to measure the amount of protein adsorbed under both transient and equilibrium conditions.*[143]* One can measure the adsorption and desorption kinetics of proteins on various surfaces, the adsorption of antibodies to the and existing protein layer, and in certain cases the conformational changes of adsorbed proteins by measuring the changes in the refractive index of the adsorbed protein layer.*[144-147]* To some extent ellipsometry can also be used to measure the 'Vroman effect' which refers to a protein solution containing different types of proteins in contact with a surface where the proteins may exchange with each other during adsorption.*[148, 149]* This is done with the use of antibodies and ellipsometry, and as amount of antibodies bound to an antigen does not follow a linear function, this method is mainly a detection technique rather than a true quantification technique. The limit of detection for proteins adsorbed on a surface using ellipsometry is about 20 ng/cm^2.*[150]*

Surface Plasmon Resonance

Surface Plasmon Waves (SPW), also known as surface Plasmon-polaritons are electromagnetic waves that travel along a metal-dielectric interface which acts as a quasi electron

plasma. A Surface Plasmon Wave is characterized by the propagation constant and the electromagnetic field distribution along the interface. The propagation constant of a SPW, β, is expressed as given by Equation 2-5.*[151]*

$$\beta = \frac{\omega}{c}\sqrt{\frac{\varepsilon_m \varepsilon_d}{\varepsilon_m + \varepsilon_d}} \tag{2-5}$$

In equation 2-5, ω is the angular frequency of the SPW, c is the speed of light, ε_m is the dielectric function of the metal and ε_d is the dielectric function of the dielectric material. This expression for SPW is valid only when the real part of ε_m is negative and its absolute value is smaller than the value of ε_d. This is possible at optical wavelengths for several metals, most common of which are gold and silver. The SPW electromagnetic field is confined to the metal-dielectric interface and decays exponential into both materials. The fact that the propagation constant of a SPW is extremely sensitive to the refractive index of the dielectric material helps determine extremely small changes in of the dielectric material properties at the interface. This change in the propagation constant can hence be used to detect and quantify the binding events of molecules and other such objects at the metal-dielectric interface.

SPW are excited at a metal-dielectric interface by a light wave. The excitation of SPW occurs only when the component of the light's wave vector parallel to the interface matches that of the SPW. This can be achieved by passing the light wave through a prism, a grating or a waveguide before it reaches the interface. The interaction between the SPW and the excitation light result in a change in the characteristics of the light wave such as a change in the amplitude, spectral distribution, polarization or phase. These changes can be correlated to the propagation constant of the SPW. Thus, binding events that induce changes in the refractive index at the interface which in turn result in a change in the propagation constant can be detected and measured by observing the changes in the characteristics of the light wave. This is the basic

principle of Surface Plasmon Resonance based detection and quantification of protein adsorption at an interface.

In one setup (Figure 2-2) using a prism to adjust the incident light wave to excite SPW, *[152]* light is made to pass through a high refractive index prism and reflect at the prism-metal interface. This generates an evanescent wave that propagates through the metal layer with a certain propagation constant. This propagation constant of the evanescent wave can be made to match the propagation constant for the SPW by changing the angle of incidence of light so as to excite the SPW. The resulting change in the characteristics of light at changing angles and fixed wavelength is studied to determine the angle or the wavelength respectively at which the strongest coupling occurs, in this case resulting in minimum intensity of reflected light. A change in the angle at which the strongest coupling occurs is a measure of the change in the propagation constant of the SPW. The change in the propagation constant of SPW is directly proportional to the change in the refractive index and the depth of the area within which the change occurs. In case of protein adsorption at interface, knowledge of the refractive index and thickness of the adsorbed protein layer can be translated to density of protein adsorbed. Similar setups where other properties of light such as wavelength, intensity and polarization can be modulated can also be used and the specific value of that property at which the coupling is strongest can be obtained.

The information obtained from SPR regarding adsorbed protein layer is the same as by ellipsometry i.e. the refractive index and the thickness of the protein layer. Thus SPR can be used to measure all the things that can be measured using ellipsometry, except that SPR requires a metal-dielectric interface. The detection limit for quantifying the amount of adsorbed protein using SPR is 0.5 ng/cm^2.*[115, 117]* SPR is more sensitive as compared to ellipsometry and has been widely used to quantify protein adsorption on gold or silver surfaces coated with self-

assembled-monolayers (SAMs) of polymeric chains.*[152, 153]* SPR is also used to measure protein adsorption on metallic nano-particles as well as in high sensitivity biosensors to measure antibody binding to adsorbed proteins on metallic nano-particles and structures.*[154-156]*

Radiolabeling

Radiolabeling of proteins with common radio labels such as ^{3}H, ^{32}P, ^{35}S, ^{14}C, ^{125}I and ^{131}I to measure the amount of a certain proteins in solution or adsorbed on a surface is one of the oldest protein quantification methods.*[157-159]* A specific protein is labeled with a certain radioactive isotope using specific chemical reactions. In some cases, a specific hormone is labeled with radioactive isotope and bound to a specific protein. Chemical processes for Radiolabeling are described in related literature*[158]* and differ based on the isotope as well as the protein or the hormone being labeled. Each of these processes has a different yield i.e. only a fraction of the molecules get labeled with the isotope. To be able to quantify the proteins, it is necessary to determine this yield. This can be easily found out from the known concentration of the molecule of interest, the radioactivity of the solution and the specific activity of the labeled isotope. Usually, the labeled protein is mixed with an unlabeled protein solution in a known ratio. To detect amount of protein adsorbed, either the decrease in the radioactivity of the solution can be measured or the radioactivity from the surface can be measured. Radioactivity is measured in decays per second (dps), but the measuring instruments usually detect only a fraction of the decay events known as counts per second (cps). The counts per second are related to the decays per second by a factor know as the counting efficiency.

The intensity of radioactive emission can be measured by various methods. These methods could employ one of the following properties of radiation from radioactive isotopes – 1) Ability to excite fluorophores 2) Ability to ionize gas molecules 3) Ability to cause exposure of photosensitive emulsions. The commonly used setups for these are the scintillation counter, the

Geiger-Muller counter and autoradiography out of which the scintillation counter and the Geiger-Muller counter are mainly used for quantitative purposes while autoradiography is used for qualitative purposes.

The detection limit for measuring the amount of protein adsorbed using radioactivity of labeled protein molecules is 5 ng/cm^2.*[157]* Competitive protein adsorption and exchange of adsorbed proteins from solutions can be measured by using different labels for different proteins. However, the use of radioisotopes is discouraged and replacements are already available or being sought in most applications employing radiolabeling due to the potential hazards of handling radioactive isotopes. Furthermore residual isotope ions in solution in some cases results in erroneous measurement of absorbed protein. It should also be taken care that the labeling of a protein with an isotope does not affect the functionality or structure of the protein, which would otherwise result in erroneous measurements.

Quartz Crystal Microbalance

Quartz crystal microbalance (QCM) is a highly sensitive technique for measuring the adsorbed mass of protein layer on a surface.*[160, 161]* The basic principle behind QCM is as follows. A piezoelectric material such as a quartz crystal oscillates as an alternating current is applied to it. The frequency of oscillation is a function of the total oscillating mass including the mass of adhered water molecules. Hence due to the adsorption of proteins to the top of a surface couple to the crystal, the frequency of oscillation under the same alternating current decreases. This decrease in the oscillation frequency of the quartz crystal can be expressed in terms of the mass adsorbed by the Sauerbrey relation described by Equation 2-6.*[162]*

$$\Delta f = -\frac{2 f_0^2 \Delta m}{A\sqrt{\mu_q \rho_q}} \tag{2-6}$$

In Equation 2-6, f_0 is the fundamental oscillation frequency, μ_q is the shear modulus of the quartz, ρ_q is the density of the quartz, and A is the electrode area. This relation though is only valid if the adsorbed layer is rigid and the change in frequency is less than 5%.

In a simple setup for QCM, the quartz crystal is sandwiched between two thin metallic electrodes (Figure 2-3). The electrodes oscillate along with the crystal. The electrodes are in contact with the protein solution and the surface of the electrodes interacting with the protein solution can be modified. The drop in the in the oscillation frequency due to protein adsorption at the electrode surface is measured by a frequency counter. Applying the Sauerbrey equation for change in oscillation frequency, one can determine the mass of the adsorbed protein layer. The measurements can be done either in aqueous medium or in air after drying. In aquaeous medium, one needs to account for the trapped or adhered water molecules near the electrode surface.

QCM can be used to obtain protein adsorption and desorption kinetics. This measurement technique is highly sensitive to changes in the mass of adsorbed protein layer.*[161, 163]* Also, an advanced technique known as QCM-D can also be used to measure the properties of the adsorbed layer which can provide information regarding the conformation of adsorbed proteins.*[162]* The QCM-D technique in addition to measuring the frequency change, also measures the time for dissipation of oscillation once the current is switched off. This dissipation time is a measure of the viscoelasticity of the adsorbed layer. A layer of soft proteins would have a longer dissipation time as compared to a rigid protein layer and can help characterize the conformation of adsorbed proteins. The detection limit for adsorbed protein layer on surfaces using QCM is 3.5 ng/cm^2.*[164]*

Single Molecule Detection

Techniques that can detect single protein molecules adsorbed on a surface would theoretically be the most sensitive techniques to quantify protein adsorption. Using single

molecule detection, one should be able to count the total number of protein molecules on a surface to determine the density of adsorbed proteins. Detection of single molecules can be done either by optical detection techniques or mechanical transduction techniques coupled to a change in either optical or electrical signals. Some of these single molecule detection techniques are discussed below.

Detection of single molecules using optical detection techniques can be done by laser induced excitation of a single fluorophore attached to the molecule being detected. The key requirement for detecting fluorescence from single molecules is the elimination of background noise arising from Raleigh scattering, Raman scattering and impurity fluorescence. This can be achieved by the use of high-performance optical filters, ultrapure solvents and most importantly illumination of extremely small sample volumes.*[165]*

One optical detection technique where extremely small sample volumes are illuminated is Near-Field Scanning Optical Microscopy (NSOM).*[166]* In NSOM, a tapered single-mode fiber with an exposed aperture of approximately 50-100 nm at the tip is brought extremely close to the sample (5-10 nm). This distance between the sample and the tip is regulated by a feedback mechanism that measures the shear force at the tip. Vertical resolution of 1 nm can be achieved by this mechanism. The closeness of the aperture to the sample does not provide sufficient distance for diffraction of light and illuminates a very small sample volume. Detection of single molecules with a sub-diffraction spatial resolution (up to 10 times lower resolution limit compared to standard optical techniques) is possible using NSOM. *[165, 167]*

Another technique to optically detect single molecules on a surface by illuminating very small sample volumes is by the use of fluorophores excitation by evanescent wave.*[168, 169]* This can be done by using a Total Internal Reflection Fluorescence (TIRF) microscopy setup

(Figure 2-4 A).*[170]* When the excitation light reaches the glass-liquid interface at large incidence angles from the glass side of the interface, it gets totally reflected back into the glass. This internal reflection results in an evanescent wave generation at the interface that propagates into the liquid medium. The intensity of the evanescent wave decreases exponentially and only a small volume of liquid is illuminated close to the interface. This eliminates a large amount of background and detection of single fluorophores on proteins is possible. Apart from detecting fluorescence from single fluorophores, another limitation towards counting individual proteins is that they have to be further apart from each other than the spatial resolution of the microscope.

Confocal Microscopy*[171, 172]* is yet another far-field epifluorescence based microscopy technique to detect single molecules adsorbed on a surface. In confocal microscopy, a laser beam is made to focus inside a sample using a high NA, oil immersion objective. A pin-hole of about 50-100 μm diameter is placed at the image plane to cut-out any out of focus light from hitting the photon detector. This results in light from only a tiny sample volume approximately cylindrical in shape (500 nm diameter due to diffraction of light, 2 μm height due to spherical aberration) being detected.*[165]* The small probe volume cuts down a large amount of the background and detecting single fluorophores attached to proteins is possible. Due to a very small region of the surface being probed with each acquisition, the surface has to be scanned to detect and quantify the proteins adsorbed to the surface.

Non-optical single molecule detection techniques involve scanning probe microscopies such as Atomic Force Microscopy (AFM)*[173]* and Scanning Tunneling Microscopy (STM).*[174]* In these techniques a microfabricated probe tip is used to scan to the surface either in close proximity to the surface or touching the surface. The presence of a protein molecule manifests itself in case of AFM as the deflection of the probe tip measured by a change in the tip

height. In case of STM, the presence of a molecule on the surface is detected by a change in the tunnel current i.e. the current across the conducting tip and the metal or semiconductor on whose surface the protein is adsorbed. AFM can detect features on the surface with a spatial resolution of 0.1 nm in all three directions. STM also has a spatial resolution of 0.1 nm along the surface, and 0.01 nm resolution in the vertical direction. Thus using these techniques, details about the shape and configuration of the adsorbed proteins can be extracted.*[175, 176]* Details regarding these techniques can be found in related reviews.*[177-180]* The basic setup of an AFM is shown schematically in Figure 2-4 B.

While single molecule detection techniques are capable of providing sufficient information regarding the presence, adsorption state, conformation etc. for surface adsorbed proteins, they have never been used to quantify the actual amount of proteins adsorbed. This is primarily because the presence or absence of an individual protein at a specific spot on the surface can be detected, but scanning a large area ($> 10^5$ μm^2) on the surface for every single protein molecule adsorbed is practically impossible.

Summary

The most commonly used methods for quantification of proteins adsorbed to a surface have been explained in brief. Optical techniques such as ellipsometry and SPR provide information regarding the adsorbed protein layer in terms of refractive index and thickness. These can then be used to obtain information regarding the mass of the protein layer and the density of adsorbed proteins on the surface. QCM provides information regarding the mass of the adsorbed protein layer directly which can be converted to surface density of the proteins. Using recently developments in QCM known as QCM-D, information regarding the rigidity of the adsorbed protein layers can also be obtained. Radiolabeling of proteins and measurement of radioactivity from the surface provides the actual number of radiolabeled proteins on the surface,

which might be a fraction of the total number of proteins based. The actual number of proteins can be obtained by dividing the number of radioactive proteins by this fraction as long as radiolabeling the proteins does affect its functionality or adsorption characteristics. Ellipsometry and radiolabeling can be used for measuring protein adsorption on almost all surfaces while SPR and QCM require metallic surfaces at the solid liquid interface. The detection limits for these techniques are listed in Table 2-1, and correspond to approximately 0.1 % of a protein monolayer.

While the above mentioned techniques provide protein adsorption information regarding the entire surface area scanned directly, the spatial distribution of individual proteins in this area cannot be obtained. In theory, single molecule detection techniques can provide this information as well as information regarding the conformation of proteins adsorbed to the surface. But, single molecule detection requires extremely sophisticated instrumentation and is expensive. Furthermore, scanning for individual proteins over an area larger than 10^5 μm^2 using a probe area of less than 0.25 μm^2 would prove to be a very difficult task. Single molecule detection techniques have not been used to quantify protein adsorption and their application is mainly in detecting the presence and state of proteins within a small sample area only.

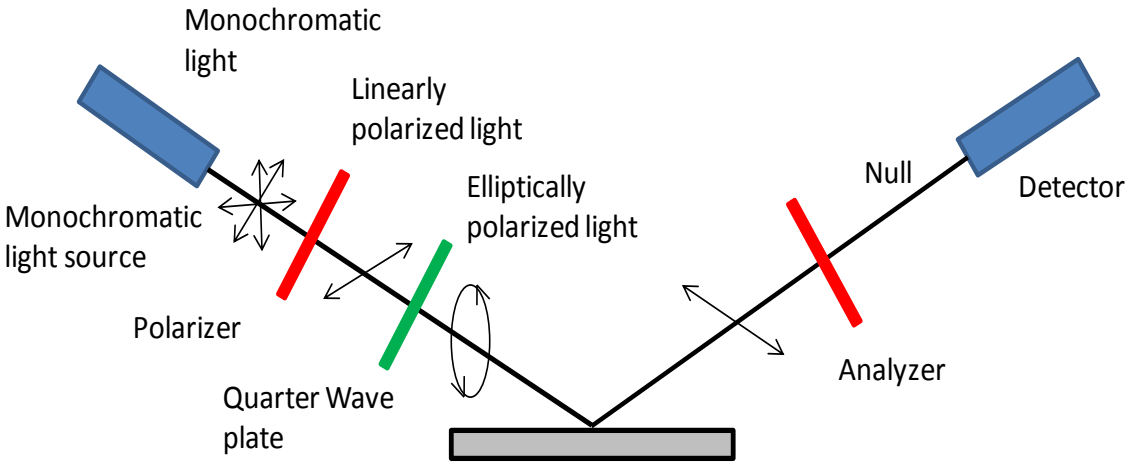

Figure 2-1. Basic Ellipsometry Setup. The setup shown is a basic setup for null ellipsometry. The quarter wave plate is held fixed at 45 deg., and the polarizer and the analyzer are rotated until a null is obtained i.e. no reflected light passes through the analyzer. Adapted from reference *[141]*.

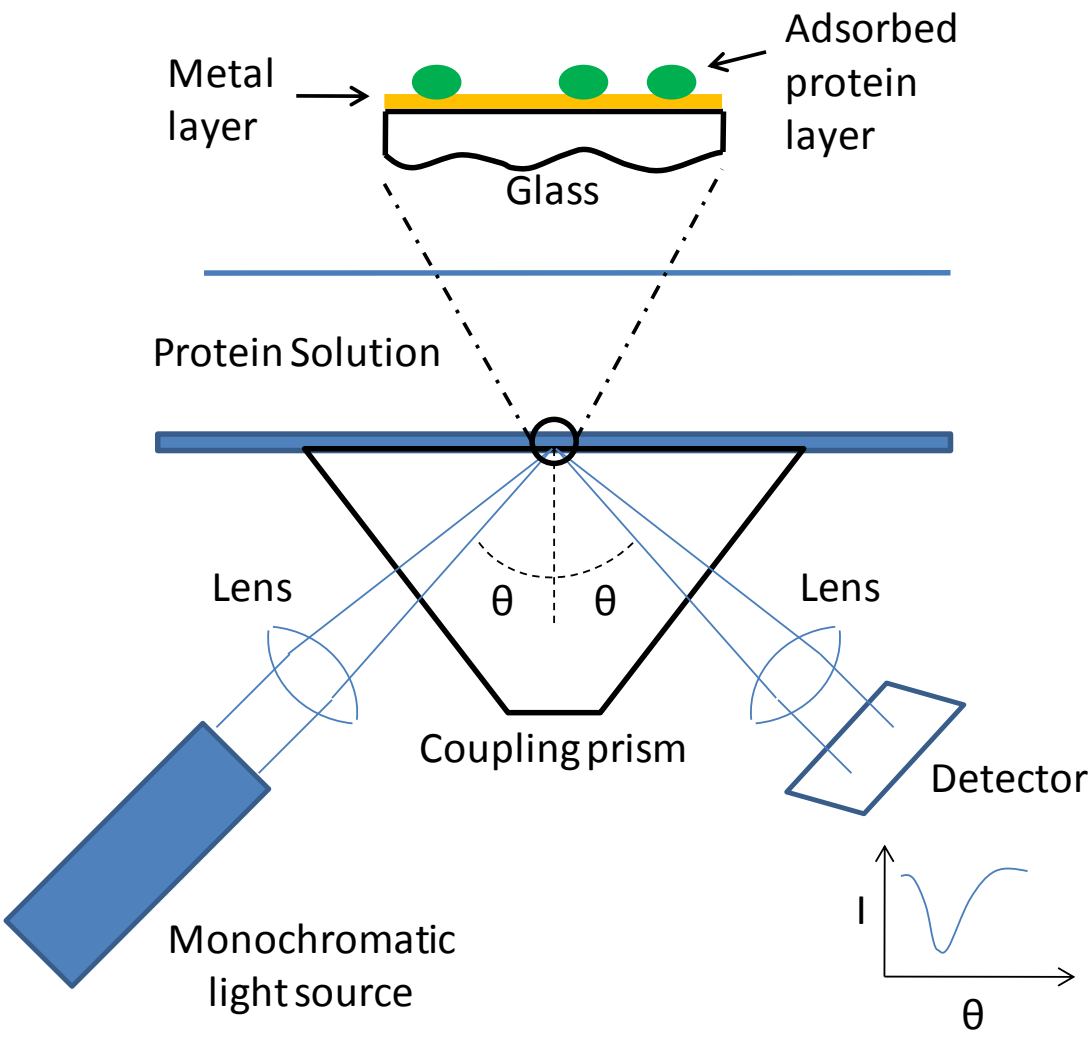

Figure 2-2. Surface Plasmon Resonance Setup. The figure shows a simple sketch of SPR measurement by using a prism to modulate the incident light wave. Surface Plasmon Waves (SPWs) are generated only when the parallel component of light matches that of the SPW. Interaction of the SPW with the incident light results in change in the properties of reflected light which can be detected. The amount of change is a function of the refractive index of the adsorbed protein layer at the interface. Adapted from reference *[152]*.

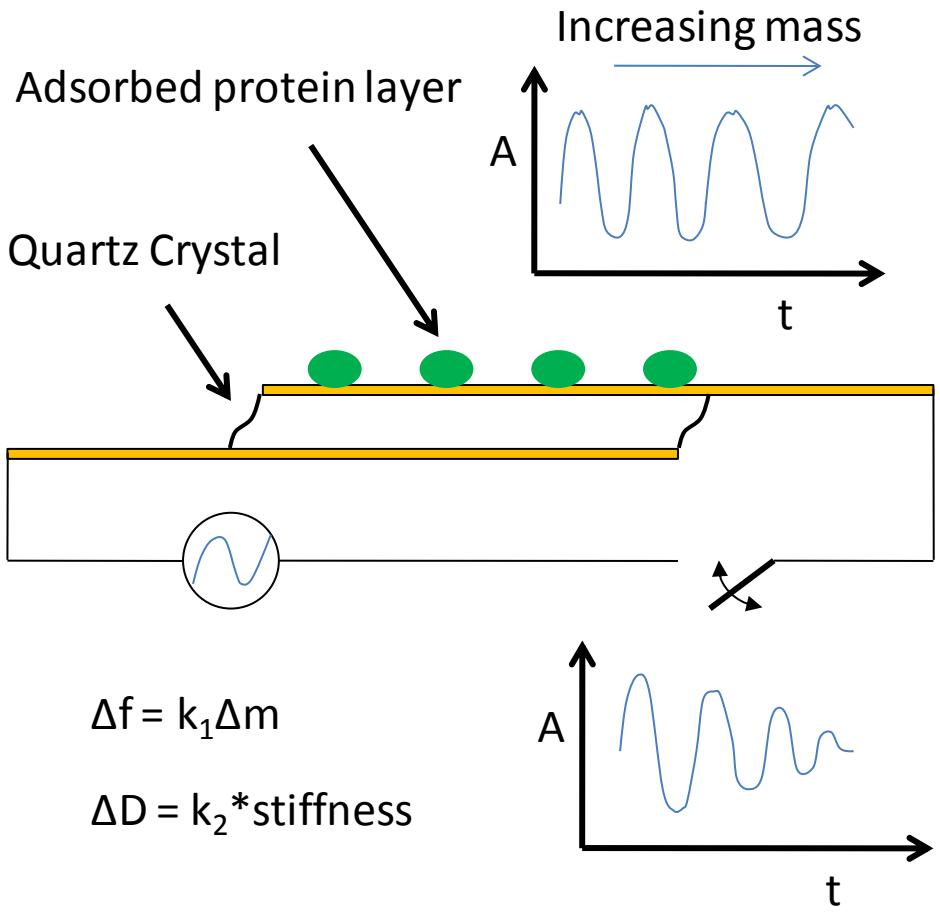

Figure 2-3. Quartz Crystal Microbalance. The figure shows a simple schematic of the QCM setup and its basic working principle. The oscillation frequency of the crystal under the influence of an AC current is a function of the adsorbed mass on top of the crystal. The change in frequency of oscillation is inversely proportional to the change in the adsorbed mass. The dissipation of oscillation frequency after the current is switched off provides information regarding the rigidity of the adsorbed film. Adapted from reference *[181]*.

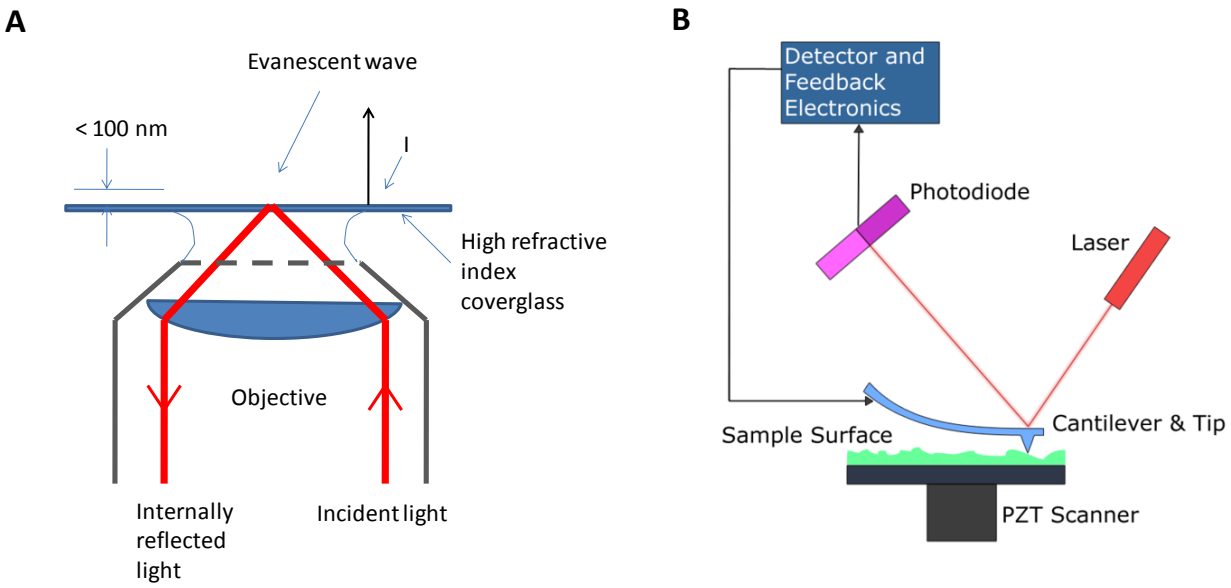

Figure 2-4. Single Molecule Detection. A) Total Internal Reflection Fluorescence (TIRF) microscopy – Total internal reflection of light at the glass liquid interface produces evanescent waves that travel into the liquid medium exciting fluorophores close to the interface. The evanescent wave intensity drops exponentially and a very small volume of sample close to the interface is illuminated. This results in extremely low background for detection of single molecules. B) Atomic Force Microscopy (AFM) – A microfabricated tip attached to a flexible cantilever is used to probe the surface. The deflection in the cantilever due to change in height of the tip is detected by change in the angle of reflection of a laser beam incident on the cantilever. AFM has a resolution of 0.1 nm in all three directions and can easily detect the presence of single molecules on a smooth surface. Adapted from *[182]*

Table 2-1. Detection Limits of Standard Quantification Techniques

Measurement Technique	Detection Limit
Ellipsometry	20 ng/cm^2 *[150]*
SPR	0.2 ng/cm^2 *[117]*
Radiolabeling	5 ng/cm^2 *[157]*
QCM	3.5 ng/cm^2 *[164]*

CHAPTER 3
A NOVEL TECHNIQUE TO QUANTIFY ULTRA-LOW PROTEIN COVERAGE

Introduction

Surfaces resistant to protein adsorption are very desirable for a variety of applications in biomedical engineering and bionanotechnology, since protein adsorption is often the first step in a cascade of events leading to systems failure. Initial efforts to create adsorption-resistant surfaces succeeded in reducing the adsorption by 80% compared to untreated surfaces to 100 ng/cm^2 by employing poly(ethylene glycol) coatings.*[183]* Recently, optimization of brush density and morphology has reduced adsorption to 1 ng/cm^2 or less.*[115]* These coverages are equal to about one tenth of a percent of a monolayer. However, biological effects can be observed for protein coverages below this limit. For example, adsorption of blood proteins can initiate the intrinsic coagulation cascade at low coverages.*[184]* Non-fouling surfaces are also a critical part of hybrid nanodevices, which utilize precisely positioned biomolecules in an artificial environment.*[23]* Controlled adsorption of motor proteins*[97, 99, 185-194]* has been utilized for the design of molecular shuttles and nanopropellers. Adsorption of motor proteins outside the intended regions at densities down to one motor per square micrometer (0.04 ng/cm^2) can lead to loss of device function, since individual motors can already bind and transport the associated filaments outside their intended tracks. Development in the quality of polymer coatings on surfaces to further improve their protein resistance needs to be supplemented with quantification techniques that can acurately characterize these surfaces. The limits of detection of current standard techniques such as SPR and Radiolabeling are close to 1 ng/cm^2 (close to the residual protein adsorption on stanadard PEO-coated surfaces). Novel surfaces that perform better than the current standards cannot be characterized accurately by these techniques. Therefore more sensitive techniques for the measurement of protein adsorption are needed.

Moreover, if protein adsorption is exceedingly slow, higher sensitivity would permit an accelerated quantification of the performance of the surface (e.g. within hours instead of days).

Working Principle of the Proposed Technique

The binding of intra-cellular filaments, such as microtubules or actin filaments, is readily observed by fluorescence microscopy in-vitro, since these filaments are composed of thousands of protein subunits and carry typically at least a thousand covalently linked fluorophores.*[195, 196]* Howard et al. demonstrated in 1989 that observing the attachment of microtubules from solution to surface-adhered kinesin motor proteins enables the determination of motor protein densities as low as 2 proteins per μm^2 by measuring the rate of microtubule attachment.*[25, 197]* Attachment rate measurements have subsequently been adapted to the determination of relative kinesin motor activity on different surfaces*[186]* and to the evaluation of guiding structures for microtubule transport.*[75, 187]* Since kinesin's long tail domain evolved to efficiently connect to cargo within cells, one can hypothesize that it serves as a particularly efficient probe for attachment points on the surface in-vitro.*[11, 198]* Measuring the attachment rate of microtubules to the surface adhered kinesins, termed as "landing rate", enables the estimation of the absolute coverage of functional kinesins in the range of 0.004 – 1 ng/cm^2, thus enabling to differentiate the performance of even the best non-fouling surfaces. While landing rate measurements in effect count individual proteins, their complexity is low compared to single molecule fluorescence measurements,*[165, 199]* due to the availability of a kinesin/microtubule kit (Cytoskeleton Inc.) and the high brightness of fluorescent microtubules which can be imaged with a standard fluorescence microscope.

In the following, it is demonstrated that the quantification of ultra-low kinesin coverages by landing rate measurements is a valuable tool in determining the performance of coatings with outstanding resistance to protein adsorption. Specifically, the adsorption model underlying the

method is described, experiments which demonstrate the determination of kinesin coverages on fouling and non-fouling surfaces are presented, and the advantages and limitations of the proposed method are discussed.

Landing Rate Model

. Microtubule attachment rate measurements are interpreted in the context of a two stage adsorption model: First, kinesin molecules adsorb from solution to the surface, filling a fraction of the available binding sites. Second, the kinesin solution is replaced by a microtubule solution and microtubules adsorb specifically to the kinesin motors bound to the surface (Figure 3-1). Both processes, kinesin adsorption and microtubule binding, are assumed to be irreversible on the timescale of the experiment (< 1 hr), since the solution exchange removes weakly bound motors, and the use of AMP-PNP (a nonhydrolyzable ATP analogue*[200]*) prevents detachment of microtubules from motors.

The surface concentration of adsorbed kinesin motors obtained for a given dosage of kinesin solution is then quantified by measuring the initial landing rate R of microtubules on the coated surfaces, and the maximal, diffusion-limited landing rate Z on a control surface densely coated with motor proteins. The initial landing rate is related to the diffusion limited landing rate as given by Equation 3-1. The probability of microtubule landing and binding to the surface, P, is the probability that there is atleast one kinesin motor in the area A of interaction between the microtubule and the surface adsorbed kinesin. Here, A=Lw is also known as the footprint of the microtubule, where the average length L of the microtubule is measured and the width is assumed to be w=25 nm*[201]* which is the diameter of the microtubule.*[30]*

$$R = Z * P \tag{3-1}$$

The probability distribution of kinesin molecules in an area on the surface can be approximated by a Poisson distribution. If the density of kinesin on surface is ρ, the average number of kinesin

molecules in an area A is ρA. Therefore, the probability that there is atleast one kinesin within the footprint of the microtubule is given by Equation 3-2.

$$P = [1 - \exp(-\rho A)] \tag{3-2}$$

From Equation 3-1 and Equation 3-2 one can express the initial landing rate of microtubules R as a function of the kinesin surface density ρ as in Equation 3-3.

$$R = Z * [1 - \exp(-\rho A)] \tag{3-3}$$

The initial landing rate R begins to substantially deviate from the diffusion-limited maximal landing rate if ρA<1, where A~0.1 μm^2 for typical microtubule lengths. Since the minimal measurable landing rate is on the order of 1 $mm^{-2}s^{-1}$, and the diffusion limited landing rate Z is on the order of 100 $mm^{-2}s^{-1}$, microtubule landing rate measurements are sensitive to motor densities between 0.1 μm^{-2} and 30 μm^{-2}.

Experimental Methods

Preparation of Surfaces

For glass surfaces, coverslips (FisherfinestTM, Premium Cover Glass, no 1, Fisher Scientific, Pittsburg, PA) were cleaned with ethanol and dried. For polyurethane (PU) surfaces, UV curable PU precursor NOA 73 (Norland Products Cranbury, NJ) was spincoated onto glass coverslips at 3500 rpm for 40 s and cured for at least 2 hrs using a 365 nm UV lamp (Spectroline EN-280L, Spectronics, Westbury, NY).

Physisorbed Pluronic surfaces were prepared according to *[107]*. Glass surfaces were cleaned twice by batch sonication for 15 min in 5% (v/v) Contrad 70 soap (Fisher Scientific, Pittsburgh, PA). Prior to the second batch sonication, all samples were sonicated in deionized distilled water for 15 min. After a final rinse with water and drying at 200ºC for 15 min, the coverslips were treated with 5% dimethyldichlorosilane in toluene (v/v, Cylon CT, Supelco Inc.,

Bellefonte, PA) and rinsed twice with toluene and thrice with methanol. These visibly hydrophobic surfaces (contact angle = 86° measured using a Rame-Hart goniometer, Model 100-00, Rame-Hart, Mountain Lakes, NJ) were treated overnight with 2 mg/ml Pluronic F108 (BASF, Mount Olive, NJ) solution in water. Unbound Pluronic was removed from the surface by rinsing twice with water and once with BRB80 buffer (80 mM PIPES, 1 mM MgCl, 1 mM EGTA, pH 6.9). After the Pluronic treatment, the contact angle changed to 71° which matches the reported contact angles for physiosorbed Pluronic.*[202]*

Self-assembled monolayers terminated in EG¬3OH were prepared by sputter-coating cleaned glass coverslips with a transparent gold layer (25 Å chromium and 150 Å gold) using a CMS-18 Multi Target Sputter Deposition machine (Kurt Lesker, Clairton, PA),*[203]* and immersing them overnight in 1mM solution of 1-Mercapto-11-undecyl tri(ethylene glycol) (Asemblon Inc., Redmond, WA) prepared in 99.9% methanol (Sigma-Aldrich, Saint Louis, MO) according to *[204]*.

PEGMA coatings: Unless otherwise specified, all chemicals were purchased from Aldrich. 2-bromoisobutyryl bromide (98%), triethylamine (TEA, 99.5%), Cu(I)Br (99.999%), Cu(II)Br2 (Fluka, 99%) were used as received. Hexanes were distilled over calcium hydride. 2,2'-dipyridyl (bpy, 99%) was sublimed. Poly(ethylene glycol) methyl ether methacrylate (PEGMA, average Mn ~475) was passed through a 20 cm column of imhibitor remover and stored at -20 °C.

Glass slides were initially modified via CVD polymerization of 4-amino [2.2]paracyclophane using a custom-built installation.*[205]* 50 mg of the paracyclophane were sublimed at 90 ºC and 0.12 torr, thermally activated, and transferred into a deposition chamber, where the polymer film was deposited at 15 ºC. Films made under these conditions had a thickness of 50 – 70 nm as determined by ellipsometry (EP3, Nanofilm AG). The resulting

amino-functionalized glass slides were immersed into an anhydrous hexane solution containing 200 µL 2-bromoisobutyryl bromide and 300 µL TEA were added subsequently. After incubated for three minutes at room temperature, the surface-modified glass slides were removed from the solution, washed sequentially with water and ethanol, and dried under a stream of nitrogen. Next, PEGMA (40 mL), deinoized water (20 mL), bpy (304 mg), and Cu(II)Br2 (40 mg) were charged into a Schlenk flask, stirred until homogeneous at room temperature, and degassed using three freeze-pump-thaw cycles. CuBr (86 mg) was then added under nitrogen purge with the contents in the flask being frozen. The flask was then evacuated and backfilled with nitrogen five times, and finally backfilled with nitrogen and warmed up to room temperature. The mixture in the flask was stirred until the formation of a homogeneous dark brown solution was observed. Finally, surface-modified glass slides were incubated with this solution in a nitrogen purged glove bag at room temperature for three hours. The substrates were then removed from PEGMA solution, washed sequentially with water and ethanol, and dried under a stream of nitrogen.

Assembly of Flowcells

The assays were performed in 75 µm high and about 1 cm wide flow cells assembled from two coverslips and double-stick tape. In all flow cells, the bottom surface and top cover surface had identical surface chemistry. Solutions were exchanged within a few seconds by pipetting the new solution to one side of the cell and removing the old solution using filter paper from the other side.

Adsorption Process

A kinesin construct consisting of the wild-type, full-length Drosophila melanogaster kinesin heavy chain and a C-terminal His-tag was expressed in Escherichia coli and purified using a Ni-NTA column*[206]*. The density of functional motors in the eluent was estimated by this technique as described later. Microtubules were prepared by polymerizing 20µg of

rhodamine labeled-tubulin (Cytoskeleton Inc., Denver CO) in 6.5 µL of growth solution containing 4 mM MgCl2, 1 mM GTP and 5% DMSO (v/v) in BRB80 buffer for 30 min at 37 °C*[207]*. The microtubules with lengths between 1 and 20 µm were 100-fold diluted and stabilized in 10µM Taxol (Sigma, Saint Louis MO).

In one set of experiments (glass, PU and Pluronic surfaces), 0.5 mg/mL casein (technical grade, Sigma, Saint Louis, MO) dissolved in BRB80 buffer was adsorbed for 5 min to reduce denaturation of kinesin.*[25]* Next, diluted kinesin solution (kinesin stock solution, BRB80 buffer, 0.5 mg/ml casein, 1 mM AMP-PNP from Sigma) was flowed in and after five minutes, exchanged against a 4µg/ml microtubule solution (sheared thrice by passing through 30G1 needles from Becton Dickinson, Franklin Lakes, NJ) in BRB80 buffer containing 1 mM AMP-PNP (Sigma-Aldrich, Saint Louis, MO), 0.2 mg/mL casein, 10µM Taxol, and an oxygen scavenging system to reduce photobleaching (20 mM D- glucose, 0.02 mg/mL glucose oxidase, 0.008 mg/mL catalase, 10mM DTT).*[208]*

In another set of experiments (all surfaces except PU and Pluronic), casein adsorption was omitted and kinesin dilutions were made directly in BRB80 containing 1mM AMP-PNP but no casein. The microtubule solution was unchanged. Time elapsed since microtubule injection was measured using a digital stopwatch with one second accuracy.

Microscopy

An Eclipse TE2000-U fluorescence microscope (Nikon, Melville, NY) with a 40X oil objective (N.A. 1.30), an X-cite 120 lamp (EXFO, Ontario, Canada), a rhodamine filter cube (#48002, Chroma Technologies, Rockingham, VT) and an iXon EMCCD camera (ANDOR, South Windsor, CT) and were used to image microtubules on the bottom surface of flow cells. Images were collected every 10 seconds with an exposure time of 0.5 s.

Determination of Landing Rates and Surface Density

Microtubule landing events were manually counted within a field of view using UTHSCSA ImageTool version 3.0 and plotted against time elapsed after microtubule solution injection. The N(t) plots were fitted (error-weighted least squares) with $N = N_{max}[1-\exp(-Rt/N_{max})]$ where N is the number of landed microtubules (in a field of view of 0.04 mm^2), t is the elapsed time and R is the initial landing rate specific to that motor density. However, for EG_3OH terminated SAM surfaces significant non-specific adsorption of microtubules was observed. This necessitated modification of the expression to $N = N_{init} + N_{max}[1-\exp(-Rt/N_{max})]$ in order to account for the non-specifically adsorbed MTs on the surface. The parameter N_{init} is independent of time, since it was observed that in the absence of kinesin the number of non-specifically adsorbed microtubules does not change within the observation time beginning 100 s after microtubule injection. In the second PEGMA experiment, a small amount of non-specific adsorption was observed, and the data points reflect a fit with N_{init}, R, N_{max} as parameters, while the error bars are extended to include the coverages derived from a fit with only R and N_{max} as parameters.

The average microtubule length L was measured by taking the arithmetic mean of at least 250 landed microtubules for every new microtubule preparation to calculate the area, A=Lw assuming a width w of 25 nm. The diffusion limited landing rate Z is assumed to be equal to the landing rate observed on casein-coated glass surface at a very high kinesin solution concentration (> 10 nM, 10-fold dilution from stock solution), since a dilution series shows a saturation of landing rates reached for 40-fold dilution of stock solution (~5nM kinesin concentration) (Figure 3-2 G, H). For gold-coated coverslips (used for EG_3OH-terminated SAM surfaces), it was observed that the maximum landing rate differed significantly from the rate measured on glass. Hence, the value of Z for EG_3OH-terminated SAM surfaces was taken to be equal to the landing

rate observed on casein-coated gold surfaces at a very high kinesin solution concentration (10-fold dilution from stock solution). Using A, Z (both measured on each day of experiments) and the landing rate R, the kinesin surface density can be calculated according to $\rho = -[\ln(1-R/Z)]/A$.

The dilution series data for casein-coated glass surfaces also enable an exact determination of the concentration of active kinesin motors in the stock solution under the experimentally validated assumption that all kinesin in the solution adsorbs uniformly to the casein-coated glass surface within 5 min.*[25]* The stock kinesin concentration is given by $C=2\rho_0/h/NA$ where h is the height of the flow cell and ρ_0 can be obtained by fitting the equation $R=Z[1-\exp(A\rho_0\xi)]$ to the landing rates on casein-coated glass surfaces as function of the dilution ξ (Figure 3-2 H).

Results

It is well-established that direct adsorption of kinesin to fouling (glass) and moderately non-fouling (Pluronic F108 coating) surfaces leads to denaturation and loss of its microtubule-binding ability.*[25, 209]* However, if the surface is covered by either denatured kinesin motors or a blocking protein (e.g. albumin or casein) interstitial binding of kinesin tails to the surface results in high motor functionality. These observations are reproduced in our measurements (Figure 3-2 H), which show that direct absorption of kinesin to glass results in a non-linear increase of the landing rate as the amount of available kinesin is increased. In contrast, pre-coating of the glass, PU and Pluronic surfaces with casein results in an initially linear dependence of microtubule landing rate (Figure 3-3 A) and surface density of active motors (Figure 3-3 B) on the amount of available kinesin.

On these surfaces, the diffusion-limited landing rate is reached for moderate (20-fold) dilutions of the kinesin stock solution (Figure 3-2 & 3-3), whose concentration can be calculated as 175 nM (see Methods). This value was used to determine dosage values in Figure 3-3. In all subsequent experiments, the diffusion-limited landing rate Z for a given microtubule preparation

is assumed to be equal to the observed landing rate on a casein-coated glass surfaces exposed to a 17.5 nM kinesin solution (10-fold dilution of stock) for 5 min.

Since physisorbed Pluronic F-108 reduces protein adsorption by ~80%,*[108]* one can interpret the observed four-fold lower density of microtubule-binding motors as a reflection of the reduced adsorption of casein. Kinesin contact to the bare surface will always lead to denaturation, whereas kinesin contact to adsorbed casein will result in a functional motor. Similarly, the density of active motors is 40% lower on PU surfaces compared to glass surfaces at equal kinesin dosages.

With the fundamental principle of the kinesin/microtubule based assay established, the focus was shifted to two types of highly non-fouling surfaces, $(EG)_3OH$-terminated SAMs and polyethylene glycol methacrylate (PEGMA) coated surfaces. To prepare protein-resistant PEGMA coatings, functional groups were first introduced onto the substrates using chemical vapor deposition (CVD) polymerization of 4-amino [2.2]paracyclophane. CVD polymerization is a vapor-based coating approach that can be used to modify a wide range of different substrate materials and geometries with a series of different chemical groups.*[210-212]* In this case, 50 nm thick films of poly(4-amino-p-xylylene-co-p-xylylene) were CVD deposited on glass substrates to provide free amino groups for further surface modification.*[116]* The amino-functionalized coating was then reacted with 2-bromoisobutyryl bromide. In the final step, bromoisopropyl groups were used as initiators for surface-initiated atom transfer radical polymerization (ATRP) of poly(ethylene glycol) methyl ether methacrylate (PEGMA).

Direct adsorption of kinesin to these highly non-fouling surfaces led to low landing rates which did not significantly increase with increasing kinesin concentration in solution (Figure 3-3). Precoating PEG-SAM surfaces with casein followed by exposure to 17.5 nM of kinesin for 5

min reduced the observed microtubule landing rate from ~ 31 $mm^{-2}s^{-1}$ to ~ 2 $mm^{-2}s^{-1}$, corresponding to a 15-fold reduction in kinesin surface density.

Our interpretation of these observations is that the highly non-fouling surface helps conserve kinesin motor function after adsorption, and that casein acts as a competitor for a very limited number of adsorption sites. Furthermore, since the surface density of adsorbed kinesin does not linearly increase with kinesin dosage, the residual kinesin adsorption is not a consequence of kinesins slowly penetrating the coating.*[49]* Instead, the surface density of adsorbed kinesins is equal to the density of defects in the coating.

EG_3OH-terminated SAM surfaces, a widely studied model system,*[109, 112, 137]* adsorbed an average of 4.2 ± 0.7 μm^{-2} (0.17 ± 0.03 ng/cm^2). This average is derived from three sets of identical surfaces prepared on different days (SAM1, SAM2 and SAM3). In comparison, the values measured using SPR for the adsorption of fibrinogen at hundred- to thousand-fold higher dosages are 0.35 ± 1.75 ng/cm^2 (1 mg/ml adsorbed for 3 min)*[153]* and 2.8 ± 1.05 ng/cm^2 (1mg/ml adsorbed for 30 min).*[204]*

PEGMA surfaces had no non-specific adsorption of microtubules and had exceptionally low landing rates as can be seen in Figure 3-2 D - F. The average motor density on these surfaces is 0.16 ± 0.02 μm^{-2} (0.0064 ± 0.0008 ng/cm^2; average of PEGMA1 and PEGMA2). These data suggest that PEGMA surfaces represent a significant improvement over $(EG)_n$OH-terminated SAM surfaces.

Conclusion

Kinesin protein adsorption followed by microtubule landing rate measurements enables the determination of active protein coverages between 0.1 and 30 μm^{-2} (0.004 – 1 ng/cm^2). This detection range extends the lower end of the detection range of established methods. In essence, microtubule landing rate measurements afford single molecule sensitivity by exploiting the

thousand-fold amplification of a fluorescence signal provided by labeled microtubules. The detection limit can be further reduced by increasing the observable number of microtubule landing events (increasing the field of view, observation time, or microtubule solution concentration). It is possible, that the ability of kinesin to bind microtubules is reduced after adsorption to the highly non-fouling surfaces. However, this reduced activity affects primarily the absolute protein coverage calculated from the data, and not the relative performance of two highly non-fouling surfaces.

While the method does not determine the performance of non-fouling surfaces in blood serum or solutions of blood proteins, the reduced detection limit enables the quantification of adsorption events which would be invisible to established techniques. As a result, the performance of highly non-fouling surfaces can be determined and optimized. For example, the adsorption of kinesin to PEGMA surfaces is twenty-fold reduced compared to EG_3OH-terminated SAM surfaces. It is hoped that the low technical requirements (fluorescence microscope with camera) and the commercial availability of a kinesin motility kit (Cytoskeleton Inc.) make this method widely accessible.

In the context of hybrid devices integrating motor proteins, the measurements demonstrate that the newly developed coatings can achieve the extreme degree of adsorption resistance desirable for the reliable placement of kinesin motors. Similar to such hybrid devices, biosensors utilizing nanowires or other nanostructures as transducing elements require highly adsorption resistant surfaces to maintain their performance advantages on the system level. These are only two examples of the diverse applications of high performance protein-resistant coatings in bionanotechnology.

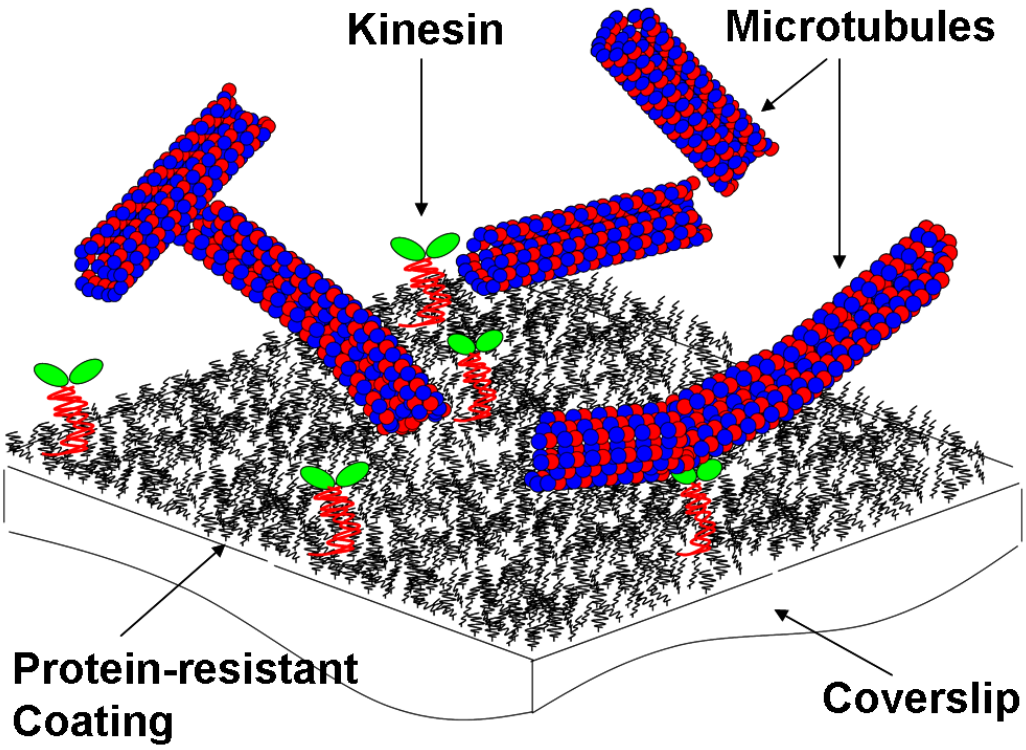

Figure 3-1. Sketch of principle for measuring kinesin density using microtubule landing rate**.** Adsorption of kinesin motor proteins to a non-fouling surface can be quantified by measuring initial microtubule landing rates. In the first step, solution-based kinesin scans the surface for 'defect sites' and adsorbs to a fraction of or all available sites. In the second step, the unbound motors in the solution are replaced by a microtubule solution containing AMP-PNP and the landing rate of microtubules on the surface is measured. This along with measurement of the average length of landed microtubules and measurement of the diffusion limited maximum landing rate on a fouling surface provides an estimate of the kinesin surface density of kinesin.

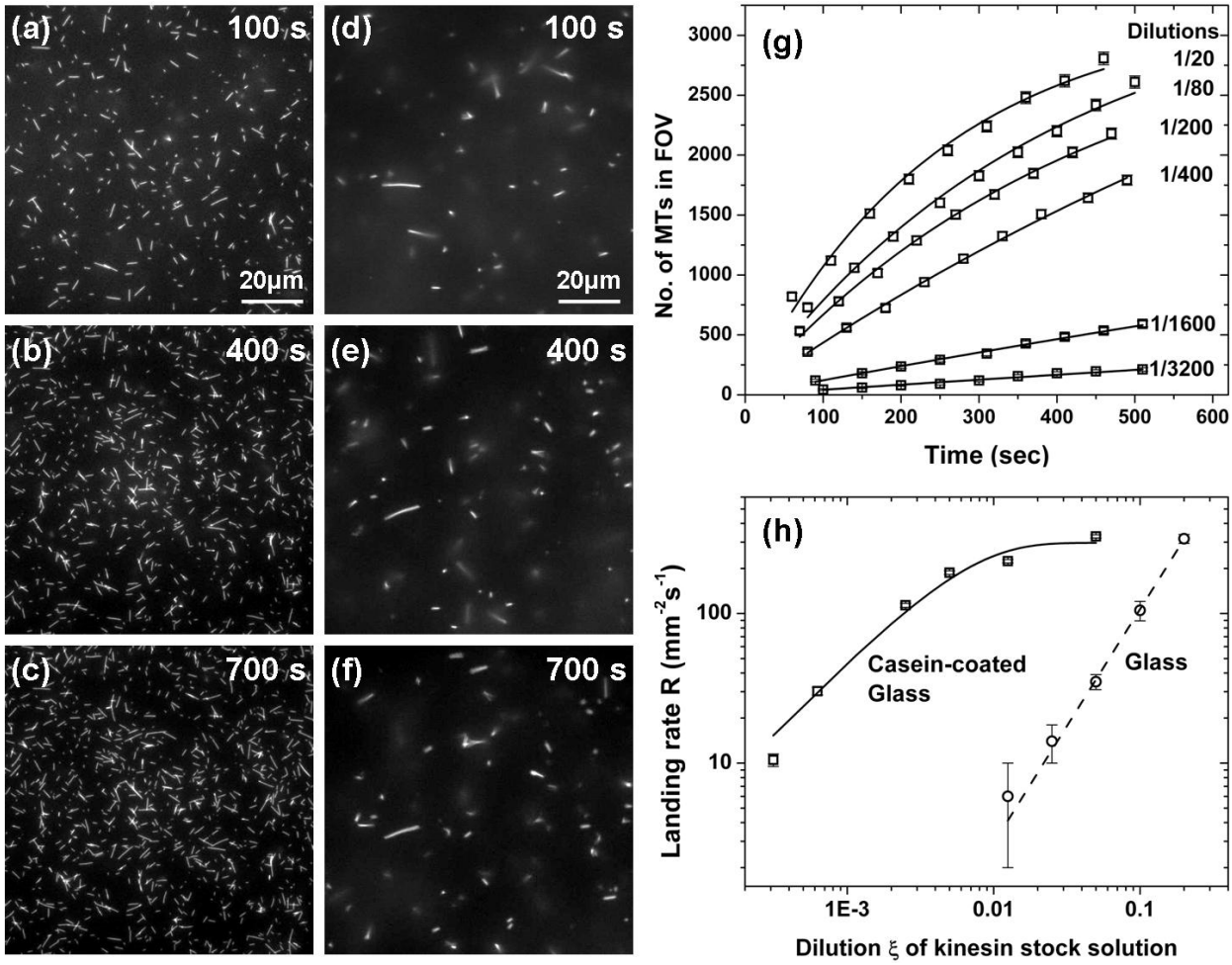

Figure 3-2. Measurement of kinesin surface densities from landing rates of microtubules. (A-C) Microtubules binding 100, 400, and 700 s after microtubule injection to a casein-coated glass surface exposed to kinesin solution twenty-fold diluted from stock (~ 9nM) for 5 min (D-F) Microtubules binding 100, 400, and 700 s after microtubule injection to a PEGMA surface exposed to kinesin solution twenty-fold diluted from stock (~ 9nM) for 5 min. The average length of microtubules for (A-C) is 1.71 ± 0.08μm and for (d-f) is 2.29 ± 0.11μm. The field of view (FOV) was 200 μm x 200 μm but (A-F) are cropped for clarity. (G) The number of microtubules attached to the surface as function of time for the casein-coated glass exposed to kinesin solutions diluted from the stock solution.(H) Landing rates R computed from the data shown in (G) and plotted against the concentration of the kinesin solution for casein-coated glass surfaces (open squares) and bare glass surfaces (open circles).

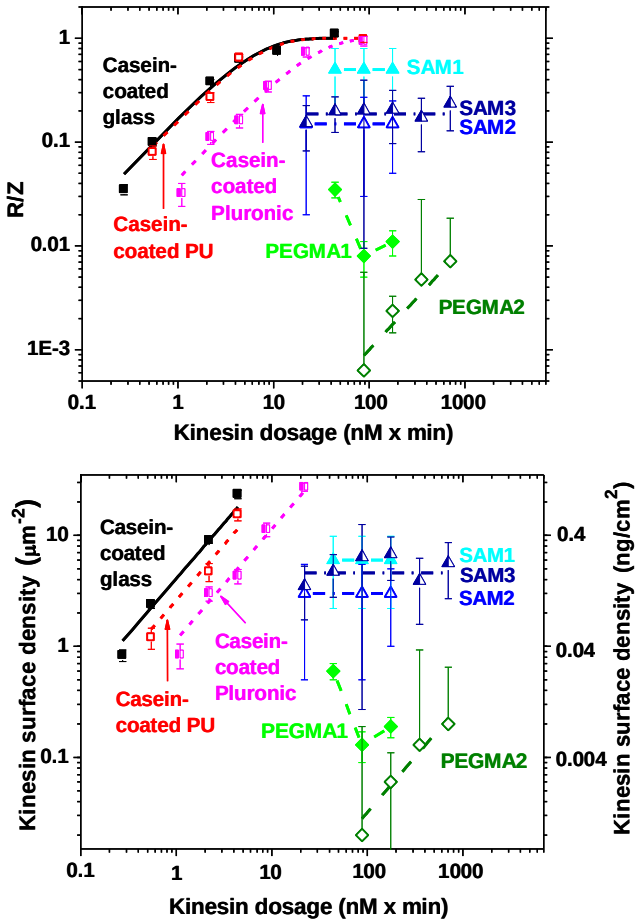

Figure 3-3. Measured Landing Rates and Kinesin Densities for Various Surfaces. A) The ratio of measured landing rate R to the diffusion-limited landing rate Z as a function of the kinesin dosage for different surfaces. B) The kinesin surface density as a function of kinesin dosage calculated from the ratio R/Z and the average microtubule length.

CHAPTER 4
PROTEIN-SURFACE INTERACTIONS – THEORETICAL APPROACH

Introduction

Adsorption of proteins to a surface is a complex phenomenon due to the variety of interaction forces that exist between a protein and a surface. The proteins can bind to surfaces by any one or more of the following mechanisms – 1) Electrostatic interactions between charged groups on the proteins and the surfaces, 2) Hydrophobic effect resulting in strong interaction forces between hydrophobic groups on the outside of the protein and hydrophobic regions on the surface, 3) Hydrogen bonding due to dipole-dipole interactions between various groups at the protein-surface interface and 4) π electron bonding between aromatic side groups in proteins and similar groups on certain polymeric surfaces.*[28, 213]* Also, once a protein adsorbs to a surface, it can undergo conformational changes that can further modify the surface properties and change the adsorption kinetics.*[45, 213]* Coating of surfaces with polymeric chains presents an additional aspect to protein adsorption. Along with protein surface interactions, polymer-protein, polymer-surface and polymer-solvent interactions also play an important part in determining protein adsorption. To understand the effect of the various parameters that influence protein adsorption, experimental data need to be complimented with physical and chemical models. Models that explain the experimental data provide valuable insight towards the mechanism of protein adsorption as well as help predict the outcome of untested scenarios.

Modeling Protein Adsorption to Surfaces

Single component adsorption of proteins to surfaces can be modeled in two simple ways. The first one is by treating the protein adsorption process as a reversible reaction followed by an irreversible conformational change.*[28, 33, 214]* Each of these processes has an associated reaction rate. The reaction rates for these processes can be obtained experimentally and using

these reaction rates one can determine the free energy change associated with each of the reaction steps. A large amount of information can be obtained by treating protein adsorption in the aforementioned method. The knowledge of free energy change in each step can give an estimate of the type of bond formation, as well as the protein coverage resulting due to the formation of specific bonds between the proteins and the surface. Different adsorption kinetics for proteins can be predicted for different protein solution concentrations based on the strength and rate of protein surface interactions during the various stages of adsorption.

The other method to model single component adsorption of proteins to surfaces is by assuming a random sequential adsorption process.*[215-217]* In this model, proteins are assumed to have a specific shape in solution (usually a sphere or a cylinder). As the proteins approach the surface, they adsorb to the surface. The adsorption rate can be modeled in as a sticking probability of protein to the surface. As the protein gets adsorbed onto a spot on the surface, the area shadowed by the adsorbed protein is inaccessible for any other protein to bind to. This implies that no protein can adsorb to a spot on the surface already occupied by and existing protein. Over time, based on the rate of protein-surface interactions, the surface gets covered with proteins. The effect of conformational change can be incorporated into the model by allowing an increase in the area occupied by the protein after adsorption. This sequential adsorption of proteins to surface can give information regarding the protein surface coverage as a function of collision rate of proteins to the surface. It has been found that in the absence of any conformational change, a random sequential adsorption of spherical, rigid proteins yields a maximum surface coverage of 54%, known as the jamming limit.*[218]* In case of flexible proteins, it is likely that the proteins can undergo conformational changes to cover the entire surface.

The primary distinction between the above mentioned approaches is that the first approach mentioned treats the adsorption process from a chemical point of view based on reaction rates and free energy, while the second approach treats it from a physical point of view based on excluded volumes and interaction areas. The two approaches need not be exclusive and a combined approach though rigorous would paint the most accurate picture.

Modeling multicomponent protein adsorption to surfaces becomes much more complex as the number of possible interactions increases. Modifications to both the above modeling methods can be made to incorporate the additional adsorption pathways. An important aspect of multicomponent adsorption is the 'Vroman effect'.*[39, 149]* When a solution containing multiple protein species is introduced to a surface, the smaller and more concentrated proteins adsorb first only to be later replaced by larger proteins that bind more strongly to the surface than the smaller proteins. This is known as the 'Vroman effect'. Another aspect of competitive protein adsorption is that time dependent denaturation or conformational change in adsorbed proteins leads to stronger binding of proteins to surfaces and makes it more difficult to displace them with a competitive protein.*[219]* Also, proteins that are less stable conformation bind strongly to the surface as compares to the more rigid proteins with stable configurations.*[220]* Modeling of these competitive protein adsorption events by considering the free energy change for every reaction step can help understand the adsorption kinetics for multicomponent systems and yet provides little information regarding the various configurations, specific protein surface interactions and mechanisms for protein exchange and denaturation. With substantial increase in computational capabilities as well as the knowledge about structure of proteins, simulations to investigate atomic level interactions between proteins and surfaces are being employed to accurately describe the complex protein surface interactions.*[221]*

Modeling Non-fouling Nature of Polymer Coated Surfaces

The importance of developing surfaces that resist protein adsorption has been discussed in chapter 1. Also various techniques employed to reduce or eliminate protein adsorption to surfaces have been discussed. While making rigid surfaces hydrophilic reduces the adsorption of certain proteins, until now they have performed poor compared to surfaces grafted with hydrophilic polymer chains such as PEO to resist protein adsorption. Surface grafted with PEO chains of number of EO units $n > 2$ at high grafting densities reduce protein adsorption to less than 0.1 % of a monolayer and close to the detection limits of standard detection techniques.*[44, 137, 153]* The protein non-fouling nature of PEO grafted surfaces can be due one or more of the following reasons – 1) Steric repulsion of proteins from the surface by grafted PEO chains, 2) Presence of water molecules trapped by the hydrophilic polymers close to the surface and 3) Same or lower affinity of the polymer chains to hydrophilic regions on the protein as to water molecules. The exact mechanism by which PEO chains prevent protein adsorption is not known. Yet, the effectiveness of high grafting densities of PEO in rendering surfaces non-fouling has led to development of a large number of PEO-like polymeric chains as well as various polymer grafting techniques to make non-fouling surfaces. These have been discussed in brief in chapter 1 and details can be found in related literature. Despite advances in non-fouling surface technology, complete prevention of protein adsorption has not been achieved as in many cases observed by the adhesion and growth of cells to these surfaces. Understanding and modeling the mechanism of protein non-fouling by PEO chains is the key towards improving the quality of polymer coatings to resist protein adsorption. Modeling the effect of PEO characteristics such as chain length and terminating group on protein adsorption can also be used to achieve better control over adsorption of proteins, adsorption of specific proteins and adsorption of proteins in specific conformations.

Early models to describe the effectiveness of PEO coatings in resisting protein adsorption are based on the De Gennes theory of polymer interfaces.*[48, 222]* These models build upon the theory that PEO chains act as steric barriers that prevent the proteins from interacting with the surface. The most notable model based on this physical view of PEO chains is the one described by Jeon and Andrade. They model proteins as rigid objects that adsorb to surface by an attractive force which is dependent on the distance of the protein from the surface. The PEO chains grafted onto the surface present a steric barrier i.e. as the proteins approaching the surface deform the PEO chains, a repulsive force acts on the proteins that prevents the protein from interacting the surface. Here the distance between consecutive PEO chains is assumed to be less than the Flory radius of the PEO chain resulting them to be in a brush conformation. The height of PEO layer determines the effectiveness of the coating to resist protein adsorption and the strength of protein adsorption. This implies that in case of electrostatic forces of attraction between the protein and the surface, the height of the PEO layer should be more than the double layer thickness to prevent protein adsorption. This is one of the earliest models for protein non-fouling by grafted PEO chains and has many shortcomings. The model can only be applied to high molecular weight PEO chains at maximum grafting densities. It fails to explain the non-fouling nature of extremely short PEO chains. The inter chain distance for short PEO chains for experimentally achievable grafting densities is more than the Flory radius and these chains are in a mushroom configuration. This model does not suggest anything regarding the role of water molecules trapped by the hydrophilic chains in prevention of protein adsorption. Though, steric repulsion by PEO chains has been modeled as a primary mechanism for protein non-fouling in only a few other early works following that by Jeon et al., most novel polymer grafting techniques have been developed based on this principle.

The current focus of modeling is towards employing molecular level interactions between polymers, polymers and proteins, the protein and the surface, polymers and the surface, and polymers and solvent molecules to understand the mechanism of protein resistance by PEO chains. The most fundamental work in this area is the work by Slzeifer and coworkers.*[49, 223]* The basic assumptions for the model by Szleifer and coworkers are – 1) The interaction force between the proteins and surface is attractive and dependent on the distance of the protein from the surface, 2) The interaction force between individual PEO chain molecules, solvent molecules (generally water molecules) and protein is same and attractive in nature, 3) The interaction of the PEO molecules with the surface is also height dependent and its nature depends on the nature of the surface, and 4) the repulsive forces that prevent protein adsorption arise to steric effects arising from packing constraints for polymer molecules, solvent molecules and proteins. The free energy of the system is obtained from the enthalpic contributions of the various interactions between the system components and the entropic contributions arising from distribution of the polymer chains, solvent molecules and the proteins. The distribution function for polymer chains can be obtained by the single chain mean field (SCMF) theory described by Szleifer and Carignano.*[224]* Based on known or assumed interaction energies of various interacting system components, the free energy of the system can be obtained for all possible configurations of the polymer chains and the distance of the protein from the surface. Minimization of the free energy of the system provides the probability distribution function of proteins in solution and the amount of proteins adsorbed at the surface. For sake of simplicity, the proteins are assumed to be rigid spheres. The model requires the knowledge of a large number of unknown parameters such as the various interaction energies between the system components. The model neglects the role of solvent molecules except in calculation of packing volumes used to determine the steric

repulsion. Following certain simplifying assumptions for the various parameters, the model has been shown to fit very well to observed protein adsorption data on PEO grafted surfaces. This model has been further expanded to predict the adsorption kinetics for proteins on polymer grafted surfaces as well as to explain the role of polymer surface interactions to result in kinetic and steric barriers for protein adsorption.*[50, 225]* The model requires numerical solutions of complex equations to determine specific adsorption characteristics and introduction of additional factors such as non-spherical proteins, solvent polymer and solvent protein interactions and non-crystalline nature of polymer grafting complicates the calculations even further. Numerical methods and simulation based models that build on the SCMF theory are being developed to focus on specific aspects of the mechanism of protein non-fouling by PEO chains. The role of solvent molecules is being investigated by employing molecular dynamic simulations.*[226, 227]*

While the model by Szleifer and coworkers suggests that proteins can adsorb to surface grafted with PEO chains by restricting the PEO chain configurations to make room for the protein, including strong affinity of water molecules to PEO chains would change this outcome of the model. The strong affinity between water molecules and PEO chains would result in a high enthalpic penalty for embedding proteins within volume excluded by the polymer chains and associated water molecules. This shifts the effect of PEO chains as being steric barriers even in the mushroom configuration as compared to a flexible polymer layer. Different modeling techniques such as molecular level simulations, chemical view based on free energy of interactions or hard sphere models, all have their benefits and provide information regarding different aspects of the system. No model or explanation is complete in itself and yet some models are more useful in understanding and predicting specific properties of the system as compared to others.

CHAPTER 5
A RANDOM SEQUENTIAL ADSORPTION MODEL FOR PROTEIN ADSORPTION ON SURFACES GRAFTED WITH PEO

Introduction

Surfaces which are designed to prevent the adsorption of proteins are of paramount importance in biomaterials science and engineering, and significant effort has been made to understand the factors contributing to the non-fouling properties of a wide variety of surface coatings. A particularly successful and common design strategy is the functionalization of the surface with poly(ethylene oxide) at a range of molecular weights and grafting densities. Theoretical attempts at understanding the effect of polyethylene oxide (PEO) grafted polymers on the adsorption of proteins to surfaces have a long history.*[33, 52, 228]* Starting with Jeon et al.'s work based on de Gennes' theory of polymer brushes,*[48, 222]* followed by the single chain mean field (SCMF) theory elaborated by Szleifer et al.*[49, 223]* to molecular dynamics simulations by Latour et al.*[221]* and Jiang et al.*[227]*, an increasingly detailed picture of the thermodynamics and kinetics of the adsorption process has been assembled. Theoretical results can be compared to experimental datasets, which measure adsorption for different proteins, polymer lengths, and grafting densities.*[109, 229]*

Hypothesis for the Model

Common to all previous theories and simulations is that the polymer chains are evenly distributed across the surface, with a constant spacing determined by the grafting density (Figure 5-1 A). However, the distribution of the polymer chains is close to random for three reasons (Figure 5-1 B): (1) the density of potential polymer attachment sites on the surface is significantly larger (e.g. 15 nm^{-2} for a gold surface*[230]*) than the grafting density of the polymer chains (ranging from 0.1 to 5 chains per square nanometer*[231]*), (2) the polymer chains interact with each other only at high grafting densities, and (3) the covalent attachment of the chains

precludes a reordering of the polymer distribution after the initial attachment. A random distribution of polymer chains leads to stochastically distributed protein binding sites defined by the absence of polymer chains. In contrast to previous theories focusing on the interactions between protein, polymer and solvent, it is hypothesized here that the existence of such "bald spots" is the primary cause of residual protein adsorption to PEO-grafted surfaces. Based on this, a Random Sequential Adsorption (RSA) model is presented which focuses on the random distribution of polymer chains on the surface leading to polymer-free "bald" spots. The calculated density of such spots with a defined minimum diameter matches the experimentally determined adsorption density of proteins for different grafting densities and chain lengths. While the calculation relies on drastic simplifications of this complex problem, the results suggest that the random arrangement of polymer chains is a critical factor in primary protein adsorption to polymer-functionalized surfaces.

The Random Sequential Adsorption Model

A random sequential adsorption (RSA) model is developed which aims to (1) predict protein adsorption based on a small number of readily accessible parameters inserted into a single equation, and (2) emphasize the stochastic placement of the grafted polymer chains on the surface (as opposed to a regular placement of grafting sites*[49]*) while neglecting every detail of the interaction of the polymer chains with solvent, surface, protein, and other chains. RSA models can be applied to a wide range of situations if the adsorption is irreversible on experimental timescales and an adsorbed particle blocks a further adsorption at that site.*[232]* Both conditions are met in the case of protein adsorption.*[218]*

Previous RSA models of protein adsorption to bare surfaces*[233]* can be extended by modeling the grafted polymers as randomly distributed, pre-existing obstacles on the surface (Figure 5-1 C). For simplicity, the space occupied by the polymer chain is modeled as spherical

with a radius equal to the radius of gyration of the polymer chain. The polymer chain excludes proteins (also assumed to be spherical*[50, 113, 222]* from this sphere, but allows partial overlap by other polymer chains up to the experimentally determined maximal grafting density (Figure 5-1 C). Under these assumptions, one can (A) calculate the open surface area required for the protein to reach the surface, (B) determine the probability that a protein encounters an open spot of sufficient size, (C) calculate the adsorption kinetics, and (D) model secondary adsorption to PEO-chains terminated with hydrophobic groups.

(A) The contact between protein and surface requires a circular opening in the polymer layer with a minimum area of $A_{poly} = 2\pi d_p R_g$, where d_p is the protein diameter and R_g is the radius of gyration of the grafted polymer (see Figure 5-1 for geometry). The radius of gyration is calculated according to $R_g^2 = nbl_k cos(\psi)/6$ for $n > 12$ and $R_g^2 = nb^2/6$ for smaller chains. Here, l_k = 1 nm is the Kuhn length of the polymer, n is the degree of polymerization, b = 0.278 nm is the monomer length and $\psi = 37.5^o$ is the angle between the chain axis and the bond between monomers.*[234]* Similarly, proteins already adsorbed within an area $A_{prot} = \pi d_p^2$ will obstruct contact between the adsorbing protein and the surface.

(B) The number of polymer chains within a surface area A is randomly distributed with a mean $\mu = \rho A$ where ρ is the surface density of polymer chains (number per area). At the maximum grafting density ρ_0 the maximum number of polymer chains within the surface area A is either $floor(\rho_0 A)$ or $ceil(\rho_0 A)$, where $floor(N)$ is the greatest integer value less than N and $ceil(N)$ is the smallest integer value greater than N. Thus, for each encounter of the protein with the surface, there are either $floor(\rho_0 A)$ or $ceil(\rho_0 A)$ separate locations for a polymer chain within the area, and each of these locations is occupied with a probability of $x = \rho/\rho_0$ (the grafting ratio). The number of polymers in each area A is therefore given by two binomial distributions with the

same probability of success *x* but two different number of trials. Since the average maximum number of polymers chains within area *A* is given by $\rho_0 A$, the binomial distribution with *floor*($\rho_0 A$) trials has to be invoked in the fraction *ceil*($\rho_0 A$) - $\rho_0 A$ of all collisions, and the binomial distribution with *ceil*($\rho_0 A$) trials has to be invoked in the fraction $\rho_0 A$ - *floor*($\rho_0 A$) of all protein-surface collisions.

The probability that there are zero polymers in the area A_{poly} is given by Equation 5-1.

$$P_{poly}(0) = (\text{ceil}(\rho_0 A_{poly}) - \rho_0 A_{poly}) * (1-x)^{\text{floor}(\rho_0 A_{poly})} + (\rho_0 A_{poly} - \text{floor}(\rho_0 A_{poly})) * (1-x)^{\text{ceil}(\rho_0 A_{poly})} \quad (5\text{-}1)$$

The Equation 5-1 can be approximated by Equation 5-2 as shown in Figure 5-6 A.

$$P_{poly}(0) = (1-x)^{\rho_0 A_{poly}} \quad (5\text{-}2)$$

Therefore, the probability that a protein scanning the surface encounters an opening of the required size in the polymer layer is approximated by Equation 5-2.

If σ is the density of adsorbed proteins on the surface, then the actual density of proteins within the area of the surface not covered by the polymers is *σ/(1-x)*. The distribution of already adsorbed proteins in the interaction area A_{prot} also is modeled as two binomial distributions with mean $\mu = A_{prot}\sigma/(1-x)$ and number of trials *floor*($A_{prot}\ \sigma_0$) and *ceil*($A_{prot}\ \sigma_0$), respectively with $\sigma_0 = 4f/\pi d_p^2$ as the maximum theoretical protein density. Utilizing the same approximation described above, the probability that there is no adsorbed protein obstructing the interaction of an incoming protein and the surface is then given by Equation 5-3. Here $f = 0.9$ is assumed for hexagonal closed packing of proteins on the surface.

$$P_{prot}(0) = \left(1 - \frac{\sigma}{\sigma_0 (1-x)}\right)^{\sigma_0 A_{prot}} = \left(1 - \frac{\sigma}{\sigma_0 (1-x)}\right)^{4f} \quad (5\text{-}3)$$

The approximated probability distributions are used for polymers as well as adsorbed proteins for all further calculations for the sake of mathematical simplicity. It is shown in Figure

5-6 B and C that this approximation has no discernible effect on the predicted protein adsorption values.

(C) The rate of collisions between proteins and surface per unit area Z is given by*[235, 236]* $Z = C_p\sqrt{k_bT/m_p}$, where C_p is the protein concentration and m_p is the mass of the protein. The probability that a collision with the bare surface results in adsorption is denoted by the sticking probability S and has values ranging from 10^{-5} to 10^{-8} for typical proteins and surfaces.*[235]*

The rate of protein adsorption on the surface grafted with polymers is then given by Equation 5-4.

$$\frac{d\sigma}{dt} = ZS * P_{poly}(0) * P_{prot}(0) \tag{5-4}$$

Solving this differential equation yields Equation 5-5.

$$\sigma = \frac{4f(1-x)}{\pi d_p^2}\{1-[1+\frac{\pi d_p^2(4f-1)SZt}{4f(1-x)}(1-x)^{2\rho_0\pi d_p R_g}]^{-1/(4f-1)}\} \tag{5-5}$$

(D) In cases where the terminal group on the hydrophilic polymer is a hydrophobic group such as OCH_3 instead of OH, high grafting coverage shows increased protein adsorption.*[231]* This can be the result of secondary protein adsorption to a close-packed layer of hydrophobic groups on top of the hydrophilic chains. Assuming that the smallest polymer island creating such secondary adsorption sites requires six close-packed polymer chains,*[113]* the probability of a protein encountering a secondary adsorption site is given by $P_{isl}(6)= x^6$. In this case, the probability $P_{prot}(0)$ of a protein-surface contact unobstructed by already adsorbed proteins can be approximated by Equation 5-6 since the proteins are distributed between and on top of polymer islands.

$$P_{prot}(0) = (1-\sigma/\sigma_0)^{\sigma_0 A_{prot}} = (1-\sigma/\sigma_0)^{4f} \quad (5\text{-}6)$$

If different sticking probabilities exist for adsorption to the bare surface and to top of the polymer islands, denoted by S and S_{isl}, the combined rate of protein adsorption to a primary or secondary adsorption site is given by Equation 5-7.

$$\frac{d\sigma}{dt} = Z*[SP_{poly}(0) + S_{isl}P_{isl}(6)]*P_{prot}(0) \quad (5\text{-}7)$$

Solving for Equation (5-7) for σ yields Equation (5-8) which reflects the dominant contribution of primary adsorption sites at low grafting densities, and the increasing contribution of secondary adsorption at high grafting densities.

$$\sigma = \frac{4f}{\pi d_p^2}\{1-[1+\frac{\pi d_p^2(4f-1)Zt}{4f}(S(1-x)^{2\rho_0\pi d_p R_g} + S_{isl}x^6)]^{-1/(4f-1)}\} \quad (5\text{-}8)$$

Results

Due to the small number of parameters, the predictions of the above model can be directly compared to published experimental results. Here three studies *[229, 231, 237]* are focused on to illustrate the excellent agreement between theory and experiment.

Prime and Whitesides mapped the adsorption of fibrinogen, pyruvate kinase, lysozyme and ribonuclease A as a function of ethylene oxide chain length (n=0-17) and fraction of oligo(ethylene oxide)-terminated alkanethiols in a self-assembled monolayer.*[229]* Figure 5-2 shows the experimental data and theoretical predictions for ribonuclease A. The size of the ribonuclease A protein d_p is taken as 3.8 nm and the molecular weight as 12.7 kDa.*[238, 239]* The maximum possible graft density ρ_0 is chosen based on experimental data when available*[112, 231]* and interpolations of the experimental data as described in Figure 5-7. Secondary adsorption is not observed for methyl-terminated PEO chains (n=17), presumably due to the rinsing step prior to measurement. The value of Zt is calculated from the protein

concentration (1 mg/ml) and the adsorption time (120 min) utilized in the experiment, while *S* is chosen as $8.8*10^{-8}$ according to measurements by Weaver et al. for the adsorption of albumin to silica.*[235]* The value of *SZt* does not greatly influence the predicted protein adsorption, thus an approximation of the actual value is sufficient (Figure 5-5 D). A comparison between model and experimental data for lysozyme can be found in Figure 5-8. The experimental data for pyruvate kinase and fibrinogen – proteins with a cylindrical rather than spherical shape – have not been fitted with the basic model presented here.

Pasche et al.*[237]* provide data for the adsorption of serum to PLL-g-PEG-coated Nb2O5 surfaces for PEG chains with molecular weights of 1, 2, and 5 kDa (n=23, 46 and 115) and varying grafting ratios (Figure 5-3). Serum (~85 mg/ml protein concentration) was adsorbed for 15 min. Since albumin constitutes a majority of serum proteins, the protein diameter is chosen as 7 nm,*[240]* and the adsorbed protein number density is calculated from the adsorbed mass using a molecular weight of 66 kDa. The value of the sticking probability S is again assumed to be $8.8*10^{-8}$. The maximum graft density for the different PEG lengths was interpolated from experimental data of maximum PEO graft densities as function of length in the literature (see Figure 5-7).*[112, 231]*

Unsworth et al.*[231]* measure protein adsorption to surfaces coated with hydroxyl-terminated (600 Da) and methyl-terminated (750 Da, 2000 Da) thiolated PEO chains as well as the transient and maximal (4 hours incubation) grafting density (Figure 5-4). Lysozyme (d_p=4.5 nm, M_w=14 kDa*[241]*) is adsorbed for 180 min at a concentration of 1 mg/ml. Methyl-terminated PEO-coated surfaces display secondary adsorption as the grafting ratio is increased, and consequently Equation 5-8 is utilized. For primary adsorption to the surface coated with hydroxyl-terminated PEO chains, again a value of the sticking probability S of $8.8*10^{-8}$ (Figure

5-4 A) is assumed. For secondary adsorption onto islands of methyl-terminated PEO grafts, the sticking probability is not known and the predictions of the RSA model are displayed for a standard sticking probability of $8.8*10^{-8}$ as well as for a two hundred-fold smaller sticking probability for 750 Da PEO chains and two thousand fold smaller sticking probability for 2000 Da PEO chains (Figure 5-4 B).

Discussion

The correspondence between the experimental data and the theoretical predictions despite the complete neglect of any thermodynamic and structural detail is striking. The calculation utilizes the protein diameter, concentration, time of exposure and sticking probability as well as the polymer chain density, chain length and maximal chain density to reproduce the non-trivial dependence of protein adsorption on polymer chain density and chain length observed in experiments by three different research groups for three different systems (PEO-ternimated alkanethiol SAMs, physisorbed PEO-grafted poly-(L-lysine), end-thiolated PEO chemisorbed to gold). This indicates that the model is robust, meaning that small changes in the experimental systems lead to small deviations between experimental results and theoretical predictions. As a result, this "single molecule" perspective, which builds on approaches taken to describe the interaction of motor proteins adhered to surfaces with cytoskeletal filaments*[25]* provides insights complementing more detailed theoretical calculations. The predictions of the RSA model for the dependence of protein adsorption on the model parameters are shown in Figure 5-5. Protein adsorption decreases rapidly with an increasing number of ethylene oxide units in the PEO chains (Figure 5-5 A), because the size of the open space required for adsorption rapidly increases with the increasing height of the polymer chain. However, the residual adsorption for very short chains becomes nearly undetectable (<0.1% of a monolayer) even for moderate grafting ratios. Since the maximum grafting density decreases and the required open space

increases with PEO chain length, the possible number of PEO chains in the required open space is maximized at an intermediate chain length. A larger number corresponds to more possibilities to encounter interfering PEO chains and thus reduced protein adsorption.

Unsurprisingly, protein size (Figure 5-5) strongly affects adsorption, suggesting that non-spherical proteins preferentially adsorb in initial orientations which minimize the required open space and that smaller proteins preferentially adsorb from protein mixtures (e.g. serum).

For a given protein size and PEO chain length, PEO chain density (Figure 5-5 C, D) is a critical parameter displaying a sharp transition between significant adsorption and almost complete resistance to protein adsorption. However, the parameter *f*, which describes the maximal fraction of the surface covered by protein, can be varied from 1 over 0.9 (representing hexagonal closed packing) and 0.78 (square net) to 0.53 (representing the jamming limit*[233, 242]*) without significantly affecting the predictions at medium and high PEO chain densities (Figure 5-5 C). The choice of f = 0.9 (hexagonal packing) permits close contact between two adsorbed proteins – a situation which cannot be ruled out at medium to high grafting densities. In contrast, adsorption at low grafting densities is dominated by the obstruction of adsorption by other, already adsorbed proteins – a situation better reflected by f = 0.53 (jamming limit).

Similarly, the kinetics of the adsorption process determined by the product of the sticking probability *S*, the landing rate *Z* and the adsorption time *t* do not have a large effect on the dependence of protein adsorption on PEO chain density (Figure 5-5 D). Changing the product *SZt* by an order of magnitude primarily shifts the chain density-dependent transition from the adsorbing to the protein-resistant regime, but by an amount which would be difficult to detect. The adsorption process is predicted to near completion on a timescale of hours, which corresponds to the typically chosen experimental conditions. The time after which the amount of

adsorbed protein reaches the detection limit of a typical adsorption measurement (10^{-3} monolayers) increases exponentially with the chain density (Figure 5-9).

Similar to the demonstrated extension of the model to methyl-terminated PEO chains which facilitate secondary adsorption, random sequential adsorption models can be readily constructed for other classes of surfaces (e.g. the glycocalix), mixed polymer layers, and mixed protein adsorption. Computer simulations promise to answer more detailed questions, for example with respect to the kinetics of the adsorption process near the jamming limit.*[218]* An application of the RSA model may also benefit a number of newly developed coating system, including "bottle" brushes of poly(oligo(ethylene glycol) methyl methacrylate)*[115]*, PEO-grafted poly-(4-benzoyl-p-xylylene-co-p-xylylene) coatings*[116]*, and plasma-deposited tetraglyme surfaces.*[117]*

The application of the RSA model may be limited in systems which permit the reorganization of PEO chains into ordered arrangements after the initial adsorption, because the model assumes a random placement. In principle, exchange reactions could lead to such ordering in self-assembled monolayers of alkanethiols, and interactions between PEO chains could drive ordering in physisorbed coatings. However, it is believed that the small thermodynamic driving forces – especially at low and medium grafting densities - render such ordering processes exceedingly slow and not important for the experimental systems discussed here.

Conclusion

The implications of the proposed RSA model for the long-standing debate about the origin of the resistance of PEO-grafted surfaces to protein adsorption are profound. Traditionally, physical (steric exclusion) and chemical (preference for water binding) contributions to the interaction of individual chains with protein and water are juxtaposed.*[52]* In contrast, the RSA model focuses on the random distribution of the PEO chains on the surface, assuming that the

presence of a single PEO chain in the protein-surface contact area completely prevents protein adsorption. The PEO coating thus presents neither a thermodynamic nor a kinetic barrier which is surmounted over time, but a perfect steric barrier with a defined number of holes. The key suggestion for the design of coating procedures is to increase the PEO chain density to reduce residual protein adsorption. While the need for a full understanding of the enthalpic and entropic interactions between PEO chains, water and protein cannot be denied*[52, 226, 228, 243]*, the agreement between the experimental data and the RSA model suggests that the random arrangement of the PEO chains is a major and previously neglected factor in determining protein adsorption to PEO-grafted surfaces.

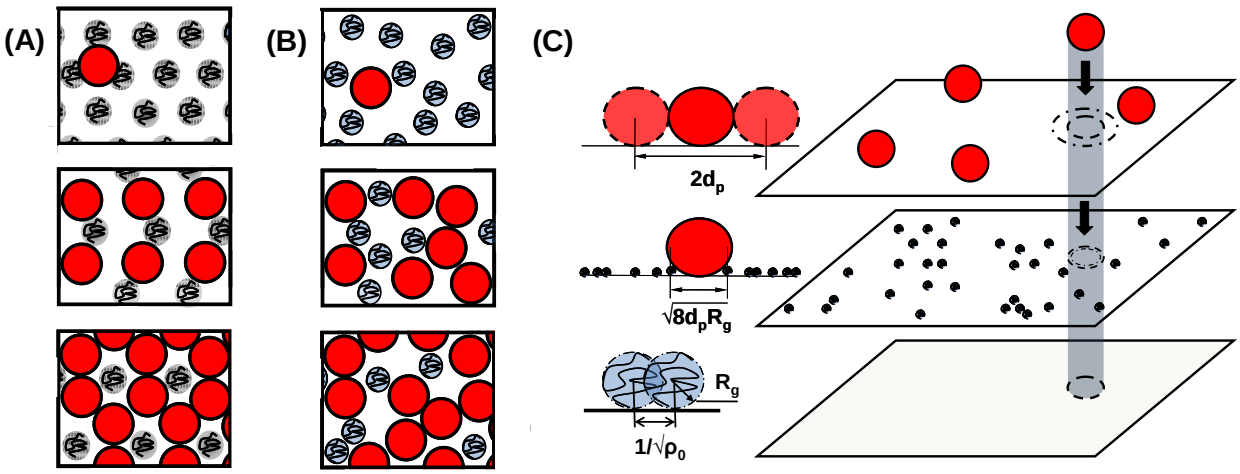

Figure 5-1. Concept of the random sequential adsorption model. (A) In previous models, polymer chains are regularly distributed on the surface and the calculation focuses on determining the fluctuating shape of the polymer and its interaction with adsorbing proteins. As the grafting density increases, the polymer chains create a thermodynamic and kinetic barrier to adsorption, which proteins can overcome over time. (B) In the random sequential adsorption model (RSA) polymer chains are randomly distributed and treated as hard spheres obstructing protein adsorption. As the grafting density increases, the number of unobstructed areas of sufficient size for protein adsorption decreases rapidly. (C) A protein diffusing in solution has to encounter an adsorption site on the surface which is free of grafted polymers as well as already adsorbed proteins in order to irreversibly adsorb to the surface.

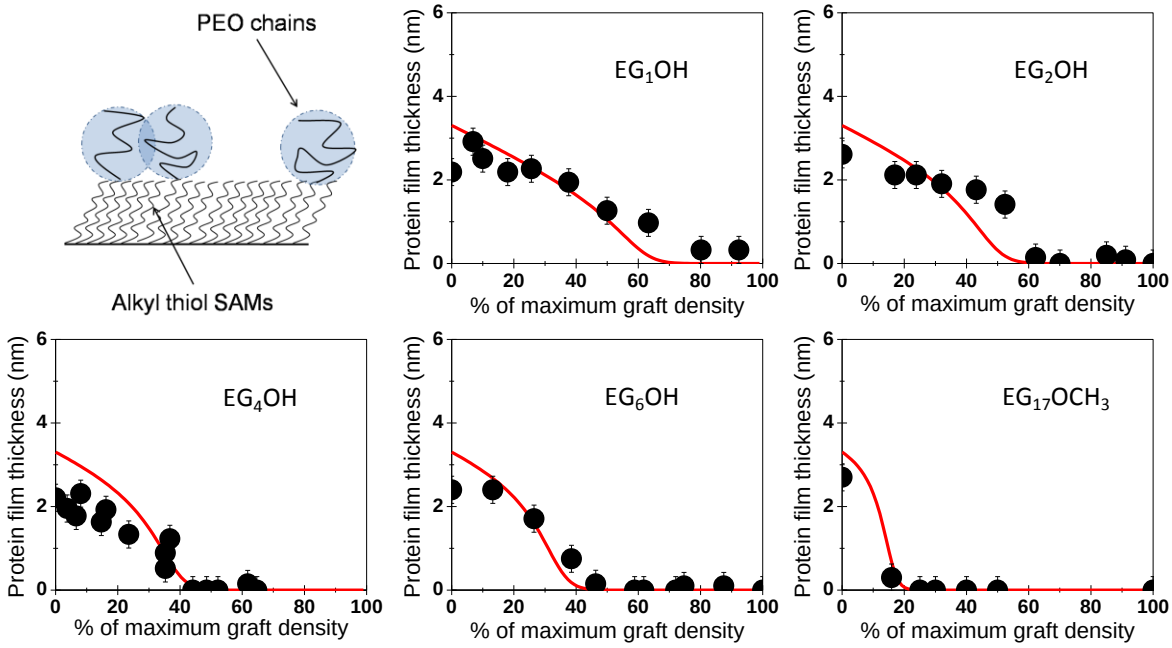

Figure 5-2. Comparison with experimental data of Prime et al. *[229]*. The adsorption of ribonuclease A to PEO-grafted SAM surfaces as a function of polymer graft coverage as experimentally observed (black circles) and as predicted by the RSA model (solid line). The maximum graft density is 4.07 nm^{-2}, 3.93 nm^{-2}, 3.6 nm^{-2}, 3.46 nm^{-2}, and 2.42 nm^{-2} for EGOH, EG_2OH, EG_4OH, EG_6OH, and $EG_{17}OCH_3$, respectively.

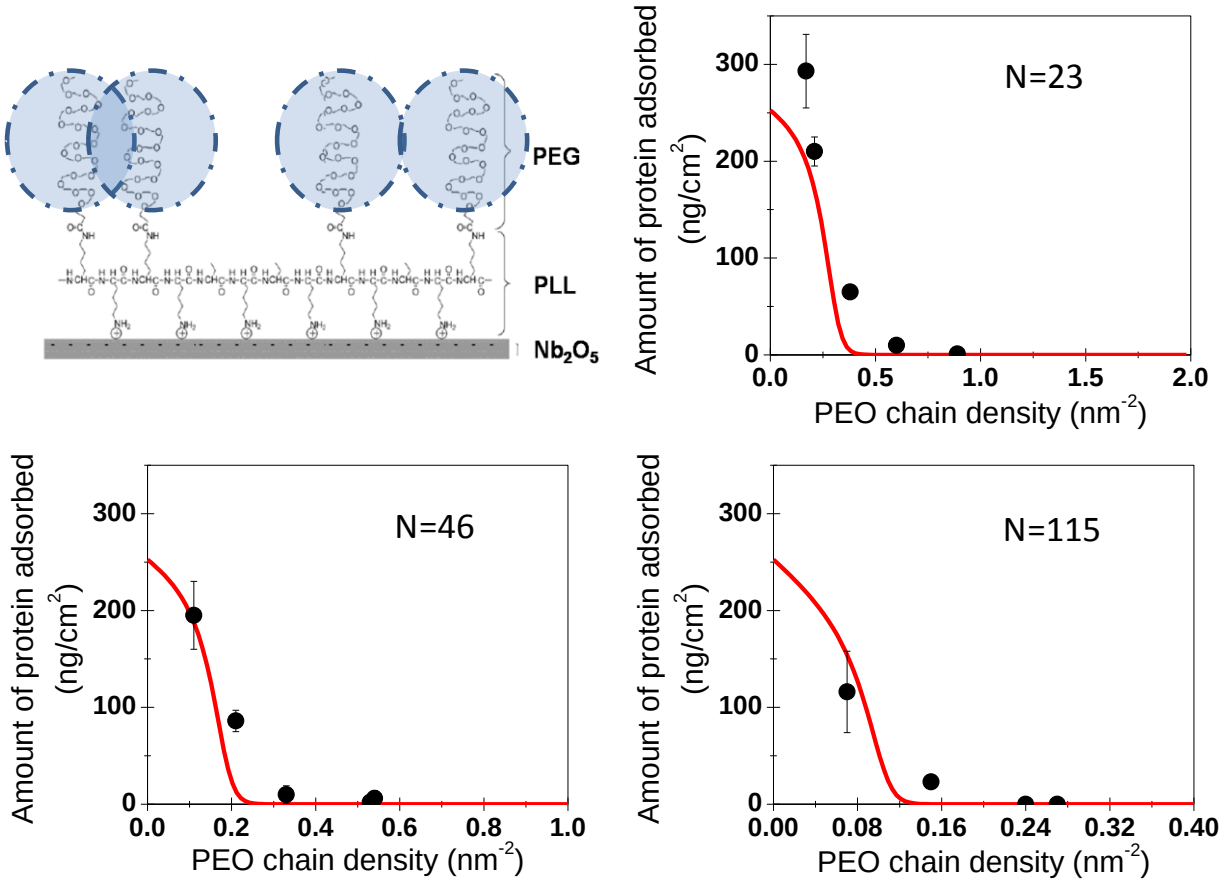

Figure 5-3. Comparison with experimental data of Pasche et al. *[237]*. The adsorption of serum protein to PEG-grafted surfaces as function of PEO chain density as experimentally observed (black circles) and as predicted by the RSA model (solid line).

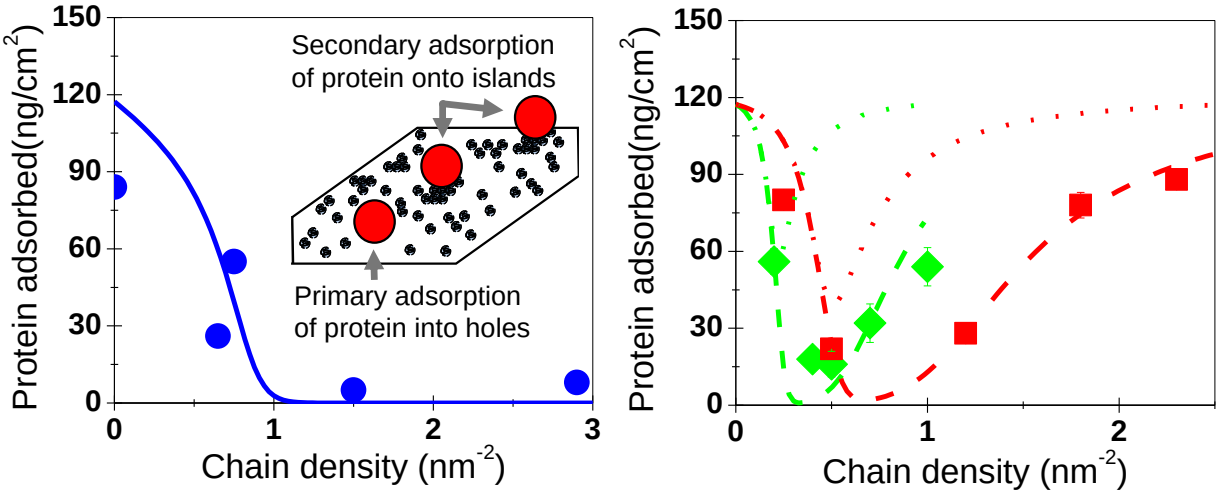

Figure 5-4. Comparison with experimental data of Unsworth et al. *[231]*. A) Primary adsorption to surfaces grafted with hydroxyl-terminated PEO chains (M_w = 600 Da) as experimentally observed (black circles) and as predicted by equation 2 (solid line). B) Primary and secondary adsorption to surfaces grafted with methyl-terminated PEO for M_w = 750 Da (squares) and M_w = 2000 Da (diamonds) as experimentally observed and predicted by Equation 5-8. Dotted lines represent a sticking probability of $8.8*10^{-8}$ for both, primary and secondary adsorption sites. Dashed lines represent a sticking probability of $8.8*10^{-8}$ for primary adsorption and a lower sticking probability for secondary adsorption ($4.4*10^{-10}$ for 750 Da, black and $4.4*10^{-11}$ for 2000 Da, gray.).

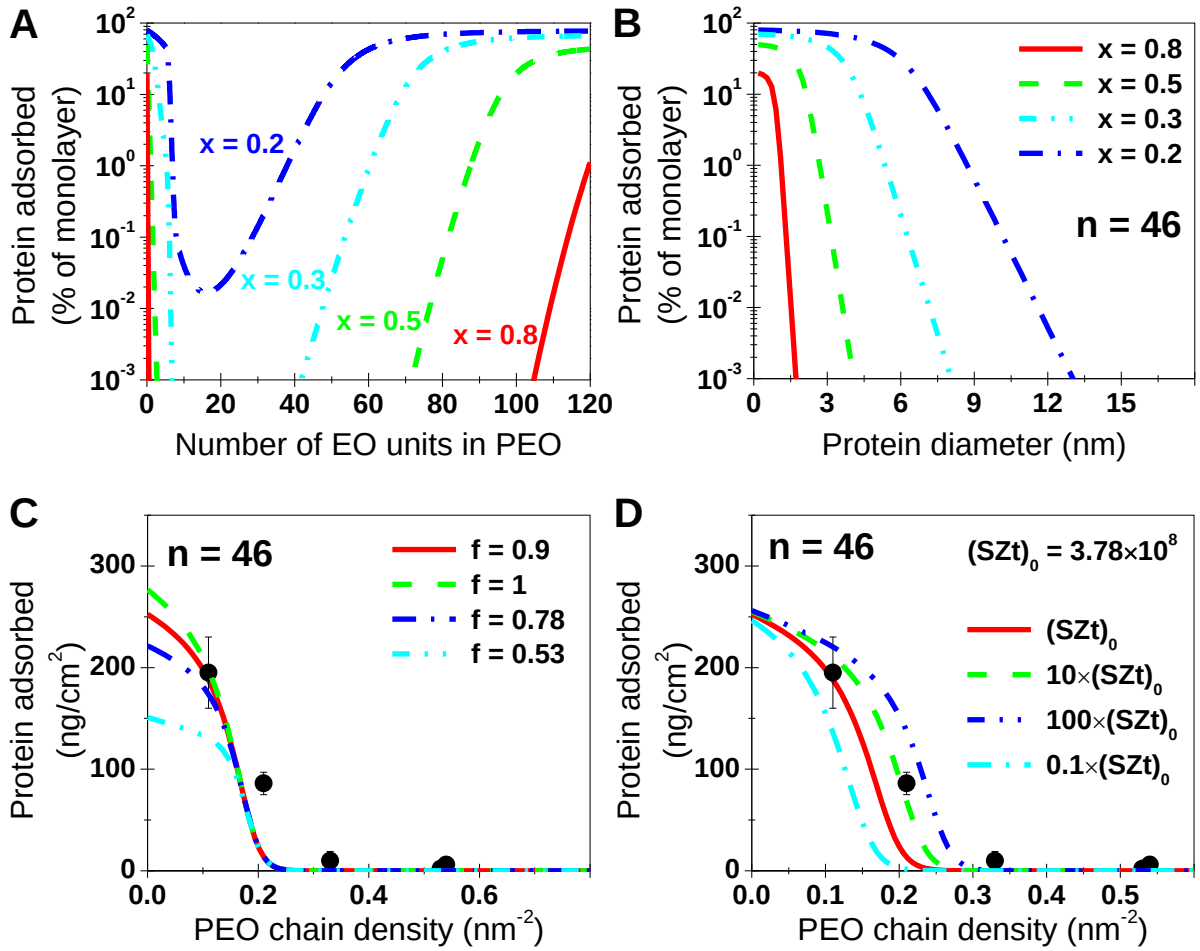

Figure 5-5. Predictions of the RSA model for primary adsorption. (A) Adsorption as function of number of EO units in a PEO chain. (B) Adsorption as function of protein diameter for chains with 46 EO units. (C) Effect of different values of the parameter f, which describes the maximum possible packing fraction. (D) Effect of variations in the product of sticking probability S, landing rate Z and adsorption time t. The adsorption conditions assumed are those used by Pasche et al.*[237]* (black circles – experimental data).

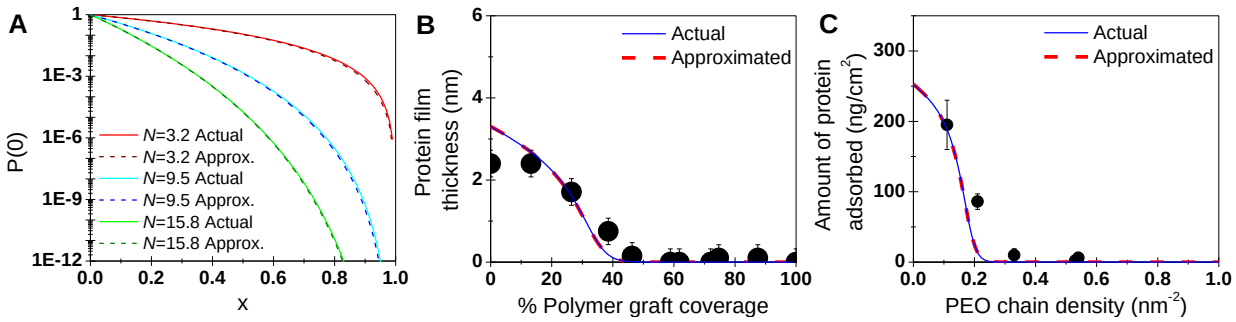

Figure 5-6. Approximation for probability distribution. (A) Figure showing the closeness of the approximation $P(0)=(1-x)^N$ to the actual $P(0)$ values for non-integer N given by a weighted average of two binomial distributions. For low and intermediate values of x, the approximation conforms closely to the actual probability values. Although the relative difference between the approximated and actual values increases at high values of x (i.e. $x>0.8$), the value of the probability $P(0)$ is also exceedingly small, which makes the effect of the approximation on the calculated amount of adsorbed protein negligible. (B) Predicted values of amount of protein adsorbed using actual and approximated probability distributions for protein adsorption on EG_6OH SAM surfaces by Prime et al. *[229]*. In this case the approximation conforms to the actual probability distribution even better as close to zero probability values have negligible effect on total amount of protein adsorbed over time. (C) Predicted values of amount of protein adsorbed using actual and approximated probability distributions for protein adsorption data on 2 kDa PEG chains (n=46) grafted onto a surface by Pasche et al. *[237]*.

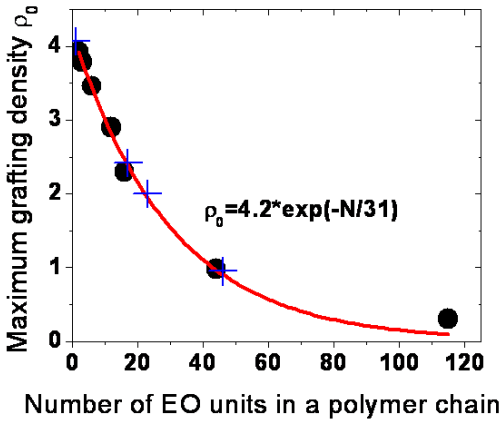

Figure 5-7. Fit of the maximum grafting density as a function of the number of PEO monomer units in the polymer to experimental data *[112, 231, 237]* (black dots). The fit function is used to determine the values of maximum grafting densities for other polymer lengths (blue crosses).

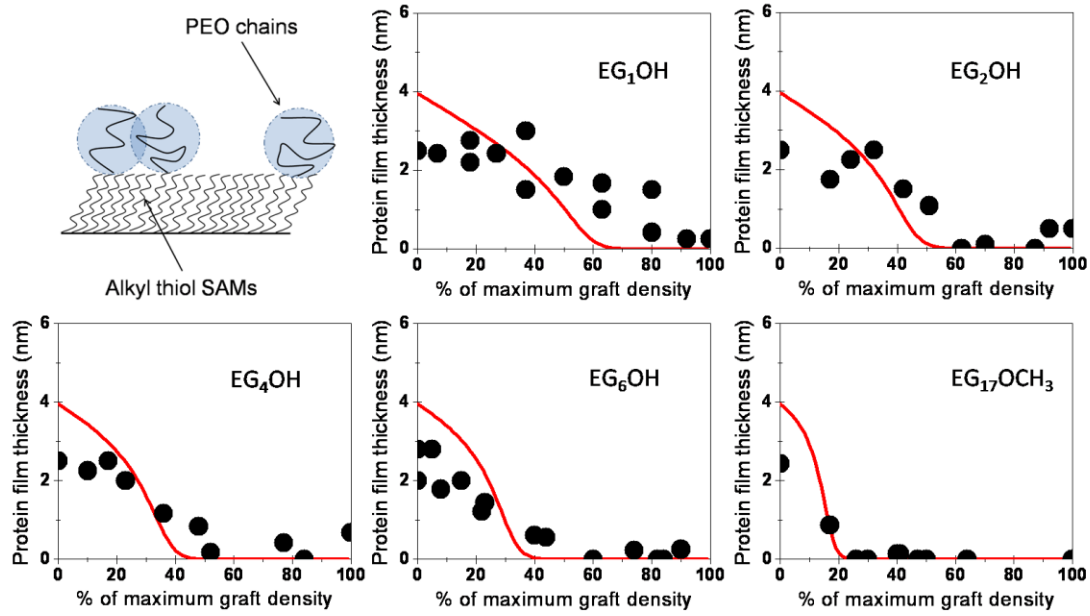

Figure 5-8. Lysozyme adsorption observed by Prime et al.*[229]* at 1 mg/ml protein concentration and predicted protein adsorption (red line) using equation (5). The size of lysozyme is 4.5 nm in diameter and 14 kDa by molecular weight*[241]*.

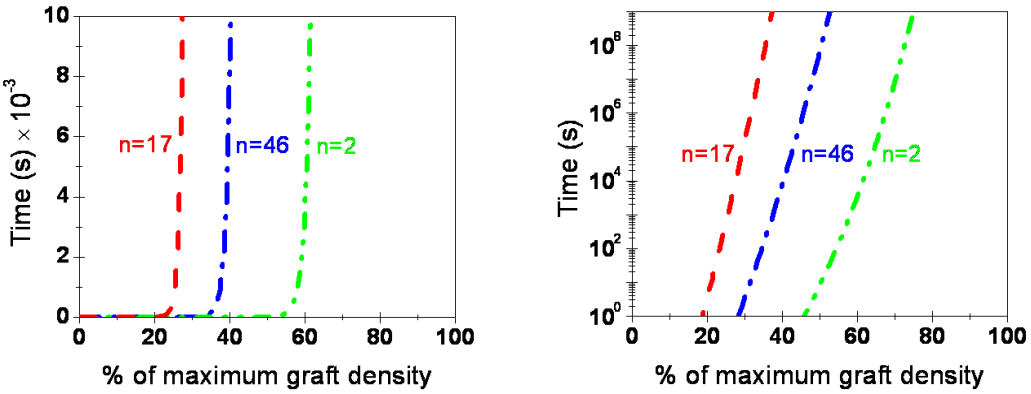

Figure 5-9. Time required for adsorption of 0.1% monolayer of proteins as a function of the grafting ratio for different polymer lengths (n=2, 17, 46). A protein concentration of 1 mg/ml and a protein size of 7 nm are assumed as used by Pasche et al. [11]. The sticking probability is assumed to be 8.8*10-8.

CHAPTER 6
DESIGN AND OPTIMIZATION OF HYBRID BIOSENSORS

Protein-Surface Interactions in Biosensors

Up to this point, the main focus of discussion has been towards characterization and modeling of protein non-fouling behavior of surfaces. In this section, specific interactions between proteins and surfaces in biosensing applications will be discussed. The role of protein adsorption has been mentioned in brief in chapter 1 and Figure 1-3 shows a schematic of a typical biosensing chip. A specific application of protein based biosensing is the detection of antigens in a solution by receptor antibodies patterned on the surface. The antibodies specifically capture their complimentary antigens from the solution. The capture event can either itself trigger a signaling event or a succeeding step of tagging the captured antigens with signaling molecules is introduced. The signal could be a change in the adsorbed mass of proteins on the surface, a change in the refractive index close to the interface, a chemical reaction resulting in the production of an optically detectable species or the attachment of a fluorescent tag. In conventional biosensors, antibodies specific to a target analyte are adsorbed close together within patterned regions on the sensor surface. This conglomeration of antibodies specific to an antigen forms the receptor. The analytes from solution are concentrated onto their specific receptors to obtain a strong detectable signal.

The receptor size in conventional biosensors is of the order of 100 μm. At high concentrations of target antigens (or any other analyte) in solution (> 1 nM) the number of analytes captured by the antibodies on the receptor is sufficiently high which results in a detectable signal. But for low analyte concentrations, the background signal, arising from non-specific adsorption of other species at the receptor as well as the large area of receptor over which the signal is collected, is comparable to the signal from the low number of analytes

captured. It is difficult to obtain a distinguishable signal using conventional biosensors for the detection of analytes at less than 0.1 pM concentrations. The current trend of biosensor research is towards using nanoscale surface features as receptors for analytes. There are two reasons for this: 1) Smaller receptor areas imply smaller sample volume analyzed which reduces the amount of background signal, 2) Nanostructures as receptors provide a strong signal enhancement (signal amplification up to 100-times) based on their design and signal transduction mechanism. Some examples of such nanoscale receptors are antibody functionalized conducting nano-wires, metallic nano-cavities, quantum dots and electromechanical nano-cantilevers. In theory, using these nanoscale receptors, one can detect analytes in concentrations below 1 fM, but in practice the performance of these sensors is limited by the time it takes to concentrate just a few analyte molecules from solution onto these receptors.*[244]* Sheehan et al. show that for receptor sizes approaching 100 nm, the time to capture just 10 molecules on these receptors is on the order of days. This is a major roadblock in the design and development of sensitive biosensors.

One of the applications of nanoscale transport systems, such as molecular shuttles and nanocars, is the capture and concentration of biological analytes and their subsequent deposition at a receptor site. Integrating active transport into a sensor platform can enhance the performance of biosensors (quantified by sensitivity AND response time) by accelerating analyte transport to the nanoscale receptor. The inspiration for this approach is of biological origin, since certain viruses “hijack” motor protein transporters to accelerate their travel from the periphery of the cell to the nucleus *[245, 246]*. Furthermore, a two step process of binding of an analyte to a surface followed by surface diffusion to the target site has been shown to be an effective approach to accelerate the interaction of dilute analytes with small target sites in a variety of biological situations*[247]*. The pursuit of such a two-stage sensor platform, where analyte capture from

solution is followed by a surface transport process, is enabled by the development of nanoscale sensing elements and of molecular shuttles capable of capturing and transporting analytes*[18, 78, 248]*. Here, the potential payoff of this design and the optimal layout of a platform is calculated. It is found that the accumulation of analyte at the sensor can be accelerated by several orders of magnitude, which would overcome the mass transfer limitations for nanoscale sensors pointed out by Sheehan and Whitman*[244]*.

Theoretical Modeling of Single-Stage and Two-Stage Analyte Capture Process

The argument is organized as follows: Consider a sensor site as it would exist on a microarray chip (Figure 6-1A) and calculate the number of analyte molecules collected at a receptor if the analyte molecules reach the receptor by three-dimensional (3D) diffusion (Figure 6-1B), by 3D diffusion to the sensor surface followed by two-dimensional (2D) transport to the receptor (Figure 6-1C), and finally by 3D diffusion to the sensor surface followed by active transport by molecular shuttles (Figure 6-1D). Since we are interested in very low analyte concentrations (less than pM) and fast response times (less than 30 minutes available for the collection of analyte), it is assumed that detection is limited by mass transport and not by the reaction rate between analytes and receptors*[249]* and that the saturation of receptors can be neglected. In this discussion, it is assumed that during the <30 min available for capture, the capture rate is determined by the steady-state flux of the analyte to the sensor surface.

Analyte Capture by 3D Diffusion

The number of analytes N accumulated on a disc-shaped sensor patch of radius r can be calculated from the diffusion-limited analyte flux $J_{3D\text{-}r}$ and the rate of dissociation of captured analytes from the receptor by Equation 6-1.

$$\frac{dN}{dt} = J_{3D-r} - k_d N \tag{6-1}$$

In Equation 6-1, k_d is the dissociation rate of the captured analyte. The steady-state flux to a disc-shaped receptor in a dilute solution of analytes is $J_{3D\text{-}r} = 4DC_m r$, where D is the diffusion constant and C_m is the bulk concentration of the analyte.*[250]* The number of analytes captured by the receptor spot in time t is then given by Equation 6-2.

$$N = \frac{4DC_m r}{k_d}(1 - e^{-k_d t}) \tag{6-2}$$

In current microarrays, the sensor patch radius varies between 10 and 200 µm and a large number of analyte molecules are rapidly accumulated.*[5, 251, 252]* However, nanoscale sensors in the size range of 1µm to 10 nm are desirable for two reasons mentioned previously: (1) a signal enhancement due to the capture of analytes into confined sensor patches *[64, 253-257]* and (2) a reduction in the background noise due to the reduced area of detection. Unfortunately, the accumulation of analyte onto such nanoscale sensors is extremely slow and necessitates collection times of hours to even days (Figure 6-2).*[244, 258]* Techniques to increase the analyte flux, e.g. stirring or flow, are effective for sensors larger than 10 µm,*[5]* but are not very effective in increasing the analyte flux to nanoscale receptors.*[244]*

Analyte Capture by 3D Diffusion to the Surface Followed by 2D Diffusion to the Sensor

Adam and Delbrueck have shown that such a two-stage capture can increase the analyte flux to the sensor if the 2D surface diffusion constant is comparable to the 3D diffusion constant and the dissociation rate of analyte from the surface is small compared to the analyte capture rate.*[247]*

The number of analytes N at the sensor patch as a result of the surface transport can be calculated from Equation 6-3.

$$\frac{dN}{dt} = \frac{N_S}{\tau_{avg}} \tag{6-3}$$

In Equation 6-3, N_s is the number of analytes on the surface at time t and τ_{avg} is the average time required for the analyte to find the sensor during the surface diffusion step.

The number of analytes at the surface N_s is determined by the 3D-diffusive flux of analytes to surface of the sensor $J_{3D\text{-}S}$, the subsequent 2D-diffusive transport of these analytes to the sensor and the concurrent dissociation of the analytes from the surface with rate k_d using Equation 6-4.

$$\frac{dN_S}{dt} = J_{3D-S} - \frac{N_S}{\tau_{avg}} - k_d N_S \tag{6-4}$$

Since the transporters do not cover the whole surface, the flux of analyte from solution to surface $J_{3D\text{-}S}$ is a fraction f of the steady-state analyte flux to the circular compartment surface of radius R from solution: $J_{3D\text{-}S} = 4fDC_mR$. The fraction f is a function of the number of transporters distributed over the compartment surface, but Berg & Purcell*[259]* have shown that even at low surface coverages it can be close to unity. Solving Equations 6-3 and 6-4 with boundary conditions $N_s = 0$ at t = 0 and N = 0 at t = 0 yields the number of analytes captured at the receptor (Equation 6-5) (Figure 6-2).

$$N = \frac{4fDC_mR}{(k_d\tau_{avg}+1)}[t - \frac{(1-e^{-(k_d+1/\tau_{avg})t})}{(k_d+1/\tau_{avg})}] \tag{6-5}$$

The average duration of surface transport τ_{avg} depends on the geometry of the surface and receptor and the character of the transport (diffusive or directed). If the sensor patch is located in a circular compartment with radius R and the motion of the analyte on the surface is diffusive, Purcell and Berg*[259]* have shown that τ_{avg} is given by Equation 6-6.

$$\tau_{avg} = \frac{R^2}{2D'}[\ln\left(\frac{R}{r}\right) - \frac{3}{4}] \tag{6-6}$$

In Equation 6-6 D' is the surface diffusion constant. If τ_{avg} is small compared to t and $k_d\tau_{avg} << 1$, Equation 6-6 can be approximated by Equation 6-7.

$$N = 4fDC_mR[t - \tau_{avg}] \quad (6\text{-}7)$$

Analyte Capture by 3D Diffusion to the Surface Followed by Active Transport by Molecular Shuttles to the Sensor

Molecular shuttles powered by biomolecular motors have been designed based on the microtubule-kinesin or the actin-myosin system.*[15, 260]* A common design for the microtubule-kinesin system is to adhere the kinesin motors to the surface and utilize the immobilized motors to propel microtubules, which serve as the transporter. Specific analytes can be captured and transported by functionalizing the microtubules with antibodies or aptamers.*[18, 87, 261-263]* The path of the gliding microtubules can be controlled by patterning tracks on the surface.*[185]* Finally, the activity of the motors can be controlled by regulating the supply of the substrate ATP.*[264]*

On an unpatterned surface (Figure 6-1C), each shuttle moves on a trajectory approximating a worm-like chain.*[24, 265]* The path can be described as a 2D random walk with a diffusion constant D' given by L_pv, where L_p is the persistence length on the microtubule trajectory.*[266]* On a surface patterned with a suitable network of tracks, the microtubule movement can be guided to the receptor spot with a microtubule velocity v.

Molecular shuttles can be integrated into a conventional microarray biosensor (Figure 6-1A), by replacing each of the spots with a compartment of radius R. The compartment surface can be coated with kinesin, which support the movement of functionalized microtubules serving as molecular shuttles. These shuttles capture analytes from the solution and transport them to a central nanoscale sensor of radius r.

If there are N_{MT} microtubules on the compartment surface, the diffusion limited steady state flux of analytes to the microtubule coated surface is a fraction f of the analyte flux to the whole surface of the compartment (given by $J_{3D\text{-}R} = 4DCR$) with f given by Equation 6-8*[250]*.

$$f^{-1} = 1 + \frac{2R}{\pi l_{MT} N_{MT}} \ln\left(\frac{2l_{MT}}{d_{MT}}\right) \tag{6-8}$$

As N_{MT}, the number of shuttles in the compartment, becomes very large f tends to 1. For a compartment with a radius of 100 μm, a typical density of one shuttle per 100 μm^2 and a microtubule length of 5 μm and width of 25 nm, the fraction of the maximal analyte flux harvested would be 80%.

The number of analytes delivered by the shuttles to the sensor patch can be determined using Equation 6-5. If microtubules move diffusively on an unpatterned surface (Figure 6-1C), the average the average time to deliver a captured analyte to the sensor patch can be determined from Equation 6-6. Neglecting the dissociation rate for sake of mathematical simplicity, Equation 6-5 can be rewritten as shown in Equation 6-9.

$$N = 4 f D C_m R\{t - \frac{R^2}{2L_p v}[\ln(\frac{R}{r}) - \frac{3}{4}] * [1 - e^{-\frac{(2L_p v t)}{R^2(\ln(R/r) - 3/4)}}]\} \tag{6-9}$$

If shuttles are directly guided to the sensor patch by tracks, the average time to deliver a captured analyte to the sensor is given by Equation 6-10.

$$\tau_{avg} = \frac{(R - r)}{v} \tag{6-10}$$

Equation 6-5 can be rewritten for this case as shown in Equation 6-11.

$$N = 4 f D C_m R[t - (\frac{R - r}{v}) * (1 - e^{-\frac{vt}{R-r}})] \tag{6-11}$$

The number of analytes captured in the two-stage capture process using molecular shuttles is plotted for different detection times (15, 30, 60 min) and sensor sizes (radius 1, 10, 100, 1000 nm) in Figures 6-3 and 6-4. Typical values for analyte diffusion constants as well as shuttle velocities and trajectory persistence lengths have been assumed.

Equations 6-9 and 6-11 can be used to optimize the design of the sensor (Figures 6-3 and 6-4). For diffusive shuttle movement on an unpatterned surface, the size of the collection compartment has an optimum at which the number of collected analytes is maximal. This optimal compartment size depends primarily on the time available for detection (Figure 6-3). For kinesin-powered molecular shuttles it is on the order of 100 μm for a 30 min detection window. For directed shuttle movement on a patterned surface, the number of collected analytes increases asymptotically with increasing compartment radius (Figure 6-4). The optimum design parameters are plotted for specific receptor sizes and detection times in Figure 6-5.

Signal-to-Noise Ratio

A counterargument to the use of molecular shuttles is that the performance comparison should be made between the molecular shuttle sensor and a diffusion-based sensor of a size equal to the size of the collection compartment. Since the analyte flux to the compartment surface is larger than the analyte flux delivered by the shuttles to the nanoscale sensor patch (see Equation 6-8), the traditional, microscale sensor should actually perform better. However, the key metric to consider is the Signal-to-Noise Ratio (SNR) of the sensor. The noise is proportional to $\sqrt{S+B+N^2}$ where S is the signal, B is the background, and N the noise introduced by the detection system. A reduction in the size of the sensor patch is often accompanied by a corresponding reduction in the size of the background. For example, in fluorescence imaging a reduction in the illuminated area is accompanied by a reduction in the illuminated solution

volume with a concomitant decrease in the fluorescence background. At the same time, problems with cross-reactivity and non-specific adsorption are drastically reduced for a smaller sensor. In summary, the Signal-to-Noise ratio is increased if the small loss in the number of collected analytes is overcompensated by a large reduction in the background signal, or if the noise introduced by the signal transduction mechanism in the sensor is significantly reduced as a result of the miniaturization to the nanoscale.*[65]*

Discussion

Figure 2 shows that for nanoscale sensor patches a two-stage capture process can significantly accelerate the analyte capture compared to a single-stage 3D diffusion capture process. Furthermore, directed movement of molecular shuttles along tracks provides a relatively small advantage over diffusive movement on an unpatterned surface. For undersized compartments, diffusive shuttle movement can even result in faster analyte collection than directed movement.

The above described analysis can be applied to two experimental systems recently described in the literature. The sensor design by Lin et al. employs capture of analytes in a compartment (radius ~90 μm) onto microtubules followed by directed transport into the sensor area (radius ~10 μm).*[78]* Assuming an initial microtubule density within the compartment of 0.05 μm^{-2} and an average microtubule length of 5 μm, Equation 6-8 yields f=0.95. In this system, the microtubules are stationary while the capturing analytes for 1 min. Then the analyte solution is replaced with a motility solution that triggers microtubule movement. After a collection period of 14 min all of the microtubules have reached the sensor area.

At a typical analyte concentration studied by Lin et al., say 1 pM, approximately 1000 analytes would be captured at the receptor. Although the sensor design by Lin et al does provide a proof of principle working of a 2-stage capture biosensor, it is not optimized for an increased

SNR. In fact, 3D diffusion based capture of 1 pM streptavidin at the 10 µm radius receptor would result in approximately 1,700 captured molecules. The sensor design utilised by Lin et al. can be modelled by modifying Equation 6-11 to incorporate analyte capture by stationary microtubules followed by directed transport towards the receptor, which yields Equation 6-12.

$$N = 4\,fDC_m R[t - t_{AT}]*[1 - e^{-\frac{vt_{AT}}{R-r}}] \tag{6-12}$$

In Equation 6-12, t_{AT} is the time for which the microtubules are actively transported towards the receptor. The optimum design for this setup and 15 minute detection time is 11 minutes for analyte capture and 4 minutes of active transport and yields 8,000 captured molecules.

Fischer et al.*[248]* developed a two-stage sensor design where the shuttles capture the analyte in the centre of a circular well and deliver it in a diffusive motion to the sensor periphery for detection. If the density of shuttles is high enough at all times that changes in f can be neglected, Equation 6-5 can be applied to this design, even though the shuttle density decreases over time. As the captured analytes are transported to the periphery rather than the centre, the average transport time in this case is given by Equation 6-13.

$$\tau_{avg} = \frac{R^2}{8D'} \tag{6-13}$$

In Equation 6-13, $D' = L_p v$ as explained earlier for the microtubule-kinesin based active random transport. For a detection time of 30 min as desired by Fischer et al., the optimum compartment radius is 375 µm (Figure 6-6), while a radius of 400 µm was employed. However, if even shorter detection times are desired (e.g. 15 min), this optimum radius should be smaller (e.g. 250 µm).

Conclusion

As Adam, Berg and Delbrueck recognized four decades ago, the scaling of diffusion processes to the nanoscale has non-obvious consequences and enables distinct approaches to the capture and detection of molecular analytes. A careful evaluation of the combination of diffusive transport with novel active transport mechanisms, such as molecular shuttles, demonstrates that analyte capture can be accelerated by orders of magnitude if the system is suitably designed. Furthermore, the analysis can be applied to transporters under development, such as nanocars *[267]*, to define the benchmarks these transport systems have to meet to be advantageously employed in a sensor system. Of course, the presented analysis of the mass transport situation does not capture the full complexity of sensor systems. For example, non-specific and adventitious adsorption of analytes to the surface,*[6]* or the complex nature of the analyte-shuttle interaction*[89]* may complicate the picture. However, an accounting of diffusion and active transport are the foundation of rational sensor design.

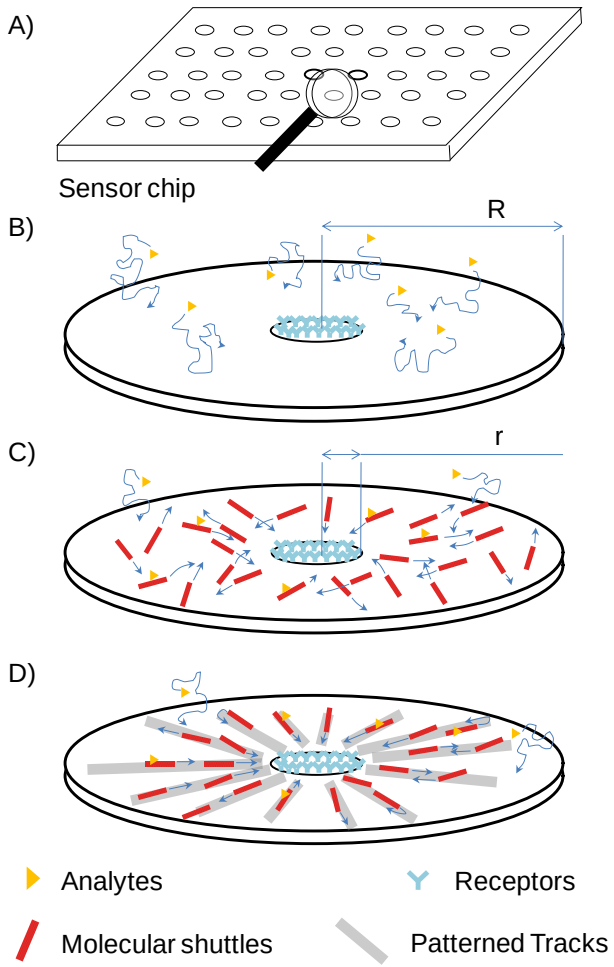

Figure 6-1. Design of Hybrid Biosensors. Sketch showing a biosensor chip (A), conventional 3D diffusion based capture of analytes to the receptors on the chip (B), analytes being captured on molecular shuttles within a compartment on the chip and being transported either by 2D diffusion (C) or directed active transport along tracks (D) and deposited at the receptor.

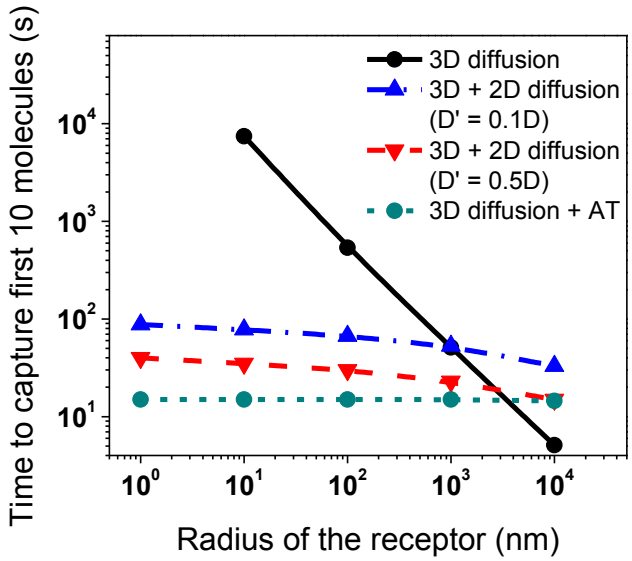

Figure 6-2. Time for capture of first 10 analyte molecules. A disc shaped receptor of radius r, analyte capture by: 3D diffusion, 3D+2D diffusion and 3D diffusion followed by directed active transport of analyte. A diffusion constant for 3D-diffusion of 80 $\mu m^2/s$ is assumed. 2D-diffusion constant is taken as one half or one-tenth of the 3D-diffusion constant. Analyte concentration C_m of 1 pM, a compartment radius R of 100 µm, an active transport v of 0.5 µm/s, a capture fraction f of 0.9, and a dissociation rate k_d of 10^{-4} s^{-1} according to*[268]* are assumed.

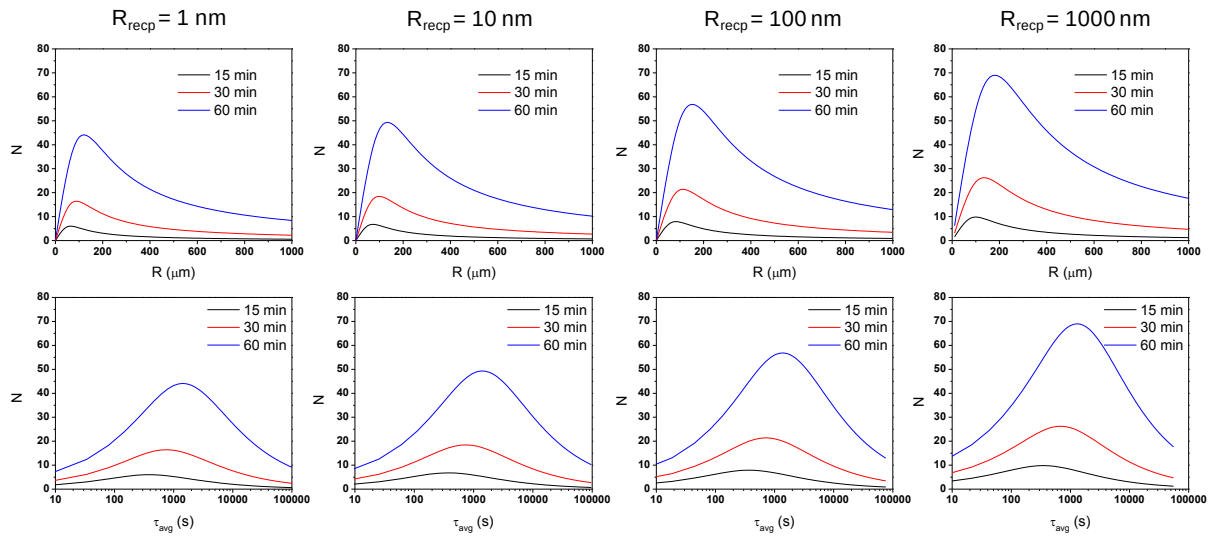

Figure 6-3. Optimizing Random Active Transport Based Biosensor Design. Plot of number of analytes collected at receptors of various sizes and at different detection times for 3D analyte diffusion onto molecular shuttles followed by diffusive transport and unloading of analytes at the receptor. The effect of sensor compartment radius R and the average analyte capture time is observed and optimum design parameter values that result in maximum number of analytes captured is obtained. Diffusion constant for 3D-diffusion of 80 $\mu m^2/s$, active transport velocity v of 0.5 μm/s, capture fraction f of 0.9 and analyte concentration C_m of 1 fM are assumed.

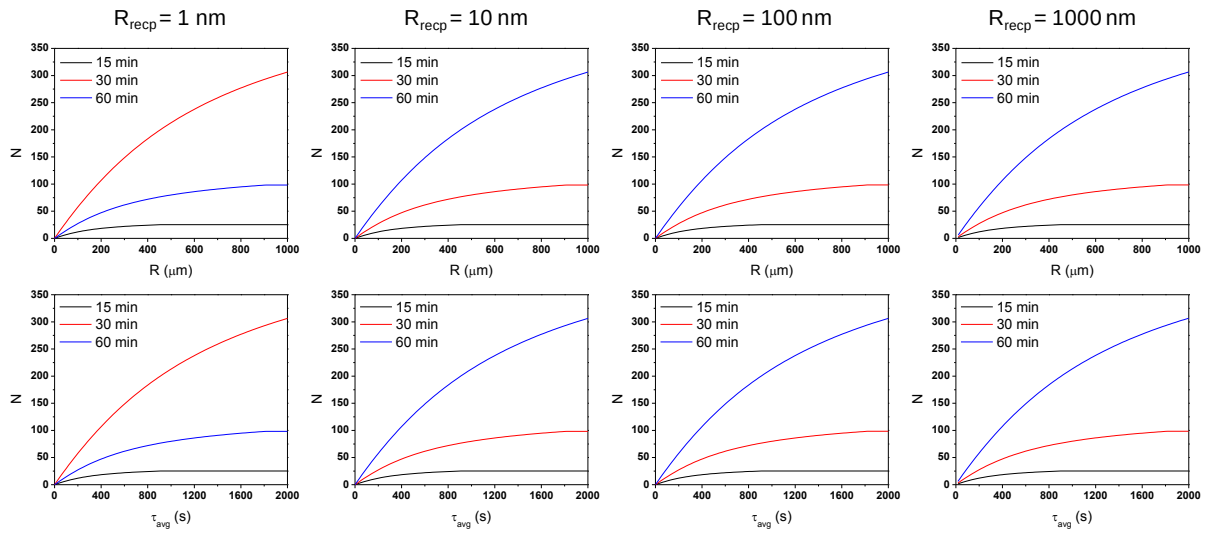

Figure 6-4. Optimizing Directed Active Transport Based Biosensor Design. Plot of number of analytes collected at receptors of various sizes and at different detection times for 3D analyte diffusion onto molecular shuttles followed by directed transport and unloading of analytes at the receptor. The effect of sensor compartment radius R and the average analyte capture time is observed and optimum design parameter values that result in maximum number of analytes captured is obtained. It is observed that increasing the compartment radius R increases τ_{avg} as well as N but once τ_{avg} = t (time for detection), the number of analytes captured in time t would remain constant. Diffusion constant for 3D-diffusion of 80 $\mu m^2/s$, active transport velocity v of 0.5 μm/s, capture fraction f of 0.9 and analyte concentration C_m of 1 fM are assumed.

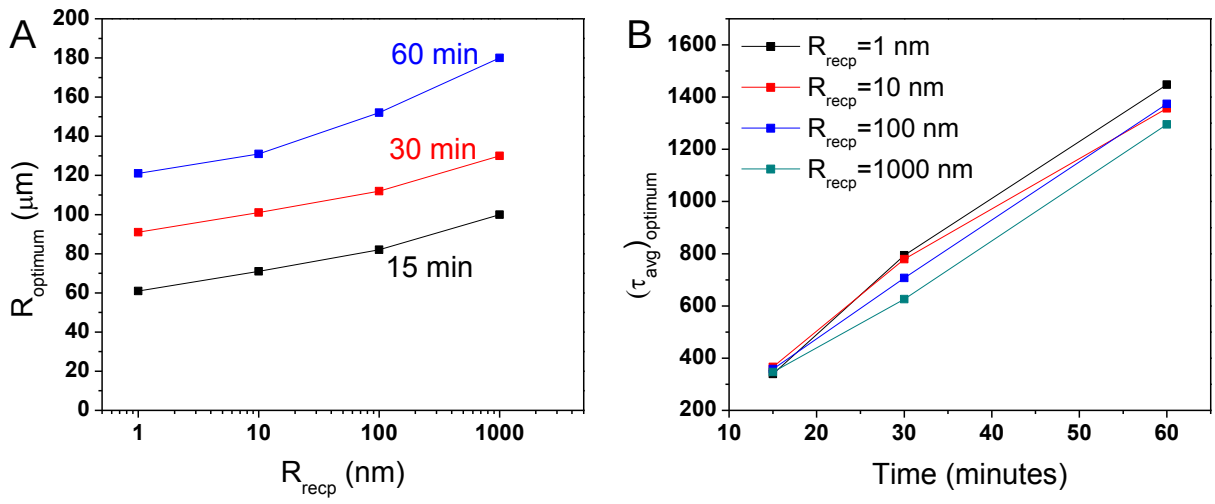

Figure 6-5. Optimum Sensor Design Parameters. A two stage capture process involving 3D diffusion to molecular shuttles followed by a random 2D motion of the shuttles along the surface to the central receptor. Diffusion constant of 80 $\mu m^2/s$ for 3D-diffusion and active transport velocity of 0.5 μm/s are assumed

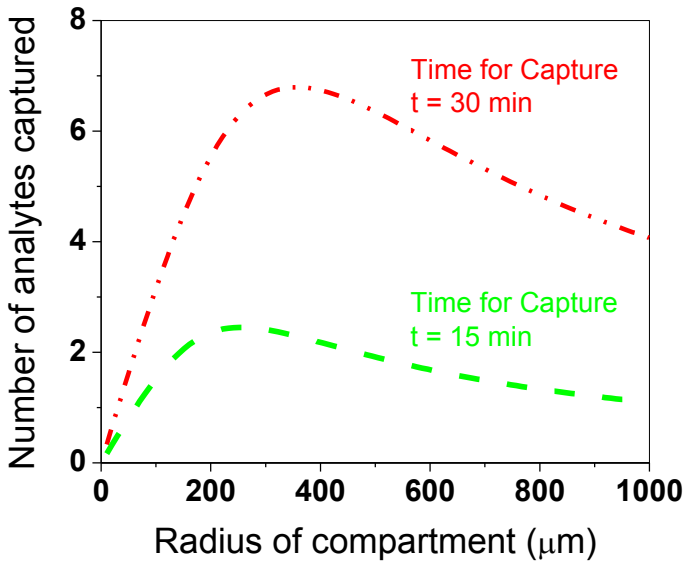

Figure 6-6. Comparing Optimum Sensor Design Parameters to Biosensing System described by Fischer et al. Analysis of the sensor design by Fischer et al.*[248]* Number of analytes captured in a 2-stage capture process involving 3D+2D diffusion based capture of analytes using microtubule/kinesin-based shuttle system. L_p = 100 μm and v = 200 nm/s.

CHAPTER 7
CONCLUSION

Research to develop surfaces that resist non-specific protein adsorption has resulted in the development of various strategies and surface coating techniques. One of the most promising techniques is grafting of surfaces with hydrophilic polymer chains. Even though complete prevention of protein adsorption has not been achieved; novel surface coatings have shown to reduce protein adsorption to less than 0.1% of a monolayer. This low coverage of proteins on surfaces is at or below the limit of detection for standard protein density quantification techniques. A technique for quantifying protein adsorption with a 100-fold lower limit for detection has been developed and demonstrated.*[269]* While the technique is demonstrated for the adsorption of kinesin protein and with the use of microtubule filaments as probes for adsorbed kinesin, it can be easily developed for other proteins as well. One example is determining the density of fibrinogen by measuring the landing rate of micron sized beads functionalized with anti-fibrinogen molecules, so that they land specifically on adsorbed fibrinogen. The detection limits are a function of the interaction area of the probe with the surface adsorbed protein. For the demonstrated setup, the lower detection limit is 0.1 μm^{-2} (about 0.001% of a monolayer). The simplicity of design and ease of detection using an epi-fluorescence microscope make this technique useful for characterization of a large variety of protein resistant surfaces.

To obtain a better understanding of protein adsorption on surfaces coated with hydrophilic polymers an analytical model has been developed and described.*[270]* While neglecting the specific interactions between individual components of a protein and a polymer chain, the model focuses on the overall distribution of the polymer chains on the surface. The model assumes that for a protein to adsorb to the surface a polymer free interaction region is required. The

predictions of this model very closely correspond to the experimentally observed protein adsorption data for various polymer-surface systems. The key insight regarding protein adsorption on polymer coated surfaces obtained from this model is that the polymer layer presents a perfect steric barrier to protein adsorption with a defined number of holes that arise from the random arrangement of the polymer chains. The obtained analytical expressions can be easily used to observe the effect of various system parameters such as polymer chain length, polymer grafting density and protein size on the amount of protein adsorbed. Protein adsorption can be minimized by increasing the polymer grafting density and adsorption of specific proteins based on size can be accomplished by adjusting the polymer grafting density and the polymer chain length to obtain specific hole sizes. The simplicity of the mathematics used to describe the model makes it easy to adapt and extend the model to various other scenarios such as multiple protein adsorption and lipid-polymer-lipid and lipid-polymer surface interactions.

A specific application for protein adsorption is biosensing. In a typical biosensor, target analytes in solution are concentrated by their specific adsorption to a receptor spot. The specific adsorption events can then be detected by various signal transduction mechanisms to determine the presence of the analyte. Nanoscale receptors are typically useful for detecting the presence of only a few analyte molecules but their applicability is limited by the extremely long analyte capture times. This limitation can be overcome by the integration of molecular shuttles in the biosensing platform to capture and concentrate analytes at the receptor. Different scenarios based on two stage capture of analytes using molecular shuttles are theoretically investigated and optimum sensor design parameters have been obtained for a kinesin-microtubule based molecular shuttle system.*[271]* Design of hybrid biosensors based on these optimum parameters

for molecular shuttle based analyte capture and concentration can result in at least a 100-fold increase in detection sensitivity.

LIST OF REFERENCES

[1] P. Angenendt, H. Lehrach, J. Kreutzberger, J. Glokler, *Proteomics* **2005**, *5*, 420.

[2] B. B. Haab, *Proteomics* **2003**, *3*, 2116.

[3] C. Wingren, C. A. K. Borrebaeck, *Expert Rev. Proteomics* **2004**, *1*, 355.

[4] W. Kusnezow, Y. V. Syagailo, I. Goychuk, J. D. Hoheisel, D. G. Wild, *Expert Rev. Mol. Diagn.* **2006**, *6*, 111.

[5] W. Kusnezow, Y. V. Syagailo, S. Ruffer, N. Baudenstiel, C. Gauer, J. D. Hoheisel, D. Wild, I. Goychuk, *Mol. Cell. Proteomics* **2006**, *5*, 1681.

[6] A. Hucknall, D. Kim, S. Rangarajan, R. T. Hill, W. Reichert, A. Chilkoti, *Adv. Mater.* **2009**, *9999*, Na.

[7] C. M. Niemeyer, C. A. Mirkin, Eds., *Nanobiotechnology*, Wiley-Vch, Weinheim **2004**.

[8] C. M. Niemeyer, *Angew. Chem. Int. Ed. Engl.* **2003**, *42*, 5796.

[9] H. Hess, G. D. Bachand, V. Vogel, In *Encyclopedia of Nanoscience and Nanotechnology*, (Eds: J. A. Schwarz, C. Contescu, K. Putyera), Marcel Dekker, New York **2004**.

[10] H. Hess, G. D. Bachand, V. Vogel, *Chem. Eur. J.* **2004**, *10*, 2110.

[11] M. Schliwa, G. Woehlke, *Nature* **2003**, *422*, 759.

[12] H. Noji, R. Yasuda, M. Yoshida, K. Kinosita, *Nature* **1997**, *386*, 299.

[13] H. Hess, *Science* **2006**, *312*, 860.

[14] D. J. G. Bakewell, D. V. Nicolau, *Aust. J. Chem.* **2007**, *60*, 314.

[15] A. Mansson, M. Sundberg, R. Bunk, M. Balaz, I. A. Nicholls, P. Omling, J. O. Tegenfeldt, S. Tagerud, L. Montelius, *IEEE Trans. Adv. Packag.* **2005**, *28*, 547.

[16] M. Sundberg, R. Bunk, N. Albet-Torres, A. Kvennefors, F. Persson, L. Montelius, I. A. Nicholls, S. Ghatnekar-Nilsson, P. Omling, S. Tagerud, A. Mansson, *Langmuir* **2006**, *22*, 7286.

[17] R. K. Soong, G. D. Bachand, H. P. Neves, A. G. Olkhovets, H. G. Craighead, C. D. Montemagno, *Science* **2000**, *290*, 1555.

[18] S. Ramachandran, K.-H. Ernst, George D. Bachand, V. Vogel, H. Hess, *Small* **2006**, *2*, 330.

[19] R. Yokokawa, S. Takeuchi, T. Kon, M. Nishiura, K. Sutoh, H. Fujita, *Nano Lett.* **2004**, *4*, 2265.

[20] R. Yokokawa, J. Miwa, M. C. Tarhan, H. Fujita, M. Kasahara, *Anal. Bioanal. Chem.* **2008**, *391*, 2735.

[21] M. G. L. Van Den Heuvel, M. P. De Graaff, C. Dekker, *Science* **2006**, *312*, 910.

[22] S. Diez, C. Reuther, C. Dinu, R. Seidel, M. Mertig, W. Pompe, J. Howard, *Nano Lett.* **2003**, *3*, 1251.

[23] T. Fischer, H. Hess, *J. Mater. Chem.* **2007**, *17*, 943.

[24] T. Nitta, H. Hess, *Nano Lett.* **2005**, *5*, 1337.

[25] J. Howard, A. J. Hudspeth, R. D. Vale, *Nature* **1989**, *342*, 154.

[26] J. D. Andrade, *Protein Adsorption*, New York: Plenum Press, **1985**.

[27] L. Stryer, *Biochemistry*, W. H. Freeman, New York **1988**.

[28] J. D. Andrade, V. Hlady, *Adv. Polym. Sci.* **1986**, *79*, 1.

[29] R. E. Dickerson, I. Geis, *The Structure and Action of Proteins*, New York: Harper & Row, **1969**.

[30] B. Alberts, A. Johnson, J. Lewis, M. Raff, K. Roberts, P. Walter, *Molecular Biology of the Cell. Fourth Edition*, Garland, New York **2002**.

[31] J. A. Tuszynski, M. Kurzynski, *Molecular Biophysics*, CRC Press, **2003**.

[32] T. A. Horbett, J. L. Brash, In *Proteins at Interfaces: Physicochemical and Biochemical Studies*, (Eds. Brash, J. L. And T. A. Horbett), Vol. 1, ACS **1987**.

[33] R. A. Latour, In *Encyclopedia of Biomaterials and Biomedical Engineering*, (Eds: G. Wnek, G. Bowlin), Taylor&Francis, New York **2005**.

[34] R. P. Ekins, "Ligand Assays: From Electrophoresis To Miniaturized Microarrays", **1998**.

[35] J. Clemmens, H. Hess, R. Doot, C. M. Matzke, G. D. Bachand, V. Vogel, *Lab Chip* **2004**, *4*, 83.

[36] A. J. Garcia, D. Boettiger, *Biomaterials* **1999**, *20*, 2427.

[37] N. D. Gallant, K. A. Lavery, E. J. Amis, M. L. Becker, *Adv. Mater.* **2007**, *19*, 965.

[38] C. J. Wilson, R. E. Clegg, D. I. Leavesley, M. J. Pearcy, *Tissue Eng.* **2005**, *11*, 1.

[39] L. Vroman, *Nature* **1962**, *196*, 476.

[40] C. A. Behling, M. Spector, *J. Biomed. Mater. Res.* **1986**, *20*, 653.

[41] D. G. Castner, B. D. Ratner, *Surf. Sci.* **2002**, *500*, 28.

[42] B. D. Ratner, D. G. Castner, T. A. Horbett, T. J. Lenk, T. J. Lewis, R. J. Rapoza, *J. Vacuum Sci. And Techn. A* **1990**, *8*, 2306.

[43] G. P. Lopez, B. D. Ratner, C. D. Tidwell, C. L. Haycox, R. J. Rapoza, T. A. Horbett, *J. Biomed. Mater. Res.* **1992**, *26*, 415.

[44] J. L. Dalsin, B. H. Hu, B. P. Lee, P. B. Messersmith, *J. Am. Chem. Soc.* **2003**, *125*, 4253.

[45] K. Nakanishi, T. Sakiyama, K. Imamura, *J. Biosci. Bioeng.* **2001**, *91*, 233.

[46] B. G. Keselowsky, D. M. Collard, A. J. Garcia, *Proc. Natl. Acad. Sci. U. S. A.* **2005**, *102*, 5953.

[47] N. Nath, J. Hyun, H. Ma, A. Chilkoti, *Surf. Sci.* **2004**, *570*, 98.

[48] S. I. Jeon, J. H. Lee, J. D. Andrade, P. G. Degennes, *J. Colloid Interface Sci.* **1991**, *142*, 149.

[49] J. Satulovsky, M. A. Carignano, I. Szleifer, *Proc. Natl. Acad. Sci. U. S. A.* **2000**, *97*, 9037.

[50] F. Fang, J. Satulovsky, I. Szleifer, *Biophys. J.* **2005**, *89*, 1516.

[51] B. D. Ratner, S. J. Bryant, In *Annual Review of Biomedical Engineering*, Vol. 6, Annual Reviews Inc., **2004**, 41.

[52] M. Morra, *J. Biomat. Sci.-Polym. Ed.* **2000**, *11*, 547.

[53] M. N. Helmus, D. F. Gibbons, D. Cebon, *Toxicol. Pathol.* **2008**, *36*, 70.

[54] J. M. Anderson, *Ann. Rev. Mater. Res.* **2001**, *31*, 81.

[55] P. Roach, D. Eglin, K. Rohde, C. C. Perry, *J. Mater. Sci.-Mater. Med.* **2007**, *18*, 1263.

[56] A. J. Garcia, B. G. Keselowsky, *Crit. Rev. Eukaryot. Gene Expr.* **2002**, *12*, 151.

[57] L. Y. Liu, G. Chen, T. Chao, B. D. Ratner, E. H. Sage, S. Y. Jiang, *J. Biomat. Sci.-Polym. Ed.* **2008**, 19, 821.

[58] G. Marletta, G. Ciapetti, C. Satriano, S. Pagani, N. Baldini, *Biomaterials* **2005**, *26*, 4793.

[59] G. R. Owen, J. Jackson, B. Chehroudi, H. Burt, D. M. Brunette, *Biomaterials* **2005**, *26*, 7447.

[60] L. Murphy, *Curr. Opin. Chem. Biol.* **2006**, *10*, 177.

[61] J. J. Gooding, *Anal. Chim. Acta* **2006**, *559*, 137.

[62] P. S. Dittrich, A. Manz, *Nat. Rev. Drug Discov.* **2006**, *5*, 210.

[63] S. Haeberle, R. Zengerle, *Lab Chip* **2007**, *7*, 1094.

[64] E. Stern, J. F. Klemic, D. A. Routenberg, P. N. Wyrembak, D. B. Turner-Evans, A. D. Hamilton, D. A. Lavan, T. M. Fahmy, M. A. Reed, *Nature* **2007**, *445*, 519.

[65] Y. D. Liu, F. Mahdavi, S. Blair, *IEEE J. Sel. Top. Quantum Electron.* **2005**, *11*, 778.

[66] B. Ilic, H. G. Craighead, S. Krylov, W. Senaratne, C. Ober, P. Neuzil, *J. Appl. Phys.* **2004**, *95*, 3694.

[67] T. Kim, E. Meyhofer, *Anal. Chem.* **2008**, *80*, 5383.

[68] E. Eteshola, D. Leckband, *Sens. Actuator B-Chem.* **2001**, *72*, 129.

[69] S. L. S. Freire, A. R. Wheeler, *Lab Chip* **2006**, *6*, 1415.

[70] B. H. Weigl, R. L. Bardell, C. R. Cabrera, *Adv. Drug. Deliv. Rev.* **2003**, *55*, 349.

[71] M. M. Stevens, J. H. George, *Science* **2005**, *310*, 1135.

[72] T. Matsuda, T. Sugawara, *J. Biomed. Mater. Res.* **1996**, *32*, 165.

[73] M. Knoblauch, W. S. Peters, *Cell. Mol. Life Sci.* **2004**, *61*, 2497.

[74] K. J. Böhm, E. Unger, In *Encyclopedia of Nanoscience and Nanotechnology*, Vol. 4 (Ed: H. S. Nalwa), American Scientific Publishers, Stevenson Ranch **2004**, 345.

[75] C.-T. Lin, M.-T. Kao, K. Kurabayashi, E. Meyhöfer, *Small* **2006**, *2*, 281.

[76] L. Jia, S. G. Moorjani, T. N. Jackson, W. O. Hancock, *Biomed. Microdevices* **2004**, *6*, 67.

[77] R. K. Doot, H. Hess, V. Vogel, *Soft Matter* **2007**, *3*, 349.

[78] C. T. Lin, M. T. Kao, K. Kurabayashi, E. Meyhofer, *Nano Lett.* **2008**, *8*, 1041.

[79] H. Hess, J. Clemmens, J. Howard, V. Vogel, *Nano Lett.* **2002**, *2*, 113.

[80] H. Hess, J. Clemmens, C. Brunner, R. Doot, S. Luna, K.-H. Ernst, V. Vogel, *Nano Lett.* **2005**, *5*, 629.

[81] H. Q. Liu, E. D. Spoerke, M. Bachand, S. J. Koch, B. C. Bunker, G. D. Bachand, *Adv. Mater.* **2008**, *20*, 4476.

[82] H. Hess, *Soft Matter* **2006**, *2*, 669.

[83] H. Hess, J. Howard, V. Vogel, *Nano Lett.* **2002**, *2*, 1113.

[84] J. L. Bull, A. J. Hunt, E. Meyhofer, *Biomed. Microdevices* **2005**, *7*, 21.

[85] Y. Tanaka, K. Morishima, T. Shimizu, A. Kikuchi, M. Yamato, T. Okano, T. Kitamori, *Lab Chip* **2006**, *6*, 362.

[86] M. J. Kim, K. S. Breuer, *Small* **2008**, *4*, 111.

[87] M. Raab, W. O. Hancock, *Biotechnol. Bioeng.* **2008**, *99*, 764.

[88] L. Rios, G. D. Bachand, *Lab Chip* **2009**, *9*, 1005.

[89] A. Agarwal, P. Katira, H. Hess, *Nano Lett.* **2009**, *9*, 1170.

[90] C. Brunner, C. Wahnes, V. Vogel, *Lab Chip* **2007**, *7*, 1263.

[91] G. D. Bachand, S. B. Rivera, A. K. Boal, J. Gaudioso, J. Liu, B. C. Bunker, *Nano Lett.* **2004**, *4*, 817.

[92] W. X. Song, Q. He, Y. Cui, H. Mohwald, S. Diez, J. B. Li, *Biochem. Biophys. Res. Commun.* **2009**, *379*, 175.

[93] R. Yokokawa, S. Takeuchi, T. Kon, R. Ohkura, M. Edamatsu, K. Sutoh, H. Fujita, *Mems-03 Kyoto. IEEE The Sixteenth Annual International Conference on, 2003*, 8.

[94] H. Hess, G. D. Bachand, *Materials Today* **2005**, *8*, 22.

[95] N. Hirokawa, R. Takemura, *Nat. Rev. Neurosci.* **2005**, *6*, 201.

[96] N. Hirokawa, *Science* **1998**, *279*, 519.

[97] M. Sundberg, M. Balaz, R. Bunk, J. P. Rosengren-Holmberg, L. Montelius, I. A. Nicholls, P. Omling, S. Tagerud, A. Mansson, *Langmuir* **2006**, *22*, 7302.

[98] J. Clemmens, H. Hess, J. Howard, V. Vogel, *Langmuir* **2003**, *19*, 1738.

[99] J. Clemmens, H. Hess, R. Lipscomb, Y. Hanein, K. F. Boehringer, C. M. Matzke, G. D. Bachand, B. C. Bunker, V. Vogel, *Langmuir* **2003**, *19*, 10967.

[100] B. D. Ratner, *J. Mol. Recognit.* **1996**, *9*, 617.

[101] B. D. Ratner, *Perspectives And Possibilities In Biomaterials Science*, Academic Press, Inc.; Academic Press Ltd., **1996**.

[102] J. J. Gray, *Curr. Opin. Struct. Biol.* **2004**, *14*, 110.

[103] P. Roach, D. Farrar, C. C. Perry, *J. Am. Chem. Soc.* **2005**, *127*, 8168.

[104] C. B. Johansson, T. Albrektsson, L. E. Ericson, P. Thomsen, *J. Mater. Sci.-Mater. Med.* **1992**, *3*, 126.

[105] J. Piglowski, I. Gancarz, J. Staniszewskakus, D. Paluch, M. Szymonowicz, A. Konieczny, *Biomaterials* **1994**, *15*, 909.

[106] B. G. Keselowsky, D. M. Collard, A. J. Garcia, *J. Biomed. Mater. Res. Part A* **2003**, *66a*, 247.

[107] M. Amiji, K. Park, *Biomaterials* **1992**, *13*, 682.

[108] S. M. O'connor, A. P. Deanglis, S. H. Gehrke, G. S. Retzinger, *Biotechnol. Appl. Biochem.* **2000**, *31*, 185.

[109] K. L. Prime, G. M. Whitesides, *Science* **1991**, *252*, 1164.

[110] L. D. Unsworth, H. Sheardown, J. L. Brash, *Biomaterials* **2005**, *26*, 5927.

[111] L. D. Unsworth, H. Sheardown, J. L. Brash, *Langmuir* **2005**, *21*, 1036.

[112] S. Herrwerth, W. Eck, S. Reinhardt, M. Grunze, *J. Am. Chem. Soc.* **2003**, *125*, 9359.

[113] E. Ostuni, B. A. Grzybowski, M. Mrksich, C. S. Roberts, G. M. Whitesides, *Langmuir* **2003**, *19*, 1861.

[114] J. P. Bearinger, S. Terrettaz, R. Michel, N. Tirelli, H. Vogel, M. Textor, J. A. Hubbell, *Nat. Mater.* **2003**, *2*, 259.

[115] H. Ma, J. Hyun, P. Stiller, A. Chilkoti, *Adv. Mater.* **2004**, *16*, 338.

[116] H. Y. Chen, J. Lahann, *Anal. Chem.* **2005**, *77*, 6909.

[117] L. Cao, M. Chang, C.-Y. Lee, D. G. Castner, S. Sukavaneshvar, B. D. Ratner, T. A. Horbett, *J. Biomed. Mater. Res. Part A* **2007**, *9999*, Na.

[118] N. B. Holland, Y. X. Qiu, M. Ruegsegger, R. E. Marchant, *Nature* **1998**, *392*, 799.

[119] K. Ishihara, N. P. Ziats, B. P. Tierney, N. Nakabayashi, J. M. Anderson, *J. Biomed. Mat. Res.* **1991**, *25*, 1397.

[120] M. Mrksich, G. M. Whitesides, *Trends Biotechnol.* **1995**, *13*, 228.

[121] R. Singhvi, A. Kumar, G. P. Lopez, G. N. Stephanopoulos, D. I. C. Wang, G. M. Whitesides, D. E. Ingber, *Science* **1994**, *264*, 696.

[122] Y. N. Xia, G. M. Whitesides, *Annu. Rev. Mater. Sci.* **1998**, *28*, 153.

[123] R. D. Piner, J. Zhu, F. Xu, S. Hong, C. A. Mirkin, *Science* **1999**, *283*, 661.

[124] G. Y. Liu, S. Xu, Y. Qian, *Acc. Chem. Res.* **2000**, *33*, 457.

[125] D. Falconnet, G. Csucs, H. M. Grandin, M. Textor, *Biomaterials* **2006**, *27*, 3044.

[126] A. Kumar, H. A. Biebuyck, G. M. Whitesides, *Langmuir* **1994**, *10*, 1498.

[127] A. Bernard, E. Delamarche, H. Schmid, B. Michel, H. R. Bosshard, H. Biebuyck, *Langmuir* **1998**, *14*, 2225.

[128] J. Spinke, M. Liley, H.-J. Guder, L. Angermaier, W. Knoll, *Langmuir* **1993**, *9*, 1821.

[129] M. Mrksich, J. R. Grunwell, G. M. Whitesides, *J. Am. Chem. Soc.* **1995**, *117*, 12009.

[130] S. Vandevondele, J. Voros, J. A. Hubbell, *Biotechnol. Bioeng.* **2003**, *82*, 784.

[131] K. Mossman, J. Groves, *Chem. Soc. Rev.* **2007**, *36*, 46.

[132] J. T. Groves, L. K. Mahal, C. R. Bertozzi, *Langmuir* **2001**, *17*, 5129.

[133] V. Verma, W. O. Hancock, J. M. Catchmark, *J. Biol. Eng.* **2008**, *2*, 14.

[134] S. M. Martin, J. L. Schwartz, C. M. Giachelli, B. D. Ratner, *Abstracts of Papers American Chemical Society* **2003**, *225*, Poly 320.

[135] NHGRI, Wikimedia. Protein-structure.png, Accessed: April 20, 2009, http://en.wikipedia.org/wiki/file:Protein-structure.png

[136] H. Zhu, M. Bilgin, R. Bangham, D. Hall, A. Casamayor, P. Bertone, N. Lan, R. Jansen, S. Bidlingmaier, T. Houfek, T. Mitchell, P. Miller, R. A. Dean, M. Gerstein, M. Snyder, *Science* **2001**, *293*, 2101.

[137] E. Ostuni, R. G. Chapman, R. E. Holmlin, S. Takayama, G. M. Whitesides, *Langmuir* **2001**, *17*, 5605.

[138] R. Marie, J. P. Beech, J. Voros, J. O. Tegenfeldt, F. Hook, *Langmuir* **2006**, *22*, 10103.

[139] M. Mrksich, G. M. Whitesides, *Annu. Rev. Biophys. Biomolec. Struct.* **1996**, *25*, 55.

[140] H. Elwing, *Biomaterials* **1998**, *19*, 397.

[141] H. Tompkins, *A User's Guide To Ellipsometry*, Dover Publications, **2006**.

[142] J. A. De Feijter, J. Benjamins, F. A. Veer, *Biopolymers* **1978**, *17*, 1759.

[143] M. Malmsten, B. Lessen, In *Proteins at Interfaces II- Fundamentals and Applications*, (Eds. T. A. Horbett, J. L. Brash), Vol. 602, ACS **1995**.

[144] H. Nygren, M. Stenberg, C. Karlsson, *J. Biomed. Mater. Res.* **1992**, *26*, 77.

[145] T. Arnebrant, T. Nylander, *J. Colloid Interface Sci.* **1988**, *122*, 557.

[146] H. Elwing, M. Stenberg, *J. Immunol. Methods* **1981**, *44*, 343.

[147] M. Werthen, H. Nygren, *J. Immunol. Methods* **1988**, *115*, 71.

[148] S.-Y. Jung, S.-M. Lim, F. Albertorio, G. Kim, M. C. Gurau, R. D. Yang, M. A. Holden, P. S. Cremer, *J. Am. Chem. Soc.* **2003**, *125*, 12782.

[149] L. Vroman, A. L. Adams, *Surf. Sci.* **1969**, *16*, 438.

[150] K. M. Hansson, S. Tosatti, J. Isaksson, J. Wettero, M. Textor, T. L. Lindahl, P. Tengvall, *Biomaterials* **2005**, *26*, 861.

[151] J. Homola, *Anal. Bioanal. Chem.* **2003**, *377*, 528.

[152] M. Mrksich, G. B. Sigal, G. M. Whitesides, *Langmuir* **1995**, *11*, 4383.

[153] R. G. Chapman, E. Ostuni, L. Yan, G. M. Whitesides, *Langmuir* **2000**, *16*, 6927.

[154] R. G. Smith, N. D'souza, S. Nicklin, *Analyst* **2008**, *133*, 571.

[155] J. S. Shumaker-Parry, C. T. Campbell, *Anal. Chem.* **2004**, *76*, 907.

[156] F. D. Stefani, K. Vasilev, N. Bocchio, N. Stoyanova, M. Kreiter, *Phys. Rev. Lett.* **2005**, *94*, 4.

[157] J. G. Archambault, J. L. Brash, *Colloids Surf. B: Biointerfaces* **2004**, *33*, 111.

[158] A. R. Ubiera, G. Carta, *Biotechnology Journal* **2006**, *1*, 665.

[159] M. S. Wagner, T. A. Horbett, D. G. Castner, *Biomaterials* **2003**, *24*, 1897.

[160] M. Rodahl, F. Hook, C. Fredriksson, C. A. Keller, A. Krozer, P. Brzezinski, M. Voinova, B. Kasemo, *Faraday Discuss.* **1997**, 229.

[161] F. Caruso, E. Rodda, D. N. Furlong, *J. Colloid Interface Sci.* **1996**, *178*, 104.

[162] J. Malmstrom, H. Agheli, P. Kingshott, D. S. Sutherland, *Langmuir* **2007**, *23*, 9760.

[163] B. S. Murray, C. Deshaires, *J. Colloid Interface Sci.* **2000**, *227*, 32.

[164] L. Rodriguez-Pardo, J. F. Rodriguez, C. Gabrielli, R. Brendel, *IEEE Sens. J.*, **2005**, *5*, 1251.

[165] S. M. Nie, R. N. Zare, *Annu. Rev. Biophys. Biomolec. Struct.* **1997**, *26*, 567.

[166] E. Betzig, R. J. Chichester, *Science* **1993**, *262*, 1422.

[167] X. S. Xie, R. C. Dunn, *Science* **1994**, *265*, 361.

[168] T. Hirschfeld, *Appl. Optics* **1976**, *15*, 2965.

[169] D. Axelrod, T. P. Burghardt, N. L. Thompson, *Annu. Rev. Biophys. Bioeng.* **1984**, *13*, 247.

[170] H. Schneckenburger, *Curr. Opin. Biotechnol.* **2005**, *16*, 13.

[171] J. B. Pawley, *Handbook of Biological Confocal Microscopy*, New York: Plenum. 2nd Ed., **1995**.

[172] M. Eigen, R. Rigler, *Proc. Natl. Acad. Sci. U. S. A.* **1994**, *91*, 5740.

[173] G. Binnig, C. F. Quate, C. Gerber, *Phys. Rev. Lett.* **1986**, *56*, 930.

[174] G. Binnig, H. Rohrer, *Sci. Am.* **1985**, *253*, 40.

[175] S. L. Mcgurk, R. J. Green, G. H. W. Sanders, M. C. Davies, C. J. Roberts, S. J. B. Tendler, P. M. Williams, *Langmuir* **1999**, *15*, 5136.

[176] K. E. Michael, V. N. Vernekar, B. G. Keselowsky, J. C. Meredith, R. A. Latour, A. J. Garcia, *Langmuir* **2003**, *19*, 8033.

[177] P. Hinterdorfer, Y. F. Dufrene, *Nat. Methods* **2006**, *3*, 347.

[178] N. Jalili, K. Laxminarayana, *Mechatronics* **2004**, *14*, 907.

[179] R. Otero, F. Rosei, F. Besenbacher, *Annu. Rev. Phys. Chem.* **2006**, *57*, 497.

[180] A. M. Moore, P. S. Weiss, *Annu. Rev. Anal. Chem.* **2008**, *1*, 857.

[181] B. Kasemo, *Surf. Sci.* **2002**, *500*, 656.

[182] Wikimedia. Atomic_force_microscope_block_diagram.png, Accessed: April 20, 2009, http://en.wikipedia.org/wiki/file:Atomic_force_microscope_block_diagram.png

[183] M. Q. Zhang, T. Desai, M. Ferrari, *Biomaterials* **1998**, *19*, 953.

[184] T. A. Horbett, *Cardiovasc. Pathol.* **1993**, *2*, S137.

[185] Y. Hiratsuka, T. Tada, K. Oiwa, T. Kanayama, T. Q. Uyeda, *Biophys. J.* **2001**, *81*, 1555.

[186] S. G. Moorjani, L. Jia, T. N. Jackson, W. O. Hancock, *Nano Lett.* **2003**, *3*, 633.

[187] L. J. Cheng, M. T. Kao, E. Meyhofer, L. J. Guo, *Small* **2005**, *1*, 409.

[188] C. Reuther, L. Hajdo, R. Tucker, A. A. Kasprzak, S. Diez, *Nano Lett.* **2006**, *6*, 2177.

[189] M. G. Van Den Heuvel, C. T. Butcher, R. M. Smeets, S. Diez, C. Dekker, *Nano Lett.* **2005**, *5*, 1117.

[190] L. Ionov, M. Stamm, S. Diez, *Nano Lett.* **2005**, *5*, 1910.

[191] A. K. Boal, J. M. Bauer, S. B. Rivera, R. G. Manley, R. P. Manginell, G. D. Bachand, B. C. Bunker, *Polymer Preprints* **2004**, 96.

[192] D. V. Nicolau, H. Suzuki, S. Mashiko, T. Taguchi, S. Yoshikawa, *Biophys. J.* **1999**, *77*, 1126.

[193] C. Mahanivong, J. P. Wright, M. Kekic, D. K. Pham, C. Dos Remedios, D. V. Nicolau, *Biomed. Microdevices* **2002**, *4*, 111.

[194] G. S. Bachand, R. K.; Neves, H. P.; Olkhovets, A.; Craighead,H.G.; Montemagno, C. D., *Nano Lett.* **2001**, *1*, 42.

[195] J. Yajima, M. C. Alonso, R. A. Cross, Y. Y. Toyoshima, *Curr. Biol.* **2002**, *12*, 301.

[196] S. Diez, W. R. Schief, J. Howard, *Curr. Biol.* **2002**, *12*, R203.

[197] J. Howard, A. J. Hunt, S. Baek, *Methods Cell Biol.* **1993**, *39*, 137.

[198] J. Kerssemakers, J. Howard, H. Hess, S. Diez, *Proc. Natl. Acad. Sci. U. S. A.* **2006**, *103*, 15812.

[199] M. J. Wirth, D. J. Swinton, M. D. Ludes, *J. Phys. Chem. B* **2003**, *107*, 6258.

[200] R. D. Vale, B. J. Schnapp, T. S. Reese, M. P. Sheetz, *Cell* **1985**, *40*, 559.

[201] J. Howard, *Mechanics Of Motor Proteins And The Cytoskeleton*, Sinauer, Sunderland, MA **2001**.

[202] D. Balazs, C. Hollenstein, H. Mathieu, *Eur. Cell. Mater.* **2002**, *3*, 7.

[203] D. Ji, C. M. Arnold, M. Graupe, E. Beadle, R. V. Dunn, M. N. Phan, R. J. Villazana, R. Benson, R. Colorado, T. R. Lee, J. M. Friedman, *J. Cryst. Growth* **2000**, *218*, 390.

[204] C. Siegers, M. Biesalski, R. Haag, *Chem.- Eur. J.* **2004**, *10*, 2831.

[205] J. Lahann, R. Langer, *Macromolecules* **2002**, *35*, 4380.

[206] D. L. Coy, M. Wagenbach, J. Howard, *J. Biol. Chem.* **1999**, *274*, 3667.

[207] F. Gittes, B. Mickey, J. Nettleton, J. Howard, *J. Cell Biol.* **1993**, *120*, 923.

[208] A. Kishino, T. Yanagida, *Nature* **1988**, *334*, 74.

[209] M. J. Decastro, C. H. Ho, R. J. Stewart, *Biochemistry* **1999**, *38*, 5076.

[210] J. Lahann, *Polym. Int.* **2006**, *55*, 1361.

[211] Y. Elkasabi, H. Y. Chen, J. Lahann, *Adv. Mater.* **2006**, *18*, 1521.

[212] K. Y. Suh, R. Langer, J. Lahann, *Adv. Mater.* **2004**, *16*, 1401.

[213] T. A. Horbett, J. L. Brash, Eds., *Proteins At Interfaces II: Fundamentals And Applications*, Vol. 602, ACS, **1995**.

[214] W. Norde, C. A. Haynes, In *Proteins At Interfaces II* (Eds. T. A. Horbett, J. L. Brash), Vol. 602, ACS, **1995**.

[215] M. J. Mura-Galelli, J. C. Voegel, S. Behr, E. F. Bress, P. Schaaf, *Proc. Natl. Acad. Sci. U. S. A.* **1991**, *88*, 5557.

[216] P. Schaaf, J. Talbot, *Phys. Rev. Lett.* **1989**, *62*, 175.

[217] A. Cadilhe, N. A. M. Araujo, V. Privman, *J. Phys.-Condes. Matter* **2007**, *19*, 12.

[218] J. Talbot, G. Tarjus, P. R. Van Tassel, P. Viot, *Colloid Surf. A-Physicochem. Eng. Asp.* **2000**, *165*, 287.

[219] C. F. Wertz, M. M. Santore, *Langmuir* **2001**, *17*, 3006.

[220] W. K. Lee, J. Mcguire, M. K. Bothwell, *J. Colloid Interface Sci.* **2004**, *269*, 251.

[221] M. Agashe, V. Raut, S. J. Stuart, R. A. Latour, *Langmuir* **2005**, *21*, 1103.

[222] S. I. Jeon, J. D. Andrade, *J. Colloid Interface Sci.* **1991**, *142*, 159.

[223] I. Szleifer, *Biophys. J.* **1997**, *72*, 595.

[224] M. A. Carignano, I. Szleifer, *J. Chem. Phys.* **1994**, *100*, 3210.

[225] F. Fang, I. Szleifer, *Proc. Natl. Acad. Sci. U. S. A.* **2006**, *103*, 5769.

[226] R. A. Latour, *J. Biomed. Mater. Res. Part A* **2006**, *78a*, 843.

[227] J. C. Hower, Y. He, M. T. Bernards, S. Y. Jiang, *J. Chem. Phys.* **2006**, *125*, 214704.

[228] I. Szleifer, *Curr. Opin. Solid State Mat. Sci.* **1997**, *2*, 337.

[229] K. L. Prime, G. M. Whitesides, *J. Am. Chem. Soc.* **1993**, *115*, 10714.

[230] J. Gottschalck, B. Hammer, *J. Chem. Phys.* **2002**, *116*, 784.

[231] L. D. Unsworth, H. Sheardown, J. L. Brash, *Langmuir* **2008**, *24*, 1924.

[232] J. W. Evans, *Rev. Mod. Phys.* **1993**, *65*, 1281.

[233] J. Feder, *J. Theor. Biol.* **1980**, *87*, 237.

[234] K. A. Dill, S. Bromberg, *Molecular Driving Forces*, Taylor & Francis, **2002**.

[235] D. R. Weaver, W. G. Pitt, *Biomaterials* **1992**, *13*, 577.

[236] L. S. Jung, C. T. Campbell, *Phys. Rev. Lett.* **2000**, *84*, 5164.

[237] S. Pasche, S. M. De Paul, J. Voros, N. D. Spencer, M. Textor, *Langmuir* **2003**, *19*, 9216.

[238] L. E. Ramm, M. B. Whitlow, M. M. Mayer, *Journal Of Immunology* **1985**, *134*, 2594.

[239] A. Rothen, *J. Gen. Physiol.* **1940**, *24*, 203.

[240] X. L. Wang, P. H. Mcmurry, *Int. J. Mass Spectrom.* **2006**, *258*, 30.

[241] A. Purice, J. Schou, P. Kingshott, N. Pryds, M. Dinescu, *Appl. Surf. Sci.* **2007**, *253*, 6451.

[242] G. Y. Onoda, E. G. Liniger, *Phys. Rev. A* **1986**, *33*, 715.

[243] S. F. Chen, S. Y. Jiang, *Adv. Mater.* **2008**, *20*, 335.

[244] P. E. Sheehan, L. J. Whitman, *Nano Lett.* **2005**, *5*, 803.

[245] E. M. Campbell, T. J. Hope, *Adv. Drug. Deliv. Rev.* **2003**, *55*, 761.

[246] K. Radtke, K. Dohner, B. Sodeik, *Cell Microbiol.* **2006**, *8*, 387.

[247] G. Adam, M. Delbrueck, In *Structural Chemistry and Molecular Biology*, (Eds: A. Rich, N. Davidson), W. H. Freeman And Co., New York **1968**, 198.

[248] T. Fischer, A. Agarwal, H. Hess, *Nat. Nano.* **2009**, *4*, 162.

[249] T. M. Squires, R. J. Messinger, S. R. Manalis, *Nat. Biotechnol.* **2008**, *26*, 417.

[250] H. C. Berg, *Random Walks in Biology*, Princeton University Press, Princeton, N.J. **1983**.

[251] M. J. Heller, *Annu. Rev. Biomed. Eng.* **2002**, *4*, 129.

[252] T. L. Vail, K. W. Cushing, J. C. Ingram, I. S. Omer, *Biotechnol. Appl. Biochem.* **2006**, *43*, 85.

[253] B. Schmidt, V. Almeida, C. Manolatou, S. Preble, M. Lipson, *Appl. Phys. Lett.* **2004**, *85*, 4854.

[254] A. G. Brolo, S. C. Kwok, M. D. Cooper, M. G. Moffitt, C. W. Wang, R. Gordon, J. Riordon, K. L. Kavanagh, *J. Phys. Chem. B* **2006**, *110*, 8307.

[255] K. A. Tetz, L. Pang, Y. Fainman, *Opt. Lett.* **2006**, *31*, 1528.

[256] J. J. Gooding, *Small* **2006**, *2*, 313.

[257] L. Senesac, T. G. Thundat, *Materials Today* **2008**, *11*, 28.

[258] J. Bishop, A. Chagovetz, S. Blair, *Nanotechnology* **2006**, *17*, 2442.

[259] H. C. Berg, E. M. Purcell, *Biophys. J.* **1977**, *20*, 193.

[260] H. Hess, V. Vogel, *Rev. Mol. Biotechnol.* **2001**, *82*, 67.

[261] M. Hirabayashi, S. Taira, S. Kobayashi, K. Konishi, K. Katoh, Y. Hiratsuka, M. Kodaka, T. Q. P. Uyeda, N. Yumoto, T. Kubo, *Biotechnol. Bioeng.* **2006**, *94*, 473.

[262] S. Taira, Y. Z. Du, Y. Hiratsuka, K. Konishi, T. Kubo, T. Q. P. Uyeda, N. Yumoto, M. Kodaka, *Biotechnol. Bioeng.* **2006**, *95*, 533.

[263] George D. Bachand, Susan B. Rivera, A. Carroll-Portillo, H. Hess, M. Bachand, *Small* **2006**, *2*, 381.

[264] D. Wu, R. Tucker, H. Hess, *IEEE Trans. Adv. Packag.* **2005**, *28*, 594.

[265] T. Nitta, A. Tanahashi, Y. Obara, M. Hirano, M. Razumova, M. Regnier, H. Hess, *Nano Lett.* **2008**, *8*, 2305.

[266] P. G. Vikhorev, N. N. Vikhoreva, M. Sundberg, M. Balaz, N. Albet-Torres, R. Bunk, A. Kvennefors, K. Liljesson, I. A. Nicholls, L. Nilsson, P. Omling, S. Tagerud, L. Montelius, A. Mansson, *Langmuir* **2008**, *24*, 13509.

[267] J. F. Morin, Y. Shirai, J. M. Tour, *Org. Lett.* **2006**, *8*, 1713.

[268] S. Kulin, R. Kishore, J. B. Hubbard, K. Helmerson, *Biophys. J.* **2002**, *83*, 1965.

[269] P. Katira, A. Agarwal, T. Fischer, H.-Y. Chen, X. Jiang, J. Lahann, H. Hess, *Adv. Mater.* **2007**, *19*, 3171.

[270] P. Katira, A. Agarwal, H. Hess, *Adv. Mater.* **2009**, *21*, 1599.

[271] P. Katira, H. Hess, *In Preparation* **2009**.

BIOGRAPHICAL SKETCH

Parag Katira was born in 1984 in Mumbai, India. Throughout his education, Parag's favorite subjects have been Physics and Mathematics. Parag earned his Bachelor of Engineering degree in Production Engineering from VJTI, Mumbai in June 2005. After that he came to the United States to pursue higher education. With a view of shifting towards science from his engineering background, Parag joined the Materials Science and Engineering Department at the University of Florida. He started his graduate studies under the guidance of Dr. Henry Hess, and earned his Ph. D. in materials science and engineering in August 2009. Parag thoroughly enjoyed his time as a graduate student at the University of Florida and his research experience as a member of the Hess group. He wishes to remain in academia and is looking forward to his time as a postdoctoral researcher.